REGULATION OF ADHERENS JUNCTION AND MECHANICAL FORCE DURING APOPTOSIS IN EPITHELIAL TISSUE MORPHOGENESIS

TENG XIANG

(B. Sc. (Hons.), NANJING UNIVERSITY, CHINA)

A THESIS SUBMITTED

FOR THE DEGREE OF DOCTOR OF PHILOSOPHY

DEPARTMENT OF BIOLOGICAL SCIENCES

NATIONAL UNIVERSITY OF SINGAPORE

2014

DECLARATION

I hereby declare that this thesis is my original work and it has been written by me in its entirety. I have duly acknowledged all the sources of information which have been used in the thesis.

This thesis has also not been submitted for any degree in any university previously.

_____

Teng Xiang

14 August 2014

Acknowledgements

Work in this study was performed in Dr. Yusuke Toyama's Lab in Temaseak Life Sciences Laboratory (TLL) and Mechano-biology Institite (MBI). I would like to address my gratitude to Yusuke for taking me as a rotation student, and decided to accept me as the first PhD student in the lab. With him, I learned not just the scientific knowledge and techniques, but also the spirit of scientific research. His talents inspired me, and his diligence encouraged me. In addition, his patient guidance for my career development and attitude towards the life will surely benefit my whole life. Under his supervision, I gradually grow up. As I always said: thank you Yusuke! I thank Dr. Roland Le Borgne from Institute of Genetics and Development of Rennes (IGDR) for guiding me the experiment of nano-ablation during my visit to Rennes, France.

I also would like to thank my lab members for supporting me on my work. I thank Qin Lei, Mikiko, Zijun, Sean, Hara-San and Ken for helping me for the fly works. I thank Mikiko and Hara-San for the discussion on molecular and imaging experimental techniques. I thank Sara and Murat for the discussion on Matlab and quantitative analysis. I thank all of them for the discussion and friendship. Besides, I would like to thank all the colleagues in TLL and MBI for generous helps and the friendly environment.

I thank my parents for supporting me to study abroad in Singapore. I also would like to thank my wife, Luo Shuyuan for bringing me with great happiness and make my research life colourful.

Last but not the least, I would like to thank Department of Biological Sciences, National University of Singapore, and Ministry of Education, Singapore for providing me the PhD scholarship.

Table of Contents

Summary

Apoptosis is known to be important during embryonic development and in the homeostasis maintenance of adult tissues. During apoptosis, the dying cell will be extruded out from the cell plane in an actomyosin ring based manner. The mechanical force generated during apoptosis was demonstrated to exist in dorsal closure during *Drosophila* embryogenesis, and the force contributes to the development. However, whether the force could help other development processes is unknown. *Drosophila* abdominal epithelial development during metamorphosis, known as histoblast expansion, is a model system to study tissue dynamics. In this project, I revealed that the apoptosis of larval epidermal cells (LECs) during histoblast expansion could mechanically promote the development. Furthermore, I also investigated how the molecules could spatial-temporally regulate the LEC apoptosis and generate the mechanical force. I revealed that the caspase-3 activity is activated before the force generation during apoptosis. Our results also indicated that in the late stage of apical constriction, the actomyosin ring will separate into two rings upon disengagement of adherens junctions between the apoptotic cell and its neighbors, where the tissue tension is released. In addition, the inner ring forms in the apoptotic cell, and starts to accumulate when the apical constriction starts to enter the fast constricting phase, which generates the intrinsic force to constrict the apoptotic cell. The outer ring forms in the neighbors, and starts to accumulate only when the adherens junction disengages in the late stage of Fast Phase. The outer ring plays the role as extrinsic force to fill in the gap left by apoptotic cell and maintain the tissue integrity, and rebuild the tissue tension to maintain tension homeostasis. Through the whole apical constriction process, the septate junction remains intact and keep the tissue integrity. In conclusion, our results suggested the apoptosis could mechanically contribute to other developmental

processes as well, which open an insight into a more universally applied active mechanical role the apoptosis may play. In addition, our results indicated the important role of the intrinsic and extrinsic forces in maintaining the tissue integrity and tissue homeostasis during apoptosis in epithelial tissue morphogenesis.

List of Figures

List of Movies

List of Abbreviations and Symbols

AJ Adherens Junction

AP Anterior-Posterior

APF After Puparium Formation

Dpp Decapentaplegic

DV Dorsal-Ventral

ECFP Enhanced Cyan Fluorescence Protein

ECM Extra-cellular Matrix

EMT Epithelial Mesenchymal Transition

FRET Fluorescence Resonance Energy Transfer

GFP Green Fluorescence Protein

LEC Larval Epidermal Cell

MARCM Mosaic Analysis with a Repressible Cell Marker

MMP Matrix Metalloproteinase

PCR polymerase chain reaction

RFP Red Fluorescence Protein

RNAi RNA inteference

ROI Region of Interest

SEM Standard Error of the Mean

Sqh spaghetti squash

SJ Septate junction

sGMCA sqh driven, Green fluorescent protein, Moesin α-helical–Coiled and Actin binding site

TNF Tumor Narcosis Factor

Chapter I: Introduction

1.1 Mechanical forces that drive tissue morphogenesis

Cells inside the tissue move not just by themselves, but also in coordination with their neighbors, which results in the tissue morphogenesis. Developmental processes are very important sources of the models to study tissue morphogenesis. Besides, tissue morphogenesis also occurs during organ growth, like mammary gland formation, and pathogenesis events, like wound healing.

While various mechanisms are adopted by the organisms to drive the morphogenesis in different tissues and different stages, mechanical force is the key player during the process. It plays key roles to coordinate the deformation and movement of cells inside the tissue. In the long run, forces drive the morphogenesis, and sculpture the tissue. For decades, researchers are interested in how the mechanical forces are generated and how the force in the cell level could incorporate with each other, and drive the morphogenesis in tissue level in different model systems.

1.1.1 Molecular and Cell level intrinsic forces

In general, organelles inside the cells generate the forces subcellularly in the molecular level, and the subcellular forces are integrated into the cell level. The cell level force, or the intrinsic force then propagates to its neighbours in the supra-cellular level through the intercellular adherens junctions (AJs). In the end, the supra-cellular cell groups affect the whole tissue and drives the tissue level morphogenesis. The missing parts are how forces are generated and how the forces in different levels are integrated. Firstly, I will discuss on the molecular and cellular level force generation.

1.1.1.1 Actin, myosin and molecular level force generation

In molecular level, actin and myosin are the basic force generators. Monomer G-actin self-assembles. Activated G-actin is bound with ATP. With the hydrolysis of ATP, G-actins polymerize into F-actin. Actin bundles polymerize faster in the barbed end of F-actin while the actin-ADP disassembles from the pointed end of F-actin. This results in the directional growth of actin bundles or called F-actin tread-milling. This F-actin tread-milling drives the formation of protrusion organelles, that are filopodia and lamellipodia, and generates the pushing force (Mogilner and Oster, 2003; Shaevitz and Fletcher, 2007).

On the other hand, non-muscle myosin II works as the molecular motor. Myosin II is a hexamer molecule with two heavy chains, two essential light chains, and two regulatory light chains (Sellers, 2000). With the phosphorylation of Myosin II regulatory light chain, the Myosin II unfolds and the heavy chains grab the anti-parallel actin bundles, and slide the bundles toward each other, which results in the contraction of actin bundles. This contraction generates the contractile force (Mahajan and Pardee, 1996; Niederman and Pollard, 1975).

1.1.1.2 Two pools of actomyosin contractile organelles

Inside the cell, the actin and myosin assemble and form the circumferential actomyosin belt along the AJs, which is also known as junctional actomyosin. Recent study revealed the myosin forms a sacromeric network circumferentially (Ebrahim et al., 2013). Inside the cell, contraction of the junctional actomyosin generates the force that tends to constrict the cell. In the tissue level, these inward forces are generated by every cells, which balance with each other, and the forces contribute to the global tissue tension homeostasis. During

morphogenesis, like neurulation during vertebrate development, contraction of the junctional actomyosin in cells at hingepoint inside the neural plate results in the decrease in the apical surface, and later leads to the neural plate folding, and neural tube formation (Copp and Greene, 2010). In other tissue morphogenesis events, like dorsal closure during *Drosophila* embryogenesis and wound healing during pathogenesis, junctional actomyosin will accumulate surrounding the constricting cell or tissue in the supra-cellular way (Brock et al., 1996; Edwards et al., 1997; Kiehart et al., 2000). These actomyosin bundles, formed inside different cells, are connected with each other through AJs and contract like the purse-string.

Besides, actin and myosin has also been revealed to be able to form the actomyosin network at the medial apical cortex below the apical membrane, which is called medial actomyosin meshwork (Martin et al., 2009). With the aid of crosslinkers, the F-actin bundles are linked with each other and form a network. The myosin contracts the network, generates the contracting force, and pulls the discrete AJ sites. Contraction of the medial actomyosin meshwork has been reported to lead the dynamics of many tissue morphogenesis events (Fernandez-Gonzalez and Zallen, 2011; Martin et al., 2009; Solon et al., 2009). For instance, during gastrulation in *Drosophila* embryogenesis, the mesoderm precursor cells accumulate medial actomyosin meshwork rather than the junctional actomyosin belt. Contraction of the meshwork, which is in the pulsatile manner, constricts the apical surface of the mesoderm precursor cells, and lead to the mesoderm invagination (Martin et al., 2009).

1.1.2 Cell-cell Adhesions

Any force needs the anchor. Studies on both *C. elegans* ventral closure and *Drosophila* mesoderm invagination revealed that the contraction of medial actomyosin not necessarily results in the cell constriction (Roh-Johnson et al., 2012). Instead, only after the plasma membrane and the contractile organelle are well engaged, the constriction could happen. Based on this study, the "Clutch Model" was proposed: like the clutch of the car, only when the engine, which is the actomyosin contractile organelle, is engaged with the effector, which is the plasma membrane in cell, through the clutch, the whole car could have the output, which is the constriction (Roh-Johnson et al., 2012). AJs work as anchors of subcellular forces inside the cell, to engage the contraction from actomyosin meshwork and junctional actomyosin to the plasma membrane. AJs also work in between the cells to transmit the force inter-cellularly. Besides, the forces are also anchored and transmitted from the cell to the ECM by focal adhesions. Here I only focus on the AJ.

In the classical model, the adhesion between cells is established by the coupling of extracellular domain of homophilic E-cadherin molecules from the neighboring cells in the calcium dependent manner. In the cytoplasmic region of E-cadherin, it is constitutively connected with β-catenin and also binds to p120-catenin. On the other hand, α-catenin, which has been reported to be important for epithelial integrity, binds to β-catenin and also F-actin(Hirano et al., 1992). Then α-catenin mediates the binding of AJ to the actomyosin bundles and cytoskeleton (Gates and Peifer, 2005). Recent studies have revealed the more dynamic interaction between α-catenin and β-catenin, that a-catenin cannot simultaneously bind to both F-actin and β-catenin (Yamada et al., 2005).

More molecules are important for the coupling between adhesion and actomyosin bundles, like vinculin, formin and Arp2/3 (Bershadsky, 2004; Yonemura et al., 2010).

The AJ anchors the subcellular level forces generated inside the cell to deform the cell itself, which is the intrinsic force. In further, the propagation of the cell level forces to the neighbours is also facilitated by the AJs between the cells, which plays the role as extrinsic force to the neighbours. With the integration of both intrinsic forces and extrinsic forces, the tissue level morphogenesis occurs.

1.1.3 Tissue-level extrinsic force

As is discussed, the intrinsic forces generated in the cell level could incorporate, and propagate within the tissue and in the end, drive the tissue morphogenesis. In turn, the tissue-level extrinsic force could also influence the morphogenesis of individual cells.

One good example is the cell sorting at the compartment boundary (Monier et al., 2010). In *Drosophila* early embryogenesis, cells on both sides of the parasegmental boundary along the DV axis are well sorted and the boundary interface, which consisted by the boundaries of cells on both sides, is formed into a straight line. High accumulation of myosin was observed on the parasegmental boundary. This tissue level myosin accumulation and the extrinsic force generation was further proved to be responsible for the cell sorting, and affects the cell packing and morphogenesis (Monier et al., 2010).

At the pupal stage during *Drosophila* metamorphosis, the contracting wing hinge generates the anisotropic tension along the proximal to distal axis. This

extrinsic force then orients the cell elongation, cell division and cell rearrangements of the wing blade epithelial cells, and results in the reorientation of the wing blade tissue (Aigouy et al., 2010). In further, the planar cell polarities of the wing blade epithelial cells are also aligned along the proximal-distal axis (Aigouy et al., 2010). This study indicated extrinsic force could not only drive the cell morphogenesis, but also affects the cells in molecular and signalling level.

1.2 Apoptosis

The notion of apoptosis was first introduced more than 40 years ago to describe cells commit suicide (Kerr et al., 1972). Apoptosis, or programmed cell death, is the process whereby animals eliminate the unwanted cells (Jacobson et al., 1997). During apoptosis, the cells undergo stereotypic morphological changes: the cells will shrink and round in their cell shape, dense their cytoplasm, fragment their nucleus and bleb their plasma membrane. In the end, the apoptotic cell will be engulfed by the macrophages (Kroemer et al., 2009).

Apoptosis is central regulated by caspases (Kuranaga, 2012). Caspases are a group of cysteine proteases that are conserved through evolution (Hengartner, 2000; Kuranaga, 2012). In *Drosophila* apoptosis signalling pathways, the apoptosis stimuli will trigger the expression of Reaper, Grim and Hid, which are the antagonists of IAP. DIAP is the *Drosophila* homolog of IAP, which is the inhibitor of caspase-9 homolog Dronc. Without the inhibitor, Dronc will express and then activates the downstream executive caspases: DrICE and Dcp-1, which are the homologs of caspase-3. Thus, the apoptosis signalling pathway is controlled by the “brake”, which is DIAP1, and the gas, that are DrICE and

Dcp-1. Once the brake is removed, the gas will initiate the apoptotic process. On the other hand, p35 in *Drosophila* is sufficient to inhibit the activity of DrICE and Dcp-1, which is another regulator of apoptosis (Hengartner, 2000; Thornberry et al., 1992).

1.2.1 Conventional role of apoptosis

Apoptosis is essential for sculpturing the tissue during development, and for maintaining the tissue homeostasis. For instance, blocking the apoptosis will result in the failure of neural tube closure in vertebrates, which is an essential process during vertebrate development (Yamaguchi et al., 2011); the removal of inter-digital webbing is also dependent on apoptosis (Lindsten et al., 2000). Here, I will focus on the role of apoptosis in epithelial tissues.

One of the most important role of the epithelial tissue is to maintain the barrier to prevent the body from invaders like bacteria and viruses. Thus, on one hand, the epithelial tissue needs to renew the cells. Cell competition is adapted to reduce the number inside the tissue. Loser cells during the competition will be extruded and undergo apoptosis (Eisenhoffer et al., 2012; Marinari et al., 2012). Besides that, the apoptotic cell also triggers the proliferation of remaining cells, or the winner cells through compensatory proliferation (Fan and Bergmann, 2008). With these processes, the tissue homeostasis is maintained and the epithelial tissue is renewed.

On the other hand, while the unwanted cells are eliminated to maintain the homeostasis, during the apoptotic process, the integrity should be maintained in the epithelial tissue. In the pathological level, poor epithelial integrity will cause the malfunctions in development and inflammation or infections in adults. In

physiological level, however, even large amount of cells undergo apoptosis in the epithelial tissues, tissue integrity is still well maintained (Rosenblatt et al., 2001).

1.2.2 Cell adhesion remodelling during apoptosis

Cell-cell junctions are the key players to maintain the tissue integrity. During apoptosis, to fully eliminate the apoptotic cell, the old junctions have to be loosen to facilitate the detachment while the new junctions have to be formed in between the remaining cells. Thus, junctions need to be remodelled.

1.2.2.1 Remodelling of adherens junctions during apoptosis

As is described previously, AJ is the interface where the actomyosin cortex connect with the plasma membrane through the E-cadherin- β-catenin- α-catenin complex. Despite the spot like AJs at the lateral side of epithelial, majority of AJ molecules locate at the apical lateral side to form the belt like structure surrounding the cells. During apoptosis, the inactive form of caspase-3, which is the executive protease, will be cleaved and activated. After activation, the caspase-3 will target to the ubiquitous cleavage target sequence on various proteins (Kurokawa and Kornbluth, 2009). In vitro studies have long identified numerous caspase-3 cleavage sites in the E-cadherin and β-catenin in the cytoplasm (Herren et al., 1998; Ivanova et al., 2011; Steinhusen et al., 2001). Besides, MMPs and ADAM have also been showed to cleave the E-cadherin in the extracellular domain (Nava et al., 2013). However, still no direct evidence shows the cleavage of E-cadherin by caspase-3 in vivo. For β-catenin, it is reported that in the induced global apoptosis during early embryo stage, the

Armadillo (*Drosophila* homologue of β-catenin) will be cleaved on its N terminus. The remaining Armadillo stays on the plasma membrane, while the DE-cadherin, which is not cleaved, detach from the cell membrane with unknown mechanism and α-catenin, which is also not cleaved, stays on the membrane (Kessler and Muller, 2009). In the later stage, the catenins will detach from the membrane. In the end, new junction forms between remaining cells (Kessler and Muller, 2009).

1.2.2.2 Remodelling of tight junction during apoptosis

Tight junction in vertebrate cells is the barrier that prevents the para-cellular movement of the fluid. At the interface of tight junction, cells are tightly associated. Tight junction locates even more apical than the AJ in vertebrates. While in *Drosophila*, the homolog of tight junction is not present. The relevant junction that is related with the tight junction in *Drosophila*, is the septate junction. Functional similarly, the septate junction prevents the fluid movement para-cellularly and maintains the blood-brain barrier like the tight junction. Septate junction locates more basally compared with AJ in *Drosophila* cells. Like AJ molecules, the molecules at tight junction have also been reported to be cleavable by caspase-3 and MMPs in vitro (Nava et al., 2013). However, in vivo study shows the remodelling of tight junction during the shed of intestine epithelial cells (Marchiando et al., 2011). Intestine epithelial cells creates the barrier to separate the gut lumen and internal tissues. Thus, tissue integrity is one of the most important issue for the epithelial cells. On the other hand, the intestine cells undergo shedding, which could be caused by both apoptosis and pathological processes like inflammation. The shed cells are extruded apically

from the intestine epithelial cell plane. Study with live imaging on high-dose TNF induced apoptosis in mice intestine revealed the redistribution of tight junction from apical to lateral after the induction of apoptosis (Marchiando et al., 2011), which confirmed the conclusion of early study (Madara, 1990). This tight junction remodelling during apoptosis maintains the tissue integrity in intestine.

In *Drosophila*, study showed that in embryo stage, the turn-over rates for the septate junction molecules are very slow, which indicates the low dynamic activity for septate junction in *Drosophila* (Oshima and Fehon, 2011). Besides, septate junction has been shown to be important to maintain the blood brain barrier, and also essential for immune barrier in the gut in *Drosophila* (Bonnay et al., 2013; Carlson et al., 2000). However, how septate junction is remodelled during apoptosis is very rarely studied.

1.2.3 Mechanical force generation for apoptotic cell extrusion

During the process of apoptosis in epithelial cells, the cell will constrict its apical surface and be extruded from the original cell plane. Pioneer study on cultured cells from J. Rosenblatt showed the stereotypical events of apoptotic extrusion: Apoptotic cell signals its neighbour. In response to the death signal, the healthy neighboring cells start to form the actomyosin ring surrounding the apoptotic cell in the supra-cellular way. On the other hand, the actomyosin ring also forms inside the apoptotic cell. Constriction of the both actomyosin rings extrude the cell from the plane (Rosenblatt et al., 2001). This serial of dynamic events indicates the dynamic nature of apoptotic extrusion. On the other hand, the involvement of actomyosin rings indicates the potential generation of

mechanical forces. In further, while the apoptosis is the programmed cell death of a specific cell, the apoptotic extrusion involves at least a patch of cells: 1.the apoptotic cell itself, which generates the intrinsic force during the process; 2. the direct neighboring cells which contribute to the neighboring actomyosin ring formation, and generate the extrinsic force. Potentially, the non-direct contacting cells could also be affected through the propagation of force by AJ. Indeed, the very recent study has shown the E-cadherin is essential for the elongation of neighboring cells and the apoptotic extrusion (Lubkov and Bar-Sagi, 2014).

1.2.4 Apoptotic force and its contribution for tissue morphogenesis

While the in vitro studies have shown that apoptosis could generate the mechanical force (Rosenblatt et al., 2001), which is called apoptotic force here, it has also been demonstrated that the apoptotic force could help the development process (Toyama et al., 2008). In the developmental process called dorsal closure during *Drosophila* embryogenesis, the transient tissue amnioserosa is restricted in the eye shape region surrounded by the lateral epidermis. All of the amnioserosa cells will delaminate during dorsal closure, and in the end, the lateral epidermis from dorsal and ventral part will meet in the midline. During the process where amnioserosa cells are delaminated, around 10% of the cells undergo apoptosis. The tissue specific expression of p35 inside the amnioserosa cells, which blocks the activity of caspase-3, resulted in the delay of dorsal closure process. On the other hand, the induction of more apoptotic events by specific overexpression of grim inside amnioserosa cells resulted in the accelerated process of dorsal closure. The results indicated

the correlation of apoptosis number and speed of dorsal closure, which means that apoptosis is important for precise control of developmental timing (Toyama et al., 2008). To further prove the mechanical role of apoptosis, the authors conducted the mechanical jump experiment by laser ablation. After ablation, the epidermal tissue will recoil. The initial recoil rate is proportional to the tension inside the tissue right before ablation. The results showed that the tension inside the tissue increases when more apoptosis events happen inside the amnioserosa cells, while on the other hand, tension inside the tissue decreases when the apoptosis of amnioserosa cell is blocked. Taking these results together, the study demonstrated the apoptotic force generation during development, and its contribution to development (Toyama et al., 2008).

1.3 Research objectives and model system

While apoptotic force have been demonstrated to contribute to development during dorsal closure (Toyama et al., 2008), there are many unsolved questions:

1. Whether the mechanical role of apoptosis globally exists during tissue dynamic process or it is just unique in dorsal closure?

2. Whether the apoptotic force could globally affect the tissue or it has just the local effects in the supra-cellular level?

3. How the cell-cell junctions remodelling and mechanical force generation are coupled during apoptosis in vivo?

With these questions, I took *Drosophila* adult abdomen epithelia development during *Drosophila* metamorphosis, known as histoblast expansion, as a model system to reveal in more details the mechanical role of apoptosis in vivo.

1.3.1 *Drosophila* as a model system and the life cycle

Drosophila melanogaster, known as fruit fly, is a model organism with the longest history, which has been used for more than a century (Rubin and Lewis, 2000). *Drosophila* has many advantages as model system: easy to raise, lay many eggs, short life cycle, and simple genetics. After such a long time of developing, the field has developed really powerful genetic tools and accumulated many resources, which make *Drosophila* from a good model system to the great model system (Rubin and Lewis, 2000). While it has been a long history for taking *Drosophila* as a model for genetics and genomics studies, the developing processes have also been chosen to study tissue dynamics, like cellularization, germ band extension, mesoderm invagination, dorsal closure, and so on (Bertet et al., 2004; Jacinto et al., 2002; Mazumdar and Mazumdar, 2002; Oda and Tsukita, 2001).

In 25 degree incubator, after the eggs are laid by the adults, it takes less than a day for the embryogenesis. Then the larva will hatch and crawl out from the egg. It takes one day for the 1st instar larva stage. After that, the larva molts and becomes 2nd instar larva. With another day for 2nd instar stage, the larva molts again and becomes 3rd instar larva. Then the larva will stay in the food eating for one day. After that, it will crawl out from the food and will start wandering on the food vial wall. This is the start of mid-3rd instar. After another one day as mid-3rd instar wandering larva, it will find a dry place, stop moving and form a pupa. After 4 days of development in the pupa stage, it will in the end eclose, and become an adult fly (Fig. 1.1). In total, it takes around 9 to 10 days for flies to develop from embryos till adults through the larval and pupal stages (Greenspan, 2004).

The process when larva develops into adult through the pupa stage, is called *Drosophila* metamorphosis. During metamorphosis, dramatic changes will take place in the larva when most of the larval organs will be reabsorbed, and the organs for the adults will develop (Greenspan, 2004). While embryogenesis contains great resources for developmental study, many of the developmental processes during metamorphosis have also attracted the interests and been extensively studied, like neuron degeneration and regeneration, development of imaginal discs into adult organs, and so on (Held et al., 2005; Yu and Schuldiner, 2014).

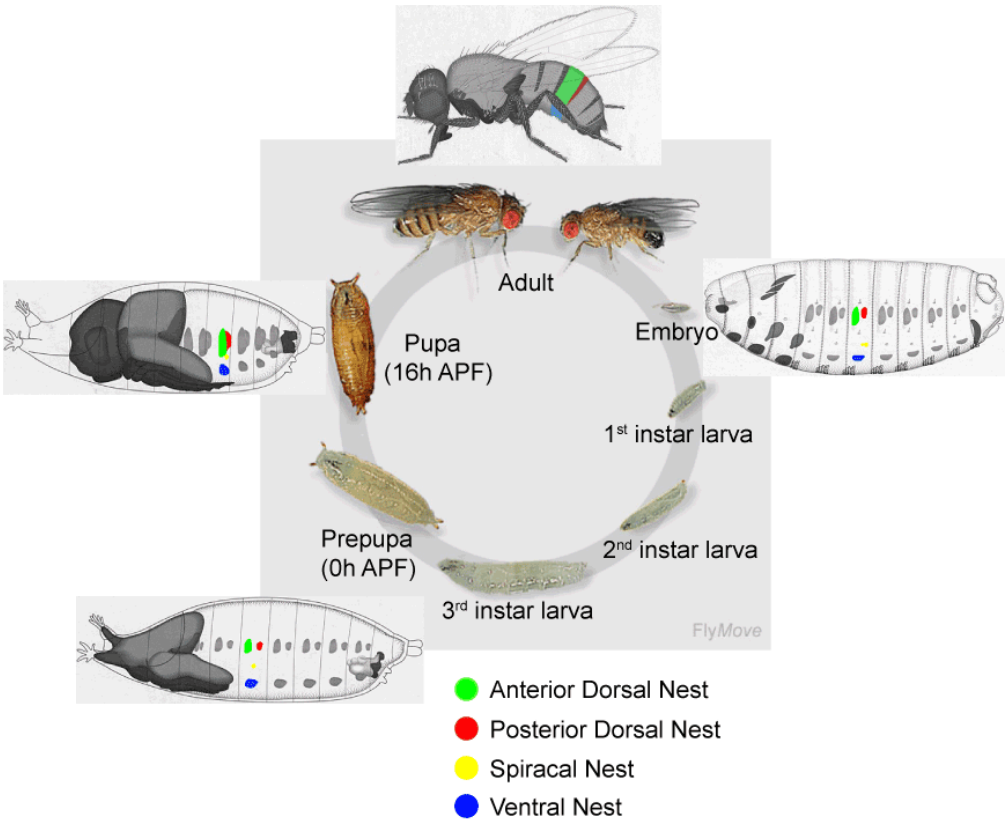

Figure 1.1 Life cycle of *Drosophila* and the development of histoblast
Schematic showing of the development process of histoblast through the life cycle of *Drosophila*. Histoblasts consist of four nests: anterior dorsal nests (green color), posterior dorsal nests (red color), spiracle nests (yellow color), and ventral nests (blue color). The four nests start to emerge from the embryo stage, when they are separate and do not proliferate (right balloon). They stay static throughout the larva stages. Until the prepupa stage, the histoblasts start to proliferate. At the beginning of pupa stage, the histoblasts only proliferate without migration, and the tissue size do not increase much (bottom-left balloon). Around 16 hour APF, the histoblasts start to migrate and invade the LECs (mid-left balloon). The nests fuse each other with the growing of histoblasts. In the end, the histoblasts will take over the whole pupal epidermis, and develop into the adult epidermis (upper balloon). (Life cycle modified from FlyMove:
http://flymove.uni-muenster.de/Genetics/Flies/LifeCycle/ LifeCycleGes.html)

1.3.2 Histoblast expansion during metamorphosis

Histoblasts are the precursors of adult abdominal epithelial cells (Madhavan and Madhavan, 1980). They start to emerge during the embryo stage. In each segment, the histoblasts form four nests among the epidermal cells: anterior dorsal nest, posterior dorsal nest, ventral nest and spiracle nest (Madhavan and Madhavan, 1980). During the embryo stage and the whole larva stages, the histoblasts are arrested in cycle G2. They only grow in their cell volume in about 60 fold, but do not divide or migrate. Until the pre-pupa stage, when the wandering lava just stops moving and starts to harden its cuticle to form the pupa case (it is defined as 0h After Puparium Formation (APF)), the histoblasts start to actively dividing, which requires string expression and Ecdysone signalling (Ninov et al., 2007; Ninov et al., 2009). The active cell division lasts until 15h APF. During this period, the histoblasts undergo the cell division with much reduced G1 phase (Ninov et al., 2007). As a result, the histoblast nests remain their original dimension while fast dividing, that is, the nests do not expand while the cell number increases, and the offspring cells have smaller apical surface compared to the mother cells (Ninov et al., 2007). From 15h APF onwards, the histoblasts slow down their dividing speed. Simultaneously, the histoblasts start to migrate and intercalate in between the surrounding Larval Epidermal Cells (LECs). The existing LECs will undergo apoptosis, which is also Ecdysone signalling dependent (Fig. 1.2 & Movie 1) (Ninov et al., 2007). While all of the LECs will undergo apoptosis and delaminate from the epithelial cell planes during histoblast expansion, around 85% of them undergo apoptosis at the tissue interface between histoblasts and LECs (Nakajima et al., 2011). At around 18h APF, the anterior dorsal nests and posterior dorsal nests sitting in

the same segment will start to fuse with each other. In the end, not just the histoblast nests in the same segment will be fused, the histoblasts from different segments will also be fused and develop into the adult epidermis (Fig. 1.2 & Movie 1) (Ninov et al., 2007).

The apoptosis of LECs and the proliferation and migration of histoblasts occurs simultaneously during the dynamic process of histoblast expansion. Coordination of the two events result in the epithelial replacement and histoblast expansion. While the majority of LEC apoptosis happens at the tissue interface, it is straightforward to think of the potential cross talk between the two types of cells. In fact, the Ecdysone signalling has been proved to be essential for both the proliferation of histoblasts and the apoptosis of LECs (Ninov et al., 2007). In further, the study showed that the block of proliferation in histoblasts leads to the ceasing of apoptosis in LECs. More detailed study revealed that the cell cycle progression from S phase to G2/M phase in the boundary histoblasts is the prerequisite for the apoptosis in LECs (Nakajima et al., 2011). On the other hand, study also showed that the blocking of apoptosis in LECs by specific expression of p35 lead to the severe delay of histoblast expansion, which in the end results in the scar on the dorsal abdominal epithelia of *Drosophila* (Ninov et al., 2007; Ninov et al., 2010). Besides, LECs secrete Dpp signal to the periphery histoblasts to increase their motility by loosening the cell-cell contacts, remodelling the cytoskeleton and modulating the attachment to the substrates. While these studies showed the crosstalk between histoblasts and LECs in signalling level, whether they have the mutual effects mechanically remains elusive.

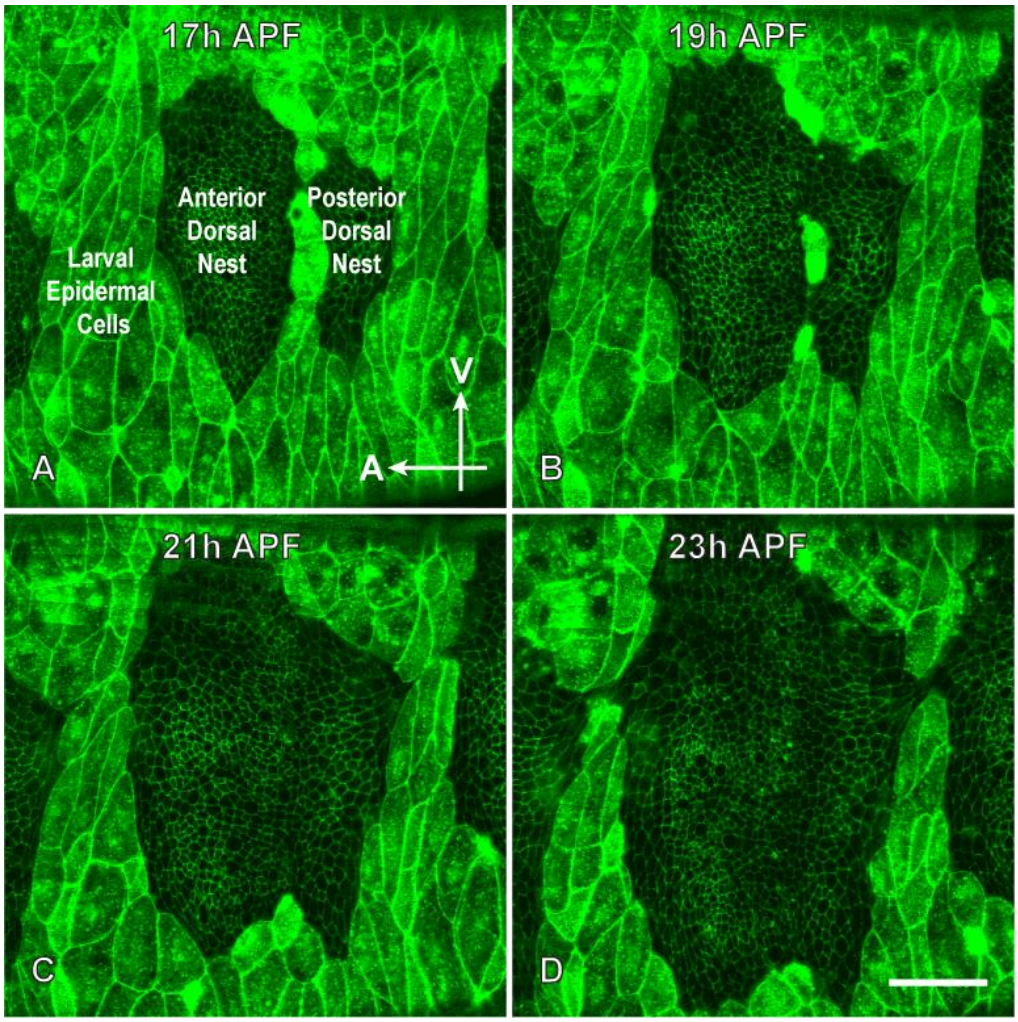

Figure 1.2 Confocal images of histoblast expansion
(A) Confocal image showing the dorsal histoblasts of the third abdominal segment at 17 hour APF. Anterior dorsal nest and posterior dorsal nest are shown in the central darker region. The surrounding bigger cells are LECs. The two nests are separated by LECs. Histoblasts from neighboring segments could be found at the edge of the image. Orientations of AP and DV are showed by the arrows. (B) The same animal at 19 hour APF. The histoblasts increase in the tissue size and the two nests start to fuse with each other. (C) The same animal at 21 hour APF. The two nests finish fusion and increase in tissue size. (D) The same animal at 23 hour APF. The fused dorsal histoblast nest keep growing and taking over the LECs. The histoblasts from different segments start to fuse. Length of scale bar: 50 μm. See Movie 1.

Chapter II: Materials and Methods

2.1 Maintenance of fly strains

2.1.1 Fly maintenance

All fly stocks were maintained at 25 ℃ under normal light dark cycling if not specified. Standard medium was prepared by Medium Preparation Facility (MPF) in Temasek Life Sciences Laboratory (TLL) as normal fly food and used for maintaining the fly stocks. Normal fly food were kept in vials or bottles. Additional brewer's yeast was added to the vials or bottles when used for crossing or fast growing.

Grape juice agar plates were also prepared by MPF in TLL. Yeast paste were freshly made by mixing brewer's yeast and sterile water until they reach the "peanut butter" status. When collecting embryos, additional yeast paste were added on top of the agar plates for higher yield.

2.1.2 Fly strains

Fly stocks used were as following:

Fluorescent protein tagged lines:

Armadillo::YFP [PBac{681.P.FSVS-1}armCPTI001198 w1118] (Kyoto Stock Center, # 115134);

DE-Cadherin::GFP [w[*]; P{Ubi-p63E-shg.GFP}5] (Kyoto Stock Center, #109007);

Endo-DE-Cadherin::GFP (on the second, gift from Yang Hong, University of Pittsburgh);

Endo-DE-Cadherin::mTomato (on the second, gift from Yang Hong, University of Pittsburgh);

Nrg-GFP [Nrg::GFP[G305] (X) (protein trap)] (on the X, gift from Erina Kuranaga, Riken CDB);

sGMCA (on the second, gift from Kiehart, Daniel P., Duke University);

Sqh-Cherry [w; sqh-sqh-cherry [A11] (III)] (on the third, gift from Adam C. Martin);

Sqh-GFP [y[1] w[*] cv[1] sqh[AX3]; P{w[+mC]=sqh-GFP.RLC}C-42] (Bloomington Stock Center, #42235);

UAS-sqh-GFP [w; UAS-sqh-GFP/ CyO] (on the second, gift from Markus Affolter, University of Basel);

UAS-Lifeact-GFP [y[1] w[*]; P{y[+t] w[+mC]=UAS-Lifeact-GFP}VIE-260B]* (Bloomington Stock Center, #35544);

Tsh-Gal4, UAS-SCAT3/CyO (on the second, gift from Masayuki Miura, University of Tokyo);

DE-Cadherin::GFP; sqh-cherry [w; Ubi-DE-Cadherin::GFP shg$^{[R69]}$; sqh-sqh-cherry$^{[M1]}$] (second and third, gift from Adam C. Martin, MIT);

UAS- sqh-GFP, Eip71CD-Gal4 (on the second, this study);

UAS-sqh-GFP; Sqh-sqh-cherry (second and third, this study);

Endo-DE-Cadherin::GFP, Eip71CD-Gal4 (on the second, this study);

Endo-DE-Cadherin::GFP, Esg-Gal4 (on the second, this study);

Gal4 lines:

Esg-Gal4 [y[*] w[*]; P{w[+mW.hs]=GawB}NP5130 / CyO, P{w[-]=UAS-lacZ.UW14}UW14] (Kyoto Stock Center, #104863);

Eip71CD-Gal4 [w[1118]; P{w[+mC]=Eip71CD-GAL4.657}TP1-1] (Bloomington Stock Center, #6871);

Tsh-Gal4/CyO (on the second, gift from Erina Kuranaga, Riken CDB);

FRT and RNAi Lines:

FRT19A [y[1]w[1118] P{ry[+t7.2]=neoFRT}19A] (Kyoto Stock Center, #106482);

FRT19A, mRFP.nls [P{w[+mC]=Ubi-mRFP.nls}1, w[1118], P{ry[+t7.2]=neoFRT}19A] (Bloomington Stock Center, #31416);

FRT19A, Gal80, hsFLP [P{ry[+t7.2]=neoFRT}19A, P{w[+mC]=tubP-GAL80}LL1, P{ry[+t7.2]=hsFLP}1, w[*]] (Kyoto Stock Center, #108063);

UAS-sqh-RNAi (Vienna Drosophila RNAi Center, #7916GD);

MARCM Ready Lines:

I: *neoFRT19A, tubP-Gal80, hsFLP; UAS-sqh-RNAi;* + (X and second, this study)

II: *neoFRT19A, ubi-mRFP.nls; Endo-DE-Cadherin::GFP, Eip71CD-Gal4;* + (X and second, this study)

2.2 Fly genetics

Standard steps were used for basic fly crossing: around 10 virgins and 8 males are picked and kept in the same vial for cross. To combine the genes on different chromosomes, the following balancer flies were used:

L/FM6; If/ CyO* for manipulation of Chromosome X and II;

L/FM6; Sb/ TM3 Ser* for manipulation of Chromosome X and III;

Pin/ CyO; TM3 Sb/ TM6B Hu Tb for manipulation of Chromosome II and III;

2.2.1 Homology Recombination

To combine genes onto the same chromosome, homology recombination was adopted. First of all, virgin females and males of P0 generation were crossed. Second, virgin females of F1 generation were picked and crossed with male single chromosome balancer flies (Sco/ CyO for Chromosome II and TM3/ TM6 for Chromosome III). Homology recombination occurs in the fertilized F1 females. To enhance the rate of recombination, vials were kept in the 29 ℃ incubator. Single male of F2 and 3 to 5 virgin females of single chromosome balancer flies were crossed in each vial. 30 to 100 vials were crossed according to the distance of the two target genes and marked with number. 4 to 5 days after the cross, when the food started to turn wet (due to the crawling of larvae), the single male from each vial was picked out for single fly PCR and the females were discarded.

To do single fly PCR, genomic DNA from each fly was extracted. Primers for target genes were designed and the PCRs were conducted. From the results, one

could tell the successfully recombined fly. The vials which contained the progenies of positive male fly were maintained.

2.2.2 Generation of MARCM clones expressing *Sqh* RNAi in LECs

MARCM (Lee and Luo, 1999) Ready Lines were first generated with the genetic methods described above and kept as a stock. Virgins of MARCM Ready Line II were picked and crossed en masse (around 100) with the corresponding MARCM Ready Line I males (around 50). Eggs were collected using grape juice agar plate with yeast paste in 25 ℃ for 1.5 hours. Eggs were then let to develop in 25 ℃ for 2.5 hours and heat shocked in 37 ℃ water bath for 50 minutes. After that, the eggs were let to develop in 25℃ for 4 days until the mid-3rd instar. Female wondering larvae were picked out and let to develop until the white pupae stage in 25℃. Pupae were then collected and processed as described earlier (Ninov and Martin-Blanco, 2007) with slight modification, and prepared for imaging at 16h APF (described in more details in the next part).

2.3 Image acquisition and processing

2.3.1 Sample preparation and live imaging on confocal microscopy

White pupae (0 hour APF pupae) were collected and washed in 1X PBS solution for 5 mins to wash off the food and to make the pupa case crisper for easier dissection. The additional liquid of the pupae were absorbed with tissue. Then the pupae were then transferred to the fly food vial and let to develop in 25℃ room for 15.5 hours. Pupae at 15.5 hour APF stage were removed from the food

vial. Slide with double-sided sticky tape was prepared. Pupae were then aligned on the slide with ventral side stick to the slide. Pupae case on the anterior dorsal abdominal part were removed (which covers around 4 segments) with needle and forceps. Then the pupae were gently freed from the slide inside 1X PBS solution. In the end, the additional PBS solution on the pupa is absorbed with tissue and the pupa is now ready for imaging.

Before mounting, the coverslip was temporarily placed on the metal coverslip holder. Halocarbon oil was added between the coverslip and the pupa to gain better imaging quality. The prepared pupa was firstly mounted on top of the coverslip on the lateral side. The pupa was then rotated 30 degrees towards the dorsal side to better imaging the histoblast expansion process.

Live images and movies were acquired in Nikon A1R MP confocal microscopy, objective Apo 40X WI λ S DIC N2, N.A 1.25, or Zeiss LSM 510 Meta Inverted confocal microscopy, objective LD C-Apo 40X, N.A 1.1. All imaging was performed in the room temperature. Ventro-lateral region of the third abdominal segment of pupa at 16 hour APF was imaged.

2.3.2 Image processing

Analysis of the mechanical impacts of apoptosis was performed using *DE-cadherin::GFP* pupae. Raw data were processed by maximum intensity z projection. Signals from basal part of cells were removed manually before projection. Cell boundaries were manually drawn in ImageJ. Cell area change and cell width change were measured in ImageJ.

Analysis of caspase-3 activity was performed separately for *Endo*-DE-cadherin::mTomato and SCAT3 (Nakajima et al., 2011; Takemoto et al., 2003). Maximum intensity z projection was conducted, boundary was manually drawn and cell area was measured in ImageJ for *Endo*-DE-cadherin::mTomato. For analysis of caspase-3 activity, sum slices projection covering apical to basal for both ECFP channel and Venus channel was conducted. Then the FRET ratio was calculated by the ratio of intensity, that is I_{Venus}/ I_{ECFP}. For individual cell, the cell boundary in SCAT3 channel was based on the signal from maximum intensity z projection of Venus channel. FRET ratio for individual cell was then measured by ImageJ with drawn ROIs.

Analysis of tissue specific myosin ring intensity was performed by sum slices of the apical signals from tissue specifically expressing sqh-GFP. The intensity was measured by free hand line tools in ImageJ. Lines were modified by fit-spline to fit the shape of cell boundaries. Width of measurement ROIs was set at 2 pixels for all the data (1 pixel = 0.24 μm). Ubiquitously expressing sqh-cherry channel was maximum intensity projected for only the apical planes after removing the basal signals.

2.3.3 Nanoablation

Laser nanoablation was performed using a TCS SP5 multi-photon confocal microscope (Leica), and a 63×/1.4-0.6 HCX PL Apo objective. Ablation was carried out at the AJ plane with a multi-photon laser-type Mai-Tai HP from Spectra Physics set to 800 nm, with a laser power of 40% out of 2.8w maximum output, gain of 80% and offset of 61%.

2.4 Quantitative data analysis

2.4.1 Phase transition

Analysis of phase transition was conducted in Matlab 2010a (MathWorks, MA) in several steps with algorithms produced in laboratory. The exactly same algorithm was adopted for each calculation of transition points.

Raw data processing

1. Data points truncation. Our algorithm was designed to calculate the transition points of the curvature, based on the slope of the interpolated curvature. Thus, the zero points had to be truncated to eliminate their effects on the curvature slope. For analysis of apical area, first zero points were considered as the last effective points, and all the later zero points were discarded. For analysis of FRET ratio, the lowest points were considered as the last effective oints, and all the later points were discarded. For analysis of myosin II intensity, the highest points were considered as the last effective points.

2. Linear interpolation. Zero-point-truncated data points (5 minutes interval between each point) were then linear interpolated into 1 minute interval.

3. Data smoothing. Simple moving average of 16 interpolated points (15 minutes) were then adopted to smooth the data.

Defining the phase transition point

Processed data were then used to calculate the velocity (absolute value) by every two points. To define the transition point, first of all, we defined the transition velocity. We used different ratio of the maximum transition velocity to test the transition lag between two curves. On the other hand, we used another method

as a reference: we shift the curvature of area to the left so that difference of integration between the two curvatures would be the minimum. Using this method, we calculated the transition lags as reference results (Fig. 2.1 A&B). After that, we found the transition lag results calculated with the ratio around 0.25 best matched the reference result (Fig. 2.1 C). So, one quarter (0.25) of the maximum velocity were then defined as the transition velocity. If the left neighboring point had smaller velocity than the transition velocity while the right neighboring point had larger velocity, then these points were defined as candidate transition points. The rightmost candidate transition points before the point of max velocity of every curvature were finally defined as the transition points.

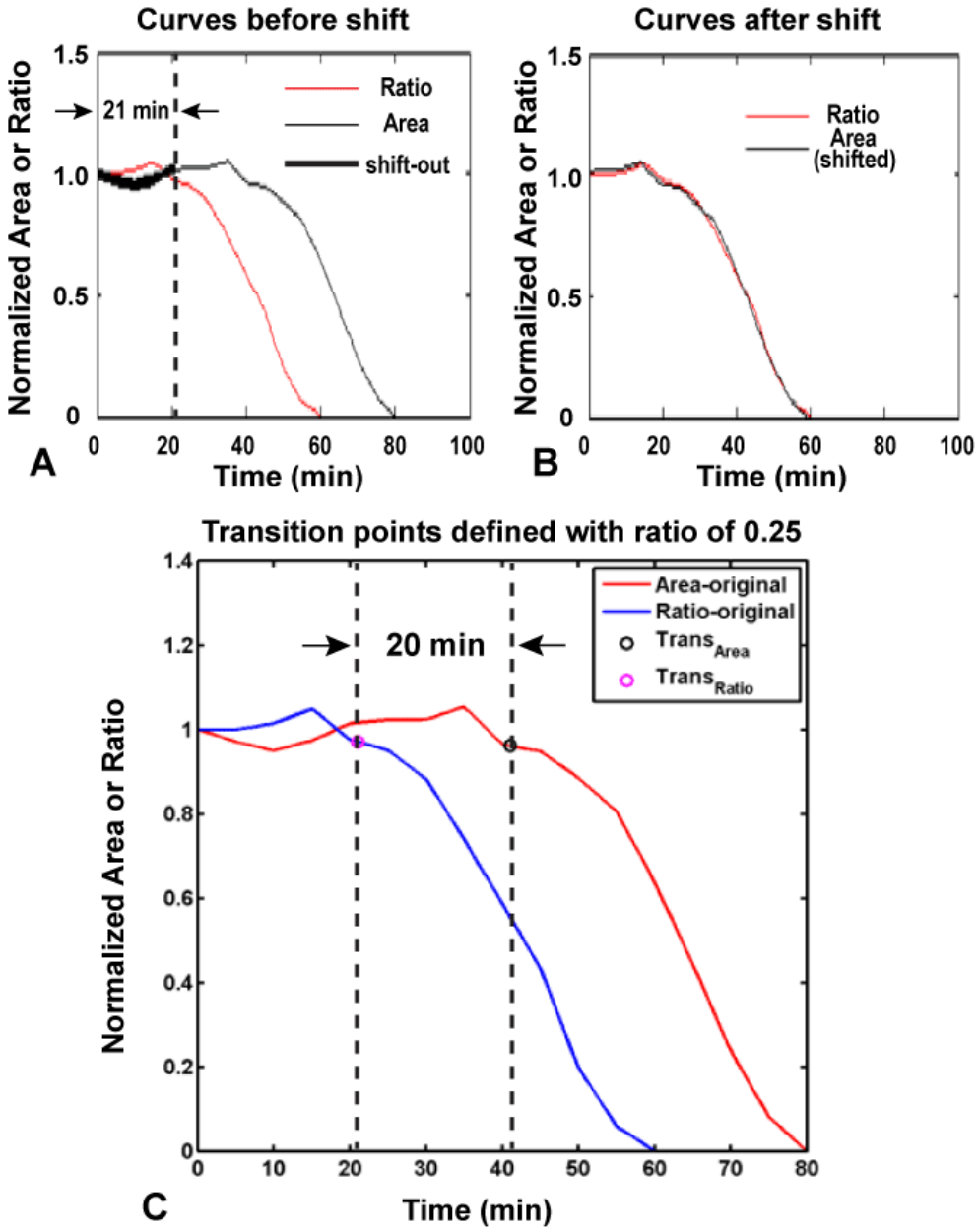

Figure 2.1 Phase transition points defining

(A) Ratio and area dynamics over time of a typical apoptotic LEC before shift. The ratio curve is in red and the area curve is in black. Double arrows and dashed line indicates the length of shift to get the minimized integration difference of the two curves is 21 minutes. The shift-out part of the area curve is highlighted with bold. (B) Curvatures with the same cell after shift. (C) Results of the transition point calculation with the ratio of 0.25. Curve of ratio is in blue and area is in red. The transition points are highlighted with magenta and black circles, respectively. The lag of the two transition points is indicated with dashed lines and two arrows. The lag is 20 minutes.

2.4.2 Apoptosis patch analysis

Ubi-DE-cadherin::GFP time lapse movie was segmented with Packing Analyzer V2.0 (Benoit Aigouy, MPI-CBG). Errors were manually corrected. Segmented images were then analysed in Matlab 2010a with image processing toolbox (MathWorks, MA). A patch of histoblast cells that located within 150 pixel (75 μm) from the edge of apoptotic LEC was selected as an apoptosis patch (for proliferating cells, only one of the offspring cell was selected and analysed). Each cell within the patch was analysed with fit-ellipse (Fig. 2.2 A). The results of fitted histoblasts were drawn to evaluate the analysis. Each cell was overlapped with the fitted ellipse with red dotted line, and the centroid of each cell was marked with blue asterisk (Fig. 2.2 B). The aspect ratio of each histoblasts within the patch was further calculated with the results of minor axis length and major axis length from fit-ellipse. Then the aspect ratio of each histoblast cell was color-coded as the overlap of the tissue (Fig. 2.2 B) to show the tissue level histoblast cell elongation during apoptosis.

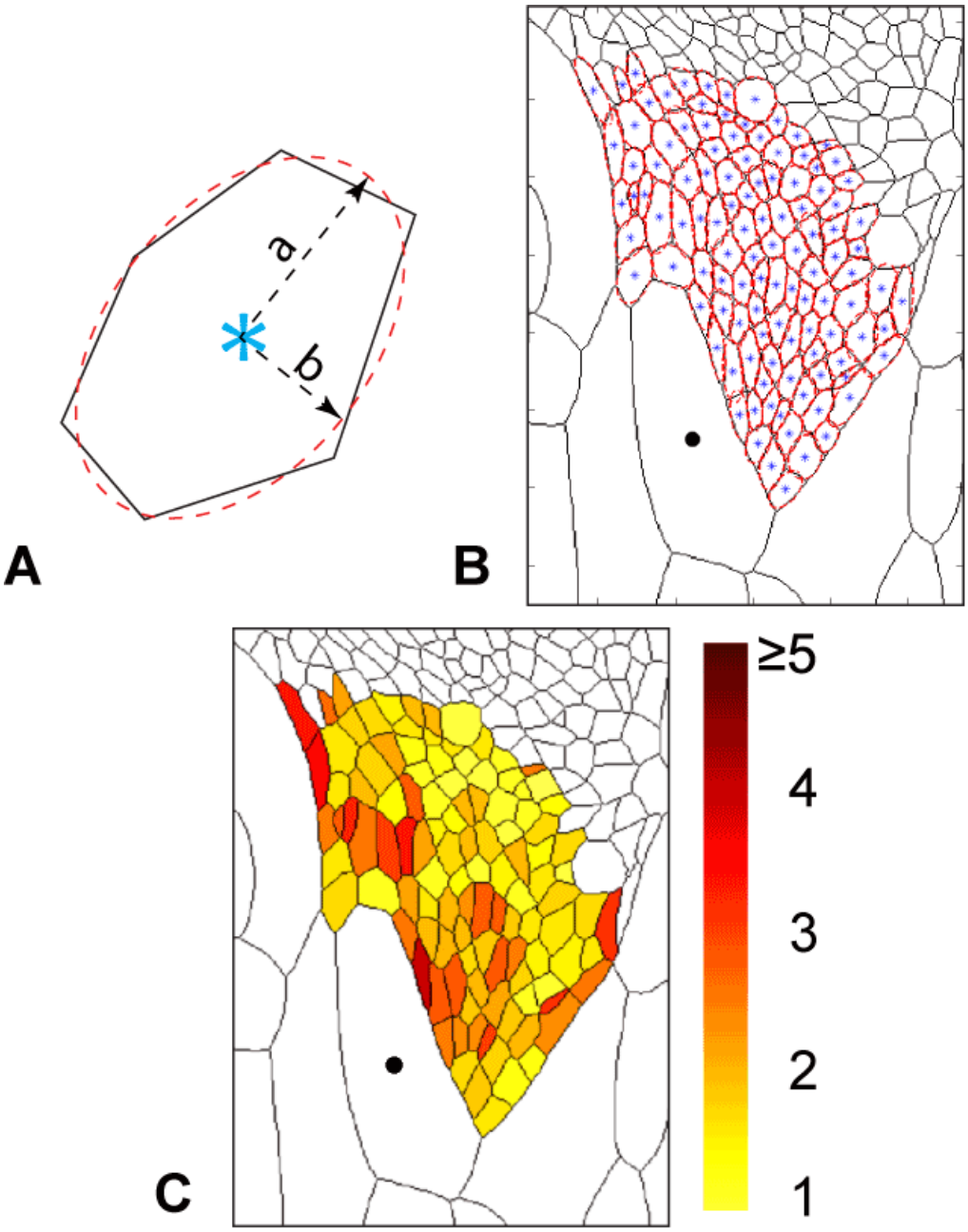

Figure 2.2 Analysis of tissue level cell elongation within apoptosis patch
(A) Illustration showing the analysis of aspect ratio of one cell. The cell shape (black line) was fitted with ellipse (red dashed line). The centroid was marked with blue asteroid. Half long axis "a" and half short axis "b" were indicated with dashed arrows. Aspect ratio was further calculated by a/b. (B) Apoptosis patch selection. The histoblasts within the patch (within 150 pixel (75 μm) from the edge of apoptotic LEC) were analysed, and the fitted ellipses of every histoblasts were drawn in red and overlapped with the segmented image. Centroid of apoptotic LEC was marked with dark circle. (C) Aspect ratios of each histoblasts within the patch were color-coded and overlapped with segmented image. Centroid of apoptotic LEC was marked with dark circle. Darker colour indicates higher aspect ratio, while light yellow indicate low aspect ratio.

2.4.3 Calculation of initial recoil velocity after ablation

To quantify the tissue tension in different stages of apoptosis, we performed calculted the initial recoil velocities for each ablation. To quantify the recoil velocity, the lengths of the ablated boundary from each frame of the movie were first measured in ImageJ using the straight line tool. Then the lengths of the ablated boundary before ablation were linear fitted, and the lengths after ablation (before reaching the plateau phase) were fitted with exponential curve in Matlab. In the end, the intersection point of the two curves was found and the initial recoil velocity was calculated in Matlab. However, for the boundaries ablated upon AJ disengagement, the recoil after ablation was in general very subtle, and the exponential fitting was not suitable for these curves. To quantify these subtle recoil curves, we calculated the lengths change in 15 seconds and defined as initial recoil velocity.

2.4.4 Calculation of linearity

To quantify the straightness of boundries during different phases, we calculated the linearity of each boundary at the frame right before ablation. Linearity was defined as Distance/ Length, where the Distance was the distance between the two vertices of the boundary and the Length was the real length of the boundaries. Distance was calculated using Staight Line tool in ImageJ, and the Length was calculated with the Segmented Line tool in ImageJ.

2.4.5 Statistical analysis

All the statistical analyses were conducted with Excel 2007, Microsoft Office. All the error bars shown in the figures are SEM. Mean values were compared using two-tailed Student's t-test between two groups.

Chapter III: Results

3.1 Mechanical contribution of apoptosis in tissue replacement

Pioneered study has demonstrated that during the development process named dorsal closure during *Drosophila* embryogenesis, the apoptosis events happened in the transient tissue amnioserosa promotes the closure event (Toyama et al., 2008). Subsequently, the mechanical role of apoptosis has been predicted to exist in other developmental systems like neural tube closure, palatal fusion and histoblast expansion during *Drosophila* metamorphosis (Teng and Toyama, 2011). Recent study have also suggested the mechanical force generated during apical constriction could promote the new bud formation during monopodial branching of the embryonic chicken lung (Kim et al., 2013). In most cases, apoptosis events initiate inside the homogeneous tissue with the neighbors of the same type and similar size. How the apoptotic cell is extruded at the tissue interface is not well studied. More particularly, whether and how the mechanical force could be generated for the apoptosis at tissue interface remains unilluminated.

Here I took development of *Drosophila* adult abdomen, or called histoblast expansion as a model system to investigate the mechanical role of apoptosis. During histoblast expansion, all the LECs will undergo apoptosis in the end. There are two types of LEC apoptosis if we categorize with the location. The majority (around 85% of the total apoptosis) of the apoptosis events happens at the tissue interface between the LEC sheet and histoblasts (Nakajima et al., 2011; Ninov et al., 2007), which I called “boundary apoptosis” (Fig. 3.1A & Movie 2), while the rest of them take place inside the LEC sheet, which I called “non-boundary apoptosis” (Fig. 3.3A & Movie 4). Whether the boundary apoptosis

could mechanically promote the tissue replacement in histoblast expansion or not is the major focus.

3.1.1 Apical constriction of apoptotic LEC

The first step is to understand the behavior of the boundary apoptosis during histoblast expansion. The constriction rate is higher in the late stage of apoptosis (Fig. 3.1A 50 & 75 min & Movie 2) compared to the early stage (Fig. 3.1A 0 & 25 min & Movie 2) according to the time-lapse movie. Quantitative analysis of the cell area of the apoptotic cell confirms the behavior (Fig. 3.1B). In further, the apical constriction process of the apoptotic LECs could be divided into two phases according to their constricting speed (Fig. 3.1B) with the developed phase transition algorithm (Chapter II 2.4.1). The cell constricts slower in Slow Phase and the apical area dramatically decreases in Fast Phase till the end of apical constriction (Fig. 3.1B). More interestingly, when I analysed the cell shape change of the apoptotic cell, I found the distinct difference of the constriction in two phases (Fig. 3.1C & D). In Slow Phase, the boundary apoptotic LEC deforms in a local manner, that is, the LEC deforms in the direction of migrating histoblasts (arrow in Fig. 3.1C), while the boundaries shared with neighboring LECs remain almost static (arrowheads in Fig. 3.1C). In Fast Phase, the LEC deforms in a self-similar way, that is, the LEC constricts in all direction and in a more even way, and the shapes of apoptotic LEC in later time points resemble its shapes in earlier points in Fast Phase (Fig. 3.1D).

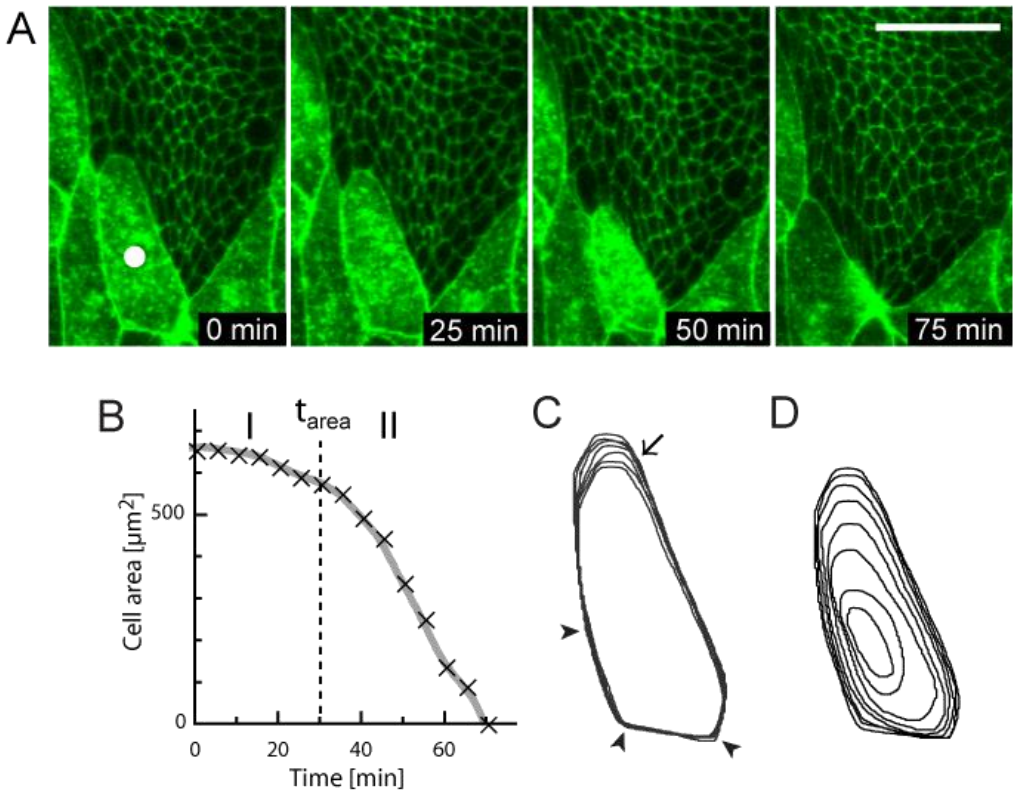

Figure 3.1 Bi-phase apical constriction of the apoptotic LEC
(A) Time lapse image showing the apical constriction of apoptotic LEC at the boundary interface between histoblasts and LECs using *Ubi*-DE-cad::GFP fly (See Movie 2). The cell of interest is marked with white circle. Length of scale bar: 30 µm. (B) Dynamic of apical surface area of the apoptotic LEC over time. The dashed line indicates the point of phase transition. It separates the curve into two different phases. (C-D) Contour plots showing the shape change of the apoptotic LEC in Slow Phase (C) and Fast Phase (D). Arrowheads in (C) indicate the static boundary of apoptotic LEC in Slow Phase, and the arrow indicate the deforming boundary of apoptotic LEC, which is contacted with migrating histoblasts.

3.1.2 Neighboring cell shape deformation upon apoptosis of boundary LECs

Previous study has shown that the histoblast expansion process will be severely delayed and a big scar will be left in the adult abdominal epidermis if the apoptosis in LEC is specifically blocked by the caspase-3 inhibitor p35 (Ninov et al., 2007). However, the mechanical role of LEC apoptosis is not well studied. To evaluate the effects of apoptosis to the neighboring histoblast cells, I first analysed the directly adjacent histoblast cells, which we called first row cells. The histoblast cells next to the adjacent histoblast cells, that are one cell away from the LECs, are called second row cells. Similarly, we defined third row cells, fourth row cells, etc. One example was shown here. Three histoblast cells belong to first row, second row and third row, respectively (yellow, white and magenta cells in Fig. 3.2A) are deformed as the apoptotic cell progress in the apical constriction. It is apparent that the first row cell is significantly elongated towards the adjacent apoptotic LEC. Besides, the second row cell is also elongated while the third row cell is slightly elongated. Then I tracked the position of the middle point of each boundaries connecting the cells (illustrated in Fig. 3.2B & C). The results showed that in Fast Phase, with the fast apical constriction of the apoptotic LEC, the first row cell is elongated dramatically (green double-head arrow in Fig. 3.2D), the second row cell is also elongated (blue double-head arrow in Fig. 3.2D), and the third row cell is slightly elongated (red double-head arrow in Fig. 3.2D), which coincide with the observation (Fig. 3.2A). Thus, the mechanical force generated during the apoptosis at tissue interface could pull the neighboring histoblast cells. Besides, the force could propagate through the tissue, and affect the non-adjacent

histoblast cells. To better understand the tissue level effects of boundary apoptosis, I conducted the tissue level cell shape analysis inside the histoblasts. I selected the histoblasts that are within 75 μm distance to the LEC boundary to form a region of interest (ROI). Inside the ROI, around 5- 10 rows of histoblasts are selected (Fig. 3.2E). I used different colors to indicate the aspect ratio of the cells inside ROI. Cells with higher aspect ratio are colored with darker color. For cells with aspect ratio larger than 5, they are all coded with dark red color (described in detail in Chapter II 2.4.2). The histoblast cells do not change much in the aspect ratio during Slow Phase of LEC apoptosis (Fig. 3.2E 25 min & Movie 3) while the aspect ratio of the cells continuously increased in Fast Phase (Fig. 3.2E 50 & 75 min & Movie 3). In particular, the histoblasts in the region along the long axis of LEC (indicated with ellipse in Fig. 3.2E 75 min) are more significantly increased in the aspect ratio while the histoblasts in other regions do not increase in aspect ratio significantly (Fig. 3.2E 75 min & Movie 3). The results indicate the mechanical effects of apoptosis are not restricted to one or two cells, but are in the tissue level.

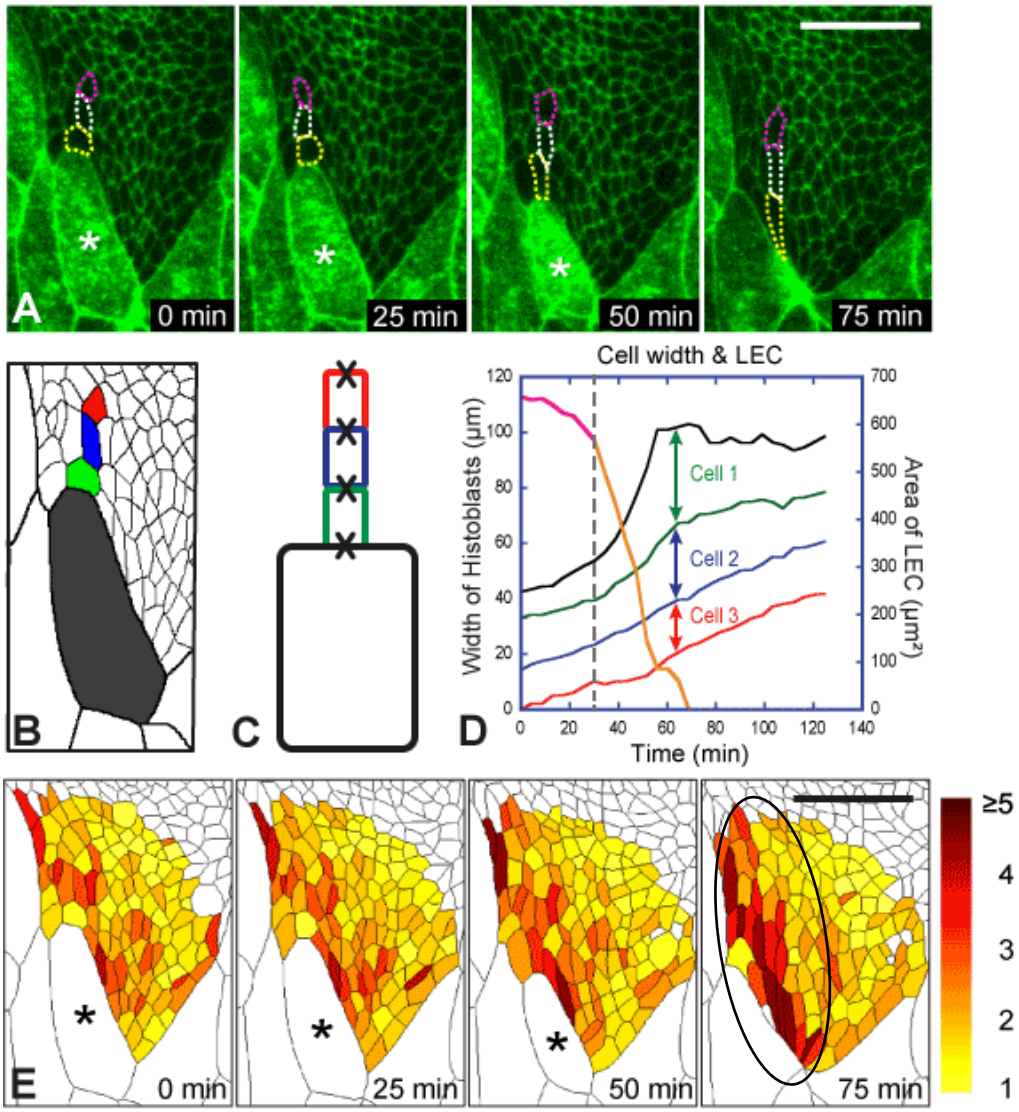

Figure 3.2 Mechanical effects of apoptosis at tissue interface

(A) Time lapse images showing the apoptotic LEC at tissue boundary (marked with asteroid) using *Ubi*-DEcad::GFP fly. Three neighboring histoblasts in a row are depicted with dashed lines. The three histoblasts are elongated during the apical constriction of the apoptotic LEC. Length of scale bar: 30 μm. (B-C) Schematic illustration of the positions of four cells. Apoptotic LEC is coloured in black, and three histoblasts in a row is coloured in green, blue and red, respectively. Black crosses indicate the midpoints of the adjacent boundaries of connecting cells (C). (D) Position changes over time of the 4 midpoints in (C) are shown in left Y-axis. The space between every two lines (indicated by double-head arrows) represent the width of the three histoblasts. Area of the apoptotic LEC is shown in right Y-axis. Two phases are separated by the dashed line. (E) Color maps showing the aspect ratio of every histoblasts within apoptotic patch. Darker color indicates higher aspect ratio of the cell. Ellipse was added for the last frame to indicate the region with elongated histoblasts after apoptosis. Length of scale bar: 30 μm. See Movie 3.

3.1.3 Neighboring cell shape deformation upon apoptosis of non-boundary LECs

Then I analysed the effects of non-boundary LEC apoptosis. As the non-boundary LEC undergoes apoptosis, its LEC neighbors are deformed accordingly (Fig. 3.3A & Movie 4). More specifically, the LEC neighbour which is not connected to histoblasts (white donut in Fig. 3.3A) are pulled and increased in its apical area as the apoptotic LEC constricts in the apical area (Fig. 3.3C). Then I drew the contour plots of this neighbour LEC. From the contour plots, I found that the LEC neighbour deforms very locally, that is, only the boundary connecting the apoptotic LEC is significantly deformed while the other boundaries stay much less deformed or even static (Fig. 3.3D). This results indicate the effects of the non-boundary LEC apoptosis are local and restricted inside the LECs.

To investigate the tissue level effects of the non-boundary LEC apoptosis, I conducted the tissue level aspect ratio analysis with the same method described above. During the whole process of the apoptosis, the global aspect ratio of the histoblasts do not significantly changed (Fig. 3.3B). The results confirm that the effects of the non-boundary LEC apoptosis are local. Taken the results together, the non-boundary LEC apoptosis may not mechanically contribute to the histoblast expansion much.

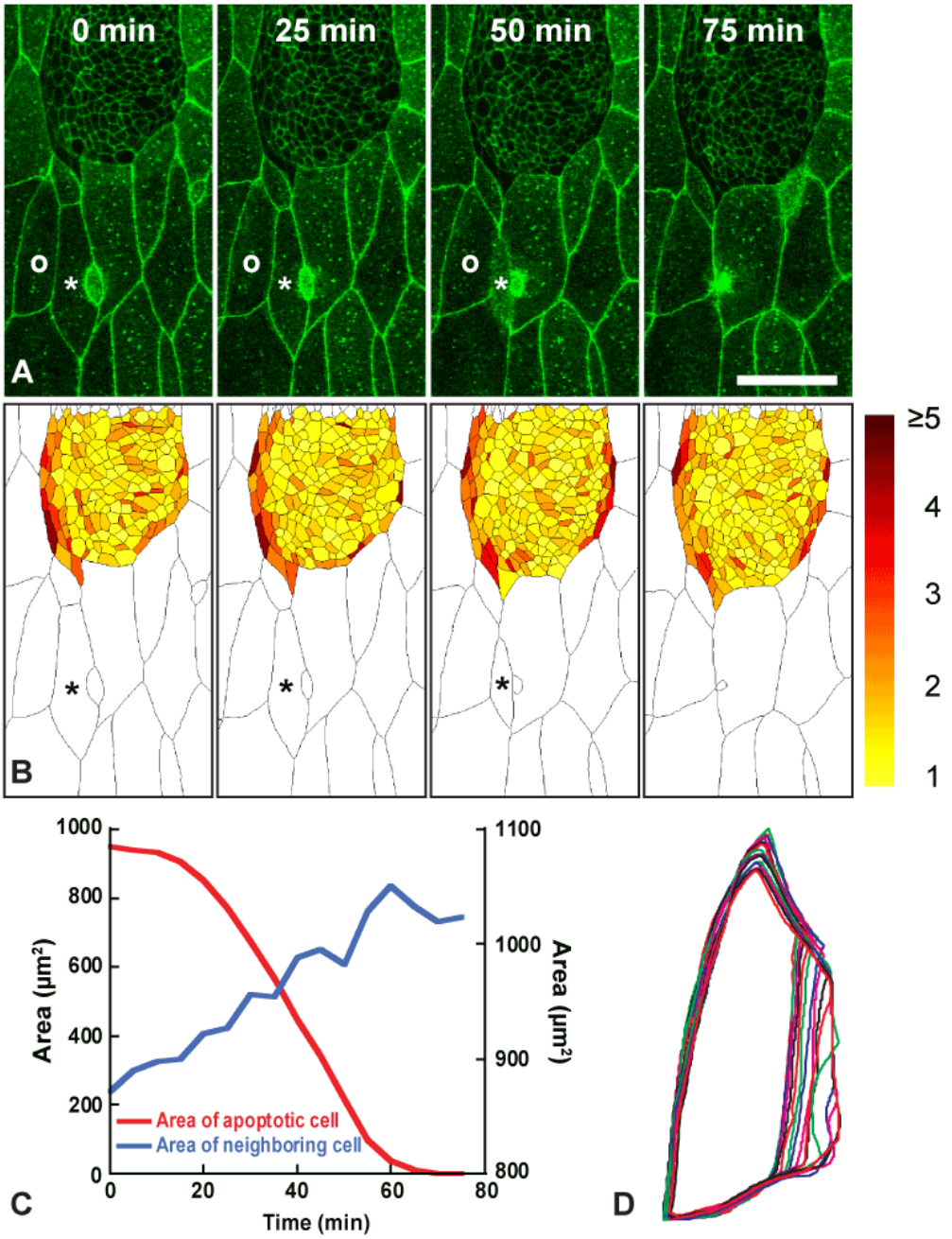

Figure 3.3 Mechanical effects of apoptosis within LECs

(A) Time lapse images showing the apoptotic LEC inside LECs (marked with asteroid) using *Ubi*-DE-cad::GFP. One of its neighbor is marked with circle. Length of scale bar: 40 μm. See Movie 4. (B) Color maps showing the aspect ratios of all the histoblasts within the image. Darker region indicates higher aspect ratio and longer cell shape. The apoptotic LEC is marked with asteroid. There is no obvious elongation of the histoblasts after apoptosis. (C) Area changes over time of the apoptotic LEC (red curve, left Y-axis) and one of its neighbour (blue curve, right Y-axis). (D) Contour plots showing the shape change of the neighboring LEC marked with circle in (A).

3.2 Apical constriction of apoptotic LECs and caspase activation

Extrusion is widely adopted by organisms to expel the unwanted cells or translocate specific cells. Besides apoptotic extrusion, live cell extrusion also occurs during cell competition and EMT (Eisenhoffer and Rosenblatt, 2013). While the extrusion during LEC apoptosis has been demonstrated to be the actomyosin ring based (Ninov et al., 2007), whether the extrusion is apoptosis-driven, or in the other case, the LECs undergo apoptosis after the extrusion is not known yet. To verify whether the extrusion is an apoptotic driven extrusion, I used SCAT3, the FRET based caspase-3 activity sensor, to monitor the caspase-3 activity inside the apoptotic LEC (Nakajima et al., 2011; Takemoto et al., 2003). Caspase-3, or DrIce in *Drosophila*, is the executive caspase (Kuranaga, 2012). Once caspase-3 is activated, the whole apoptosis signalling pathway enters the executive period (Kurokawa and Kornbluth, 2009). Thus, if caspase-3 inside the apoptotic LEC is activated before the Fast Phase of apical constriction, we could conclude that the extrusion is apoptosis-driven extrusion. Simultaneously, I imaged the cell deformation by *Endo*-DE-cadherin::mTomato to monitor the cell deformation. As the apoptotic process progresses, the mVenus signal attenuates while the ECFP signal increased (Fig. 3.4B & C & Movie 5). It indicates the attenuation of FRET ratio, which is confirmed by the FRET ratio calculation (Fig. 3.4A & Movie 5, brighter pseudo-color indicates lower FRET ratio, as shown in the color bar). It in further indicates the increase of caspase-3 activity as the apoptosis progresses. More specifically, while the caspase-3 activity significantly increases from 30 min to 60 min (Fig. 3.4A 30 & 60 min & Movie 5), the apical area of the apoptotic LEC seems not decreased much (Fig. 3.4D 30 & 60 min & Movie 5). The

quantified results confirmed the observation (Fig. 3.4D) that activation of caspase-3 precedes the phase transition of the apical constriction. In fact, the FRET ratio dynamics follow the similar behavior as the apical area dynamics, that is, there is a slow decreasing phase and fast decreasing phase, regardless of the final increasing period (dotted curve in Fig. 3.4D). To better quantify the process, I took the same algorithm (Chapter II 2.4.1) to separate the ratio dynamics into two phases, and applied to all the data. On average, the phase transition, or the activation of caspase-3 activity, precedes the phase transition of apical 21.75 $\pm$3.97 mins (n = 8, from 7 animals, Fig. 3.4E). From the results, it is shown that the caspase-3 was activated before the apical constriction entering Fast Phase. This result further indicated that the apical extrusion is the apoptosis driven extrusion.

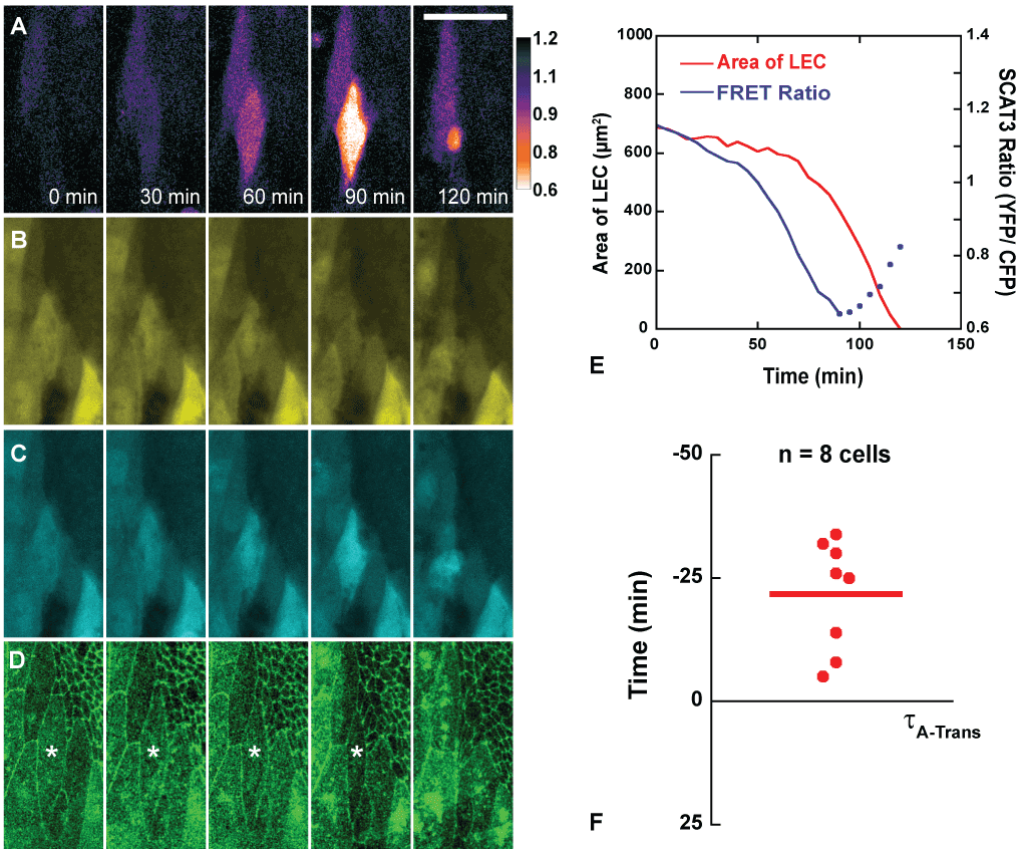

Figure 3.4 Caspase-3 activity activation precedes phase transition
(A-D) Representative apoptotic LEC showing both the caspase-3 activity and shape change over time. See Movie 5. (A) Pseudo-coloured image showing the FRET ratio of the apoptotic LEC over 2-hour period. Brighter color indicates lower FRET ratio, and higher caspase-3 activity. Length of scale bar: 40 μm. (B & C) Venus channel (B) and ECFP channel (C) time lapse images. SCAT3 was expressed in both histoblasts and LECs under the driving of *tsh*-Gal4. Ratio images are produced with these images. (D) *Endo*-DE-cadherin::mTomato channel image showing the shape change over time of the apoptotic LEC (marked with asteroid). (E) Quantification of the FRET ratio (blue curve, right Y-axis) and area (red curve, left Y-axis) change over time. Late stage increasing FRET ratio is depicted by dotted line. (F) Statistical analysis of the caspase-3 activation time. X-axis represents the phase transition time of apoptosis ($\tau_{A\text{-}Trans}$). Y-axis represents the time of apoptosis. Negative value indicates Slow Phase while positive value indicates Fast Phase. Red bar indicates the mean value of activation time and each red dot indicates one sample cell. Sample number is 8, from 7 animals.

3.3 Regulation of cell adhesion and tissue tension during apoptosis

Apoptotic cells need to leave the cell plane to finish the extrusion. During this process, the old junctions between apoptotic cell and its neighbors need to be degraded, and in the end, new junctions between the remaining cells will form. Besides, as the epithelial tissue works as the first physical barrier to protect the organism, the tissue integrity needs to be maintained. In the mechanical aspect, while the mechanical force is generated during apoptosis, the tissue tension homeostasis also need to be well maintained. In fact, how the junction remodelling and mechanical force generation is coupled during apoptosis-driven extrusion in vivo is not well studied yet.

3.3.1 DE-cadherin

Firstly, I imaged *Ubi*-DE-cadherin::GFP expressing pupa to monitor the AJ during apical extrusion (Fig. 3.5A & Movie 6). I found that during Late Fast Phase of the apical constriction, the DE-cadherin between the apoptotic cell and neighboring cells blurs (Fig. 3.5A 100 min & Movie 6). In the end, when apical constriction finished, new junction was formed between the remaining cells (Fig. 3.5A 130 min & Movie 6). Then I conducted the analysis to find the Phase transition of apical constriction. The cell started Fast Phase at round 75 min (76 min according to the analysis, illustrated with black square in Fig. 3.5B), when DE-cadherin still maintained intact (Fig. 3.5A 75 min). After around 25 min, when the cell is in the late stage of the Fast Phase, the clear boundary blurs (Fig. 3.5A 100 min, illustrated with blue circle in Fig. 3.5B), which indicates the junction disengagement. In addition, there was a gap formed between the

apoptotic cell and its neighbours (more obvious for the gap between apoptotic LEC and the histoblast neighbours, Fig. 3.5A 100 min). For the histoblast neighbours, there is not much DE-cadherin accumulated at the nascent edge (white arrowheads in Fig. 3.5A 100 min), which is previously connected with apoptotic LEC. Besides, there is dot shaped accumulation at the tip of the junction (connected to the nascent edge) between the histoblast neighbours (red arrowheads in Fig. 3.5A 100 min), which could be the punctate AJ (Takeichi, 2014). In the end, when the apical constriction finished, new junction forms between the remaining cells (Fig. 3.5A 130 min). Statistic results confirmed that the DE-cadherin dissociation occurs 29.75 $\pm$2.05 mins (n = 20, from 11 animals) after the apical constriction enters the Fast Phase (Fig. 3.5C).

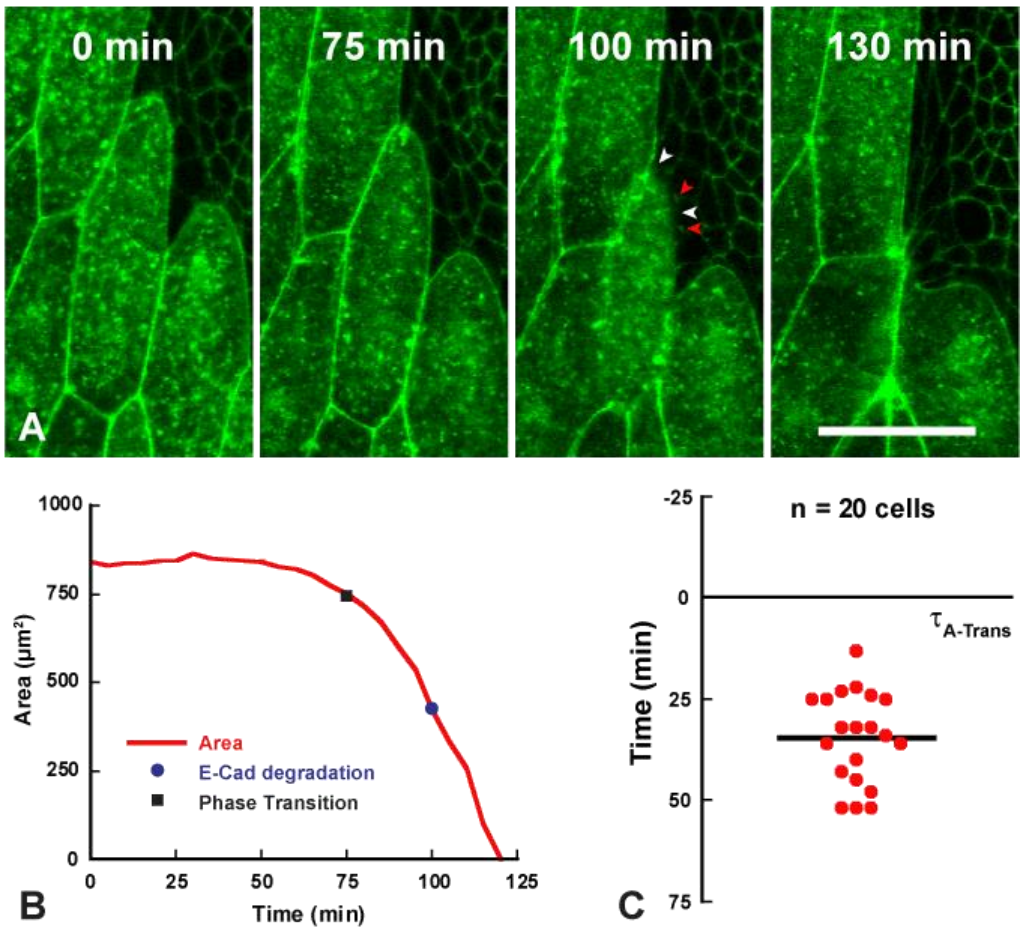

Figure 3.5 DE-cadherin is dissociated in Late Fast Phase

(A) Representative apoptotic LEC at tissue boundary in *Ubi*-DEcad::GFP animal. In late stage of apoptosis, the DE-cadherin is dissociated in the apoptotic LEC (100 min). Gap is formed between the LEC and its neighbors, while week accumulation of DE-cadherin still remains at the nascent edge of the neighbors (white arrowheads). Punctate DE-cadherin spots are formed in the nascent edge of neighboring cells (red arrowheads). DE-cadherin boundary is formed between remaining cells after the completion of apical constriction (130 min). Length of scale bar: 30 μm. See Movie 6. (B) Area change over time of the apoptotic LEC. Phase transition point and the DE-cadherin degradation point are indicated with black square and blue circle, respectively. (C) Statistical analysis of the DE-cadherin degradation time. X-axis represents the phase transition time of apoptosis ($\tau_{A\text{-}Trans}$). Y-axis represents the time of apoptosis. Negative value indicates Slow Phase while positive value indicates Fast Phase. Red bar indicates the mean value of degradation time and each red dot indicates one sample cell. Average degradation time for DE-cadherin is 29.75 ±2.05 mins. Sample number is 20, from 11 animals.

3.3.2 α-catenin and β-catenin

To investigate the destiny of other molecules at AJ during the apical constriction, I imaged the Dα-catenin and Dβ-catenin.

The expression of Dα-catenin-RFP was driven by LEC specific *Eip71CD*-Gal4. The cell have the stable Dα-catenin boundary during Slow Phase and Early Fast Phase of the apical constriction (Fig. 3.6A 0, 30 min & Fig. 3.6B). In the late stage of Fast Phase, Dα-catenin was dissociated from the boundary, and internalized into the cytoplasm (Fig. 3.6A 60 min, dissociation time was illustrated with blue circles in Fig. 3.6B). After the apical constriction finished, new junction was formed between the remaining cells (Fig. 3.6A 90 min). Statistic results confirmed that the Dα-catenin was dissociated from the cell boundary around 24.44 ± 1.12 mins (n = 9, from 3 animals) after the apical constriction enters the Fast Phase (Fig. 3.6C).

The fly with Dβ-catenin-YFP has the similar results. Dβ-catenin was stabilized at the boundary during Slow Phase and Early Fast Phase of the apical constriction (Fig. 3.7A 0 & 40 min & Fig. 3.7B). In the late stage of Fast Phase, Dβ-catenin was dissociated from the boundary, and internalized into the cytoplasm (Fig. 3.7A 60 min, dissociation time was illustrated with blue circles in Fig. 3.7B). Simultaneously, weak accumulation of Dβ-catenin still remains at the nascent edge of the neighbors (yellow arrowheads in Fig. 3.7A 60 min). Punctate Dβ-catenin spots are formed in the nascent edge of neighboring cells (white arrows in Fig. 3.7A 60 min). After the constriction finished, new junction was formed between the remaining cells (Fig. 3.7A 80 min). Statistic results confirmed that the Dβ-catenin was dissociated from the cell boundary 29.08 ±

2.63 mins (n = 12, from 4 animals) after the apical constriction enters the Fast Phase (Fig. 3.7C).

In further, statistical study was conducted to investigate the difference between the dissociation timing of the AJ molecules. The statistical results showed that none of the occurring time of dissociation events of the three molecules at AJ are significantly different (p = 0.107 between DE-cadherin and Dα-catenin, p = 0.164 between Dα-catenin and Dβ-catenin, p = 0.843 between DE-cadherin and Dβ-catenin, Fig. 3.8), which is around 30 mins after the transition from Slow Phase to Fast Phase during apical constriction. Considering the temporal resolution is 5 mins for all the data sets, my data suggested that the dissociation events of the three molecules at AJ occur at the same time.

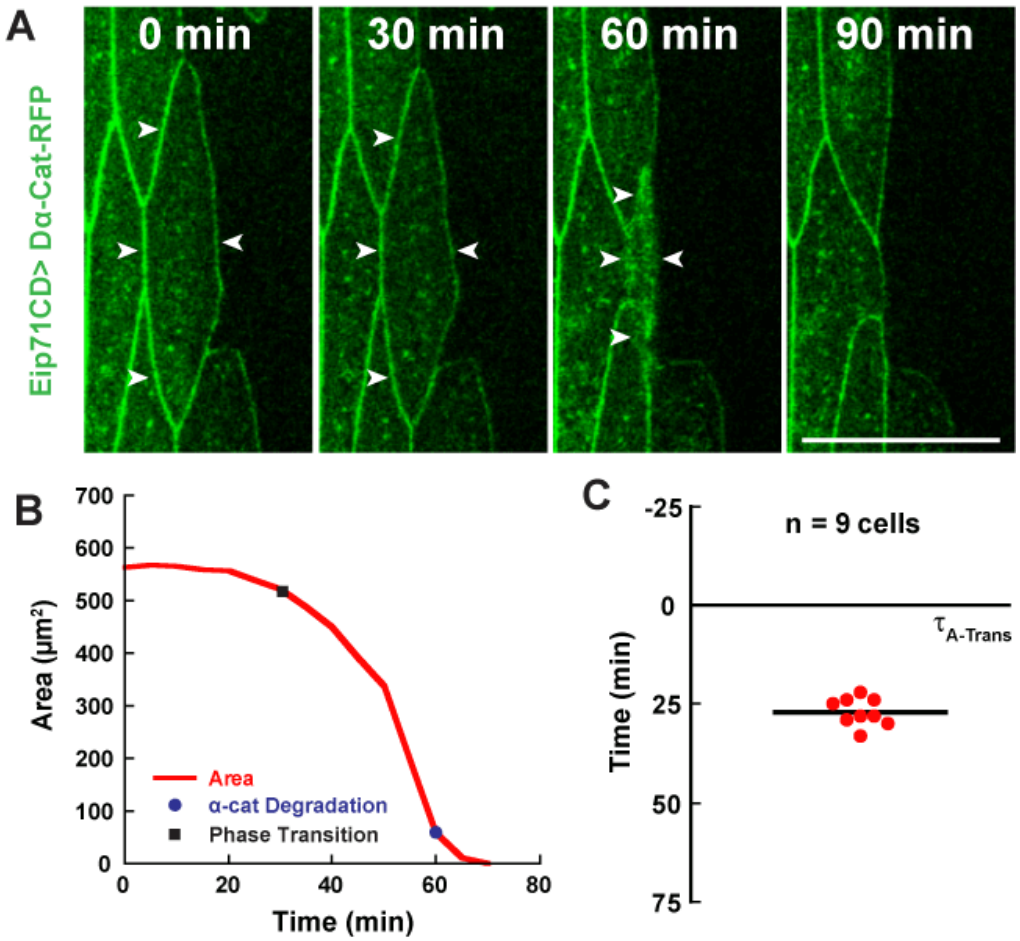

Figure 3.6 Dα-catenin is dissociated in Late Fast Phase

(A) Representative apoptotic LEC at tissue boundary (indicated by white arrowheads) with *UAS*-Dα-catenin-RFP driven by LEC specific *Eip71CD*-Gal4. In late stage of apoptosis, the Dα-catenin is dissociated and internalized in the apoptotic LEC (40 min). DE-cadherin boundary is formed between remaining cells after the completion of apical constriction (60 min). Length of scale bar: 30 μm. (B) Area change over time of the apoptotic LEC. Dα-catenin degradation point is indicated with blue circle at 60 min. Phase transition point is indicated with black square at 32 min. (C) Statistical analysis of the Dα-catenin degradation time. X-axis represents the phase transition time of apoptosis ($\tau_{A\text{-}Trans}$). Y-axis represents the time of apoptosis. Negative value indicates Slow Phase while positive value indicates Fast Phase. Black bar indicates the mean value of degradation time and each red dot indicates one sample cell. Average degradation time for Dβ-catenin is 24.44 ±1.12 mins. Sample number is 9, from 3 animals.

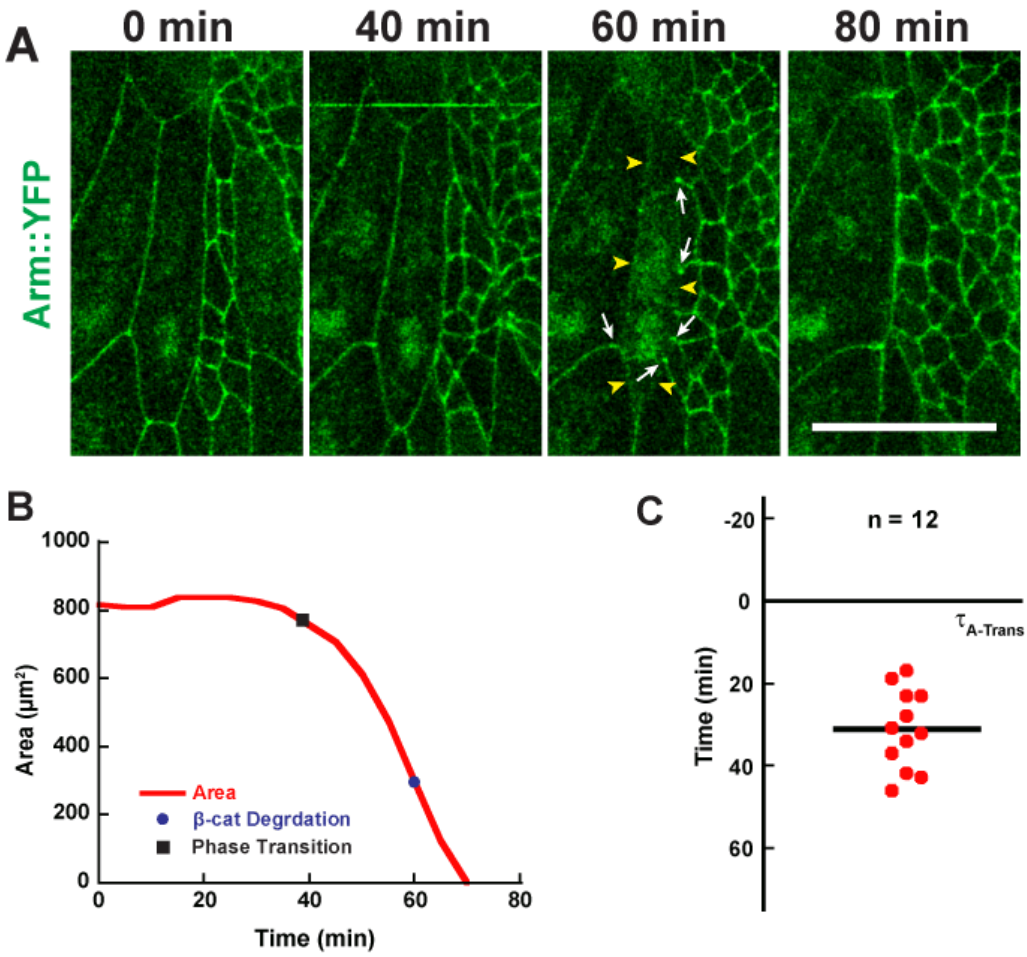

Figure 3.7 Dβ-catenin is dissociated in Late Fast Phase and the AJ molecules degrade at the similar time of apoptosis

(A) Representative apoptotic LEC at tissue boundary in Armadillo-YFP (Dβ-catenin-YFP) animal. In late stage of apoptosis, Dβ-catenin is dissociated and internalized in the apoptotic LEC (60 min). Weak accumulation of Dβ-catenin still remains at the nascent edge of the neighbors (yellow arrowheads). Punctate Dβ-catenin spots are formed in the nascent edge of neighboring cells (white arrows). Dβ-catenin boundary is formed between remaining cells after the completion of apical constriction (80 min). Length of scale bar: 30 μm. (B) Area change over time of the apoptotic LEC. Dβ-catenin degradation point is indicated with blue circle at 60 min. The phase transition point is indicated with black square at 37 min. (C) Statistical analysis of the DE-cadherin degradation time. X-axis represents the phase transition time of apoptosis ($\tau_{A\text{-}Trans}$). Y-axis represents the time of apoptosis. Negative value indicates Slow Phase while positive value indicates Fast Phase. Red bar indicates the mean value of degradation time and each red dot indicates one sample cell. Average degradation time for Dβ-catenin is 29.08 ± 2.63 mins. Sample number is 12, from 4 animals.

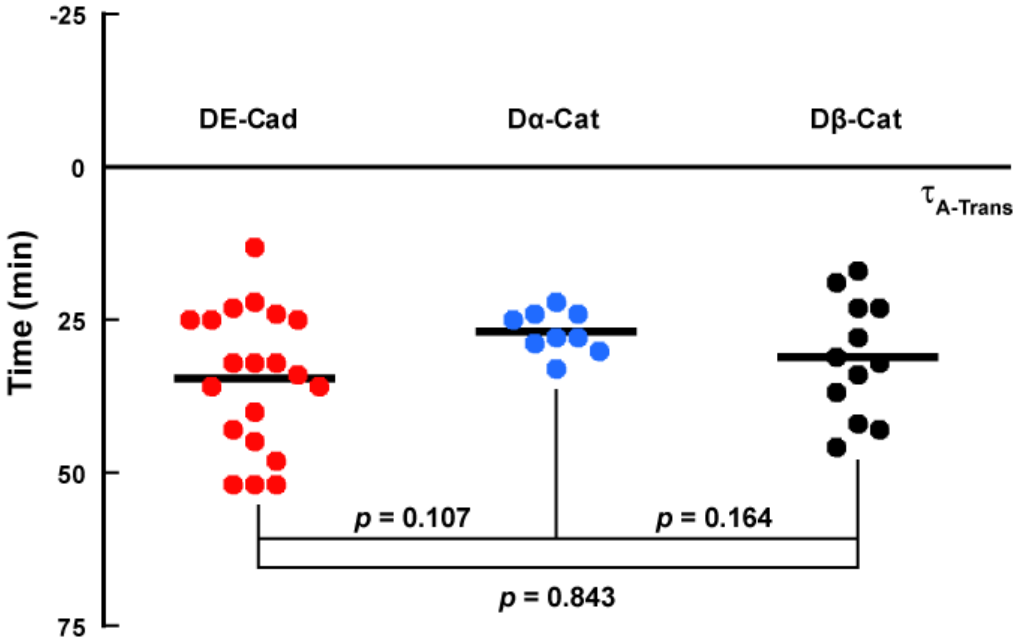

Figure 3.8 AJ molecules are dissociated at the similar timing
Summary of the statistical analysis of the AJ molecule (DE-cadherin, Dα-catenin, and Dβ-catenin) dissociation time. X-axis represents the phase transition time of apoptosis ($\tau_{A\text{-}Trans}$). Y-axis represents the time of apoptosis. Negative value indicates Slow Phase while positive value indicates Fast Phase. Black bars indicate the mean value of degradation time. Each dot in red or blue or black indicates one sample cell from DE-cadherin, Dα-catenin, and Dβ-catenin, respectively. Average degradation times for DE-cadherin, Dα-catenin, and Dβ-catenin are 29.75 ± 2.05 min (n = 20, from 11 animals), 24.44 ± 1.12 mins (n = 9, from 3 animals), and 29.08 ± 2.63 mins (n = 12, from 4 animals), respectively. The degradation times of the three AJ molecules are statistically not significantly different. The p-values of the degradation time between DE-cadherin and Dα-catenin, Dα-catenin and Dβ-catenin, DE-cadherin and Dβ-catenin are 0.107, 0.164 and 0.843, respectively.

3.3.3 AJ disengagement and actomyosin ring separation

Previous work showed that during the apoptotic extrusion of MDCK cells from the cultured cell sheet, two actomyosin rings will form both inside the apoptotic cell and inside the neighbors (Rosenblatt et al., 2001). However, when the two rings start to accumulate is not well studied. Specifically, in histoblast expansion, while the majority of apoptosis is the boundary apoptosis, how the two rings are formed and cooperate in the tissue boundary to facilitate the extrusion in heterogeneous tissue is still an open question.

To investigate the question, I imaged the *sqh*-sqh-cherry simultaneously with *Ubi*-DE-cadherin::GFP. As described above, DE-cadherin will disengage in the late stage of Fast Phase (Fig. 3.5 & Movie 6). Before the DE-cadherin disengagement and after the apical constriction finished when new junction formed, the myosin ring colocalize well with the cell boundary (Fig.3.9A 0 & 45 min, Movie 7). Interestingly, coincide with the DE-cadherin disengagement (Fig.3.9B 15 & 25 min, Movie 7), the myosin ring separate into two rings: inner ring (single-head arrows in Fig.3.9B 15 & 25 min, Movie 7) and outer ring (double-head arrows in Fig.3.9B 15 & 25 min, Movie 7). The inner ring colocalizes with the apoptotic LEC, and the outer ring colocalizes with the nascent edge of histoblast neighbours (Fig. 3.9E), where there is dot shaped punctate DE-cadherin accumulation at the tip of the junction (connected to the nascent edge) between the histoblast neighbours (arrowheads in Fig. 3.9D). Besides, weak DE-cadherin still localized at the nascent edge (arrowhead in Fig. 3.9D).

Similar results were also revealed for Dα-catenin and Dβ-catenin (Fig. 3.10, Movie 8 & Fig. 3.11, Movie 9): before the AJ disengagement and after the apical constriction finished when new junction formed, the myosin ring colocalize well with the cell boundary (Fig. 3.10 0, 30 & 90 min for Dα-catenin, Fig. 3.11 0-40 & 80 min for Dβ-catenin); when the AJ disengaged, the myosin rings separate into two rings (Fig. 3.10 60 min for Dα-catenin, Fig. 3.11 60 min for Dβ-catenin) while the outer ring colocalizes with the nascent edge of histoblast neighbours (Fig 3.10A 60 min & Fig. 3.11A 60 min).

Besides, I imaged sGMCA fly to investigate the dynamics of actin ring during apoptosis. Similarly as myosin ring separation, the actin ring also separates into two rings in the late stage of apical constriction (Fig. 3.12 & Movie 10). The results confirmed the actomyosin ring separation in the late stage of LEC apoptotic constriction.

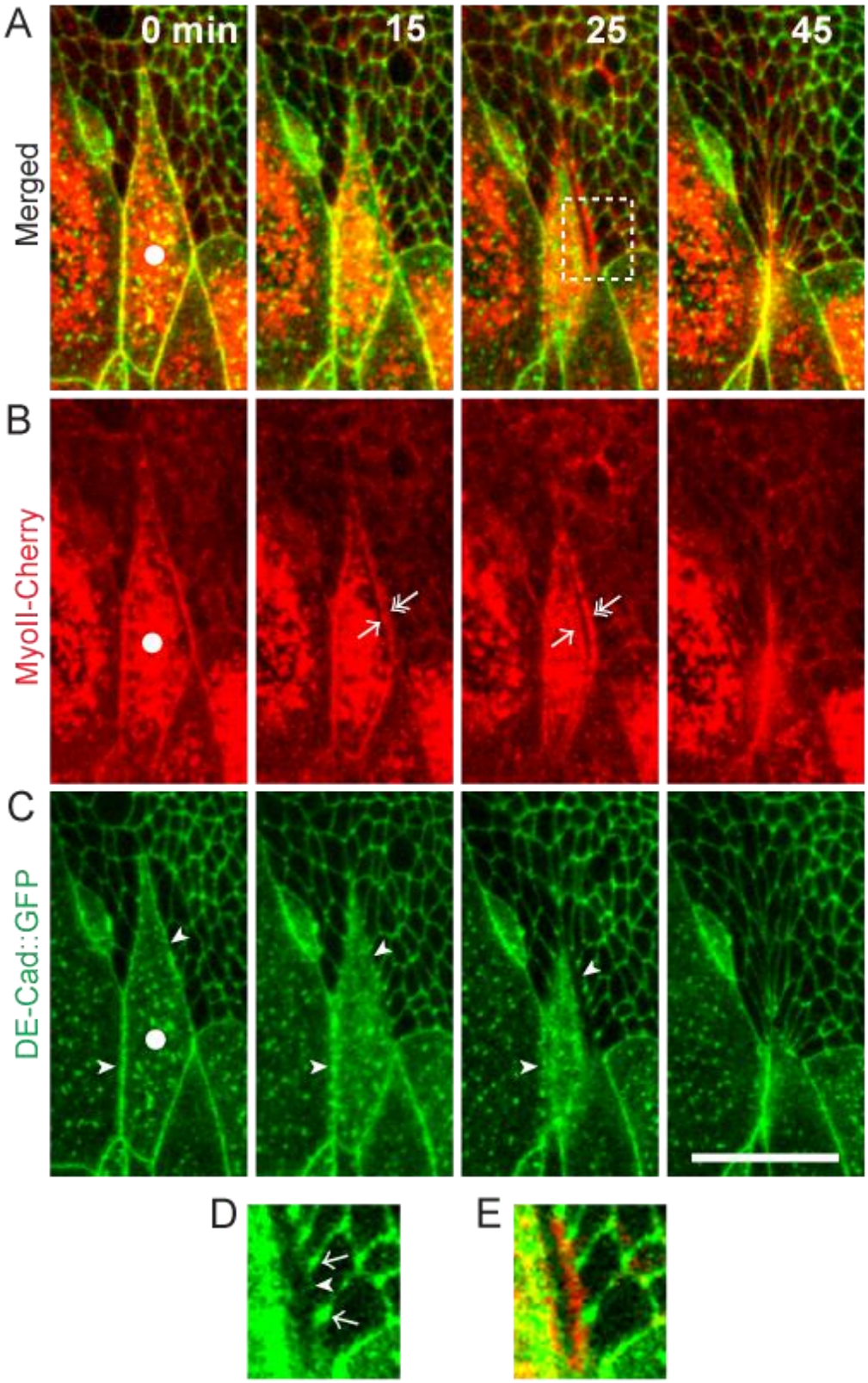

Figure 3.9 Myosin ring separates into two when DE-cadherin degrades
DE-cadherin and actomyosin colocalize well in the early stage of apoptosis (A-C, 0 min. Apoptotic LEC is indicated with white circle), and the DE-cadherin boundary is intact (C, 0 min, indicated with white arrowheads). In the late stage of apoptosis, DE-cadherin degrades, and gap is formed between the apoptotic LEC and its neighbors (C, 15 & 25 min). Simultaneously, the myosin ring

separate into two rings (B, 15 & 25 min, inner ring and outer ring are indicated with arrowheads and double arrowheads, respectively). Region of dashed box in 25 min was zoomed out and shown in D & E. Punctate DE-cadherin accumulates at the front of edge of the neighboring cells (D, white arrows). Weak accumulation of DE-cadherin still located at the nascent edge (D, white arrowhead). The inner ring colocalized with the apoptotic LEC, and the outer ring colocalized with the nascent edges (E). New junction forms between remaining cells when apical constriction finishes, and myosin and DE-cadherin colocalized well again (A-C, 45 min). Length of scale bar in C: 30 μm. See Movie 7.

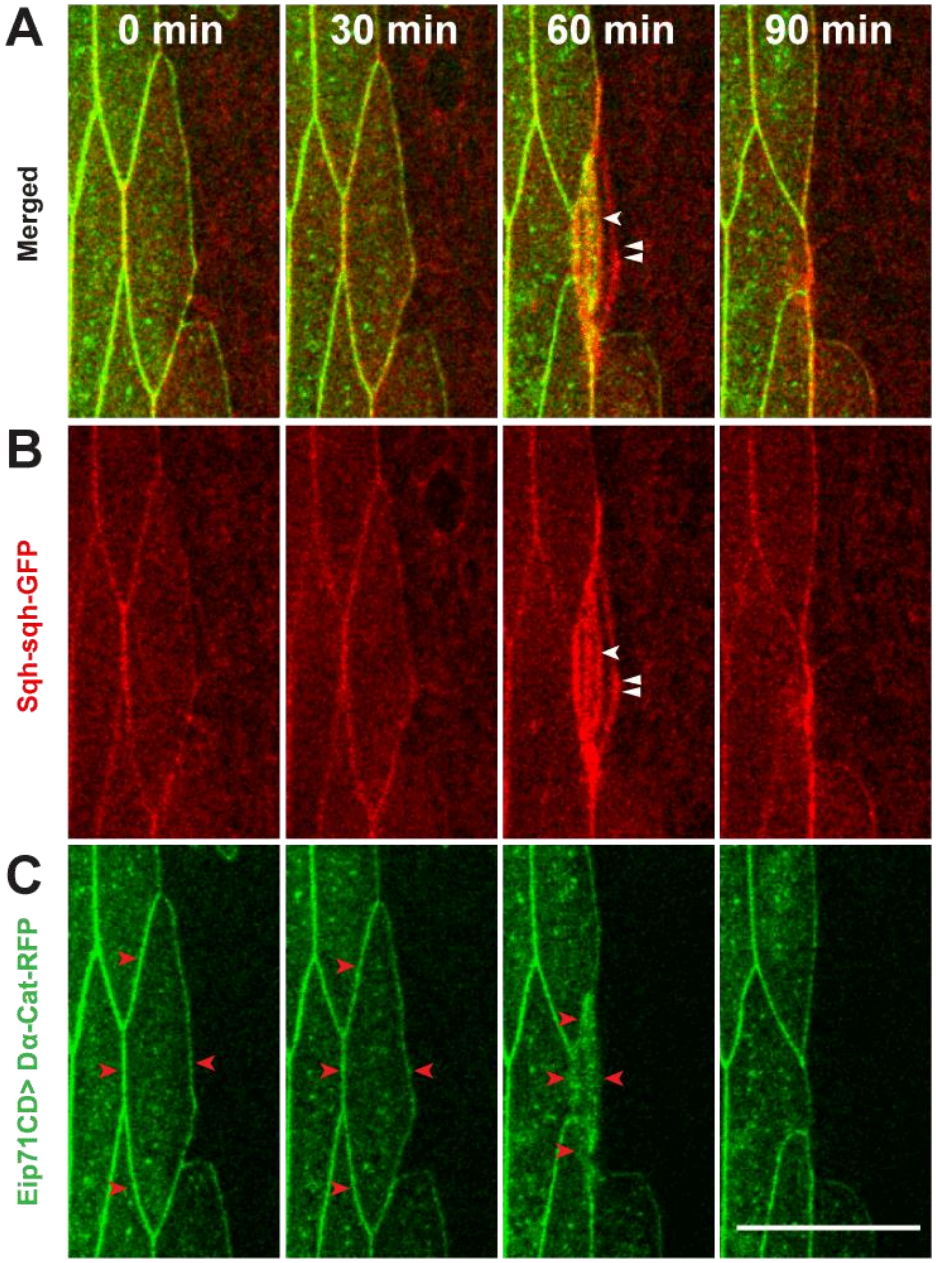

Figure 3.10 Myosin ring separates into two when Dα-catenin degrades
Dα-catenin and myosin ring colocalize well in the early stage of apoptosis (A-C, 0 & 30 min). In the late stage of apoptosis, Dα-catenin degrades and is internalized from the boundary (C, 60 min). Simultaneously, the myosin ring separates into two rings. Inner ring and outer ring are indicated with single arrowhead and double arrowheads, respectively (A&B, 60 min). The inner ring colocalizes with the apoptotic LEC, and the outer ring colocalize with the nascent edges (red arrowheads in C 60 min). New junction forms between remaining cells when apical constriction finishes, and myosin and Dα-catenin colocalize well (A-C, 90 min). Length of scale bar in C: 30 μm. See Movie 8

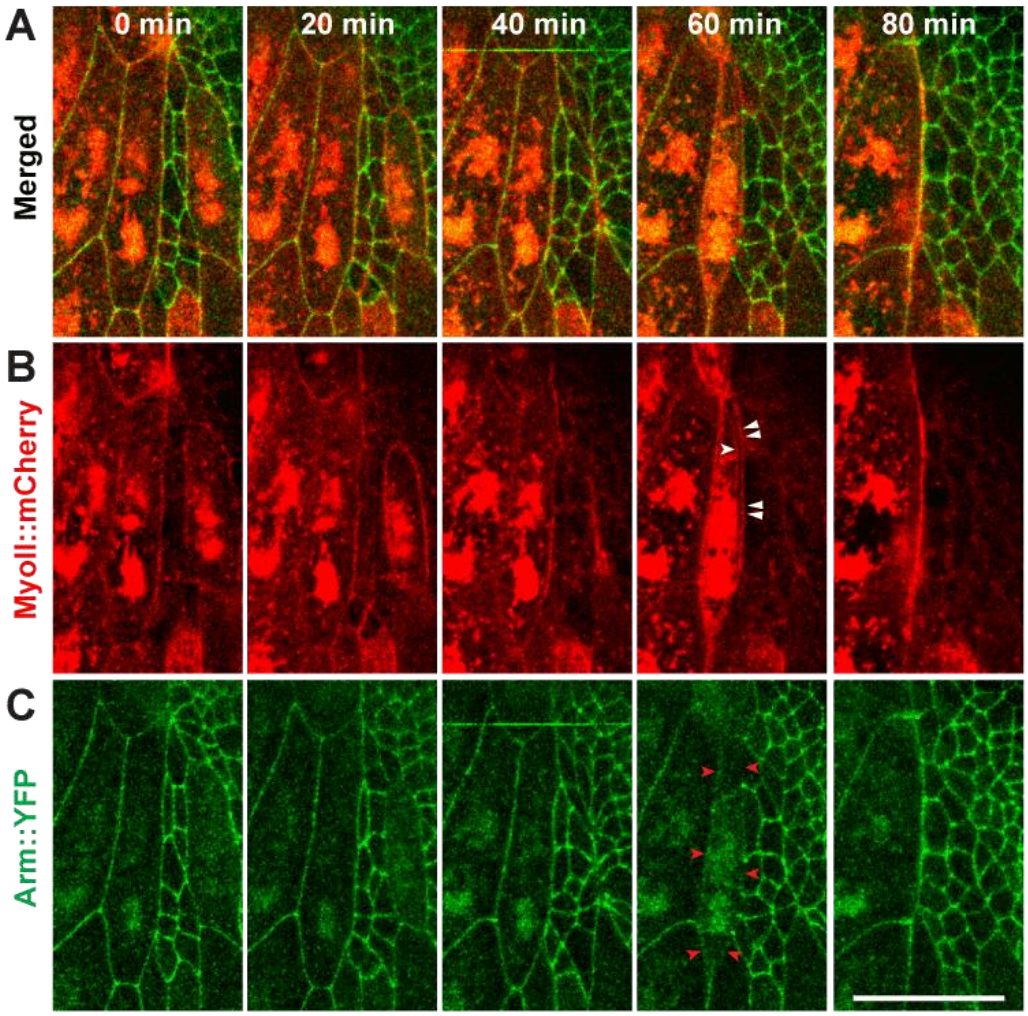

Figure 3.11 Myosin ring separates into two when Dβ-catenin degrades
Dβ-catenin and actomyosin colocalize well in the early stage of apoptosis (A-C, 0-40 min). In the late stage of apoptosis, Dβ-catenin degrades (C, 60 min). Simultaneously, the myosin ring separate into two rings. Inner ring and outer ring are indicated with arrowheads and double arrowheads, respectively (B, 60 min). The inner ring colocalizes with the apoptotic LEC, and the outer ring colocalizes with the nascent edges (red arrowheads in C 60 min), and the punctate Dβ-catenin accumulation at the front of edge of the neighboring cells (A, 60 min). New junction forms between remaining cells when apical constriction finishes, and myosin and Dβ-catenin colocalize well (A-C, 80 min). Length of scale bar in C: 30 μm. See Movie 9

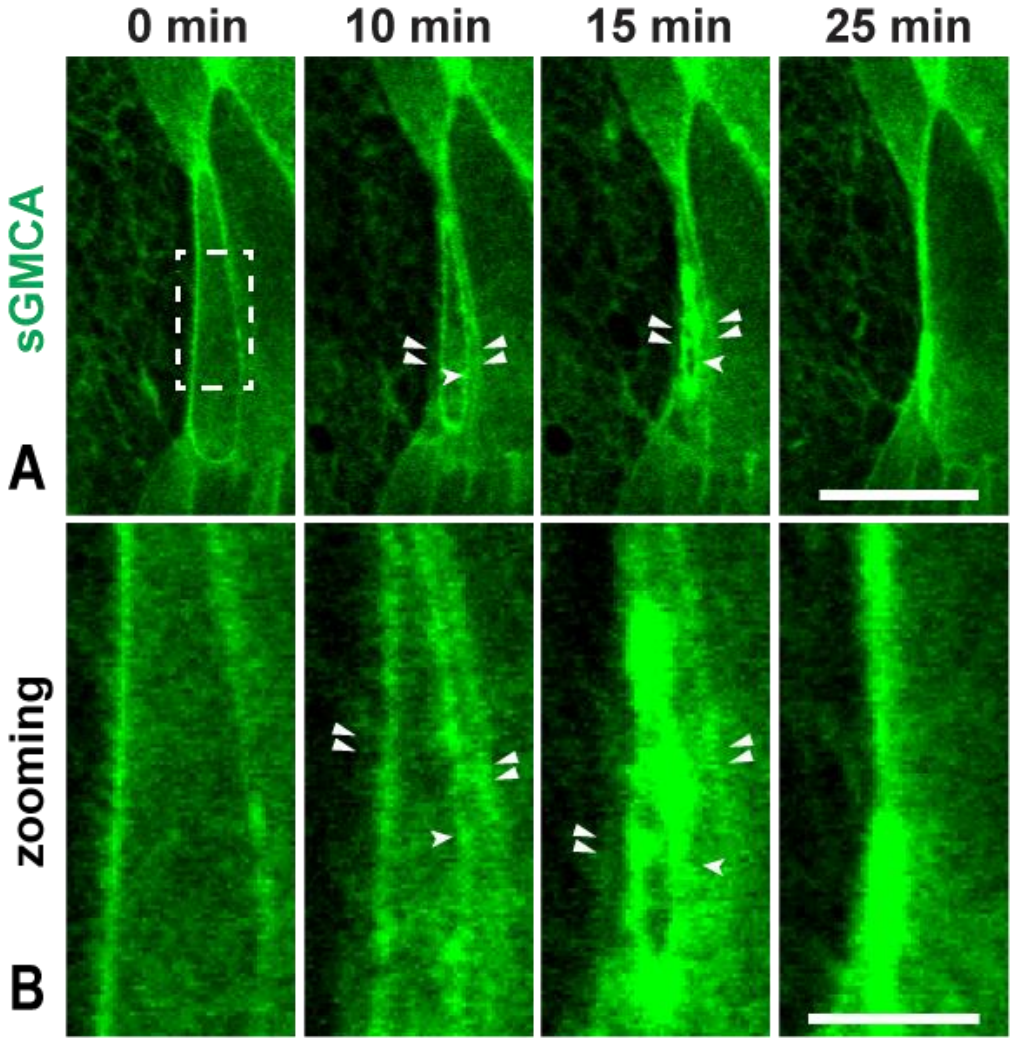

Figure 3.12 Actin ring separates in the late stage of apoptosis
(A) Time lapse images showing that in late stage of apoptosis, the actin ring also separates into to rings (0- 15 min). Region of dashed line was zoomed out in (B). Inner ring was indicated with single arrowhead, and outer ring was indicated with double arrowheads (A& B, 10 & 15 min). Length of scale bar: 30 μm in (A) and 10 μm in (B). See Movie 10.

3.3.4 Tissue tension regulation during AJ disengagement

Epithelial cells are connected through cell-cell adhesions. Cortical actomyosin rings in each epithelial cells are connected through the AJ belt located at the apicolateral side of each cell. While the cortical actomyosin ring contracts and generates the contractile force, the force is balanced by many other epithelial cells within the cell plane, which results in the tissue tension. Previous results showed the AJ disengagement during late stage of apical constriction of apoptotic LECs. The remaining question is whether it will result in the tissue tension release.

To investigate this question, I expressed the *UAS*-sqh-GFP under the driven of LEC specific Gal4, *Eip71CD*-Gal4. This tissue specific expression could have better image contrast. On the other hand, I increased the time resolution from 5 mins to 2.5 mins to better record the dynamics. Fig. 3.13A &B show the two frames right before actomyosin ring separation and right after the separation. The merged image shows the red ring locates in between the two cyan rings (Fig. 3.13C). This result indicates that right after the AJ disengagement (myosin ring separation as a marker), the outer ring will retract outwards, which in further indicates the junctional tension release upon apoptosis.

To confirm the tissue tension dynamics during different stages, I analyzed the linearity of the neighboring histoblast boundaries connecting to the LECs at distinct time points (Chapter II 2.4.1). Upon AJ disengagement, when two actomyosin rings are forming (Fig. 3.14B), the linearity of the boundary decreases (0.856±0.024, n=12 from 7 animals) compared with control in Slow Phase (0.960±0.007, n=17 from 9 animals) when the AJ is still intact. This results indicates the tension release upon AJ disengagement in the tissue (Fig.

3.14F, $p<0.001$), which is consistent with previous observation (Fig. 3.13). When the apical constriction enters the late stage, which is hallmarked by the well separated two actomyosin rings, the linearity of the boundary rebuilds (0.981±0.005, n=27 from 15 animals), which indicates the tissue tension is rebuilt during the late stage of apical constriction (Fig. 3.14F, $p<0.001$). The boundary linearity in late disengagement is slightly, but significantly higher than the control (Fig. 3.14F, $p<0.05$).

To further quantify the actual tissue tension dynamics in different stages of apoptosis, I performed nano-ablation and analyzed the initial recoil velocities of each ablation (Chapter II 2.3.3 & 2.4.3). Upon AJ disengagement (Fig. 3.14B & B'), the initial recoil velocity of the boundary is significantly lower (0.0286±0.007 μm/sec, n=12 from 7 animals) than the control in Slow Phase (0.184±0.027 μm/sec, n=17 from 9 animals, Fig. 3.14A & A',) when the AJ is still intact (Fig. 3.14D, $p< 0.001$). During the late stage of apical constriction (Fig. 3.14C & C'), the initial recoil velocity of the boundary is significantly higher (0.312±0.019 μm/sec, n=27 from 15 animals) than the control (Fig. 3.14D, $p<0.001$), and is much higher compared to the boundary upon AJ disengagement (Fig. 3.14D, $p<0.001$). Besides the initial recoil velocity, the average recoiled distances were also quantified (Fig. 3.14E). The results showed that the recoiled distances after ablation upon AJ disengagement (red line with red circle in Fig. 3.14E) are shorter than the recoiled distances at the Slow Phase (green line with green cross in Fig. 3.14E) at all time points. Besides, the recoiled distances at late disengagement (blue line with blue squares in Fig. 3.14E) are longer than the distances of both Slow Phase and early disengagement at all time points.

All together, our results showed that the tissue tension is released upon AJ disengagement, and is rebuilt when the constriction goes on. In further, the results showed that the tissue tension is well regulated during AJ disengagement.

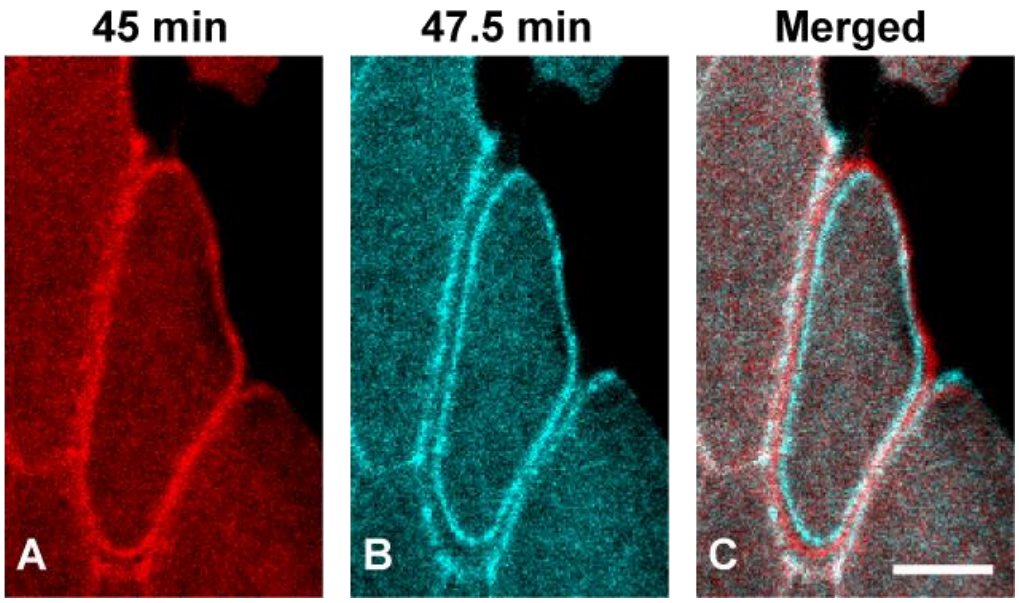

Figure 3.13 Junctional tension is released during AJ disengagement
UAS-sqh-GFP driven by *Eip71CD*-Gal4 to express sqh-GFP only in LECs. (A) Time point showing the myosin ring right before the separation. (B) 2.5 mins later, the myosin ring separate into two rings. Part of the outer ring is formed inside histoblasts, which is not visible. (C) Overlapped image of the two time points. The red myosin ring (signal from time point 45 min) locates in between two cyan myosin rings (signal from time point 47.5 min). Length of scale bar in C: 10 μm.

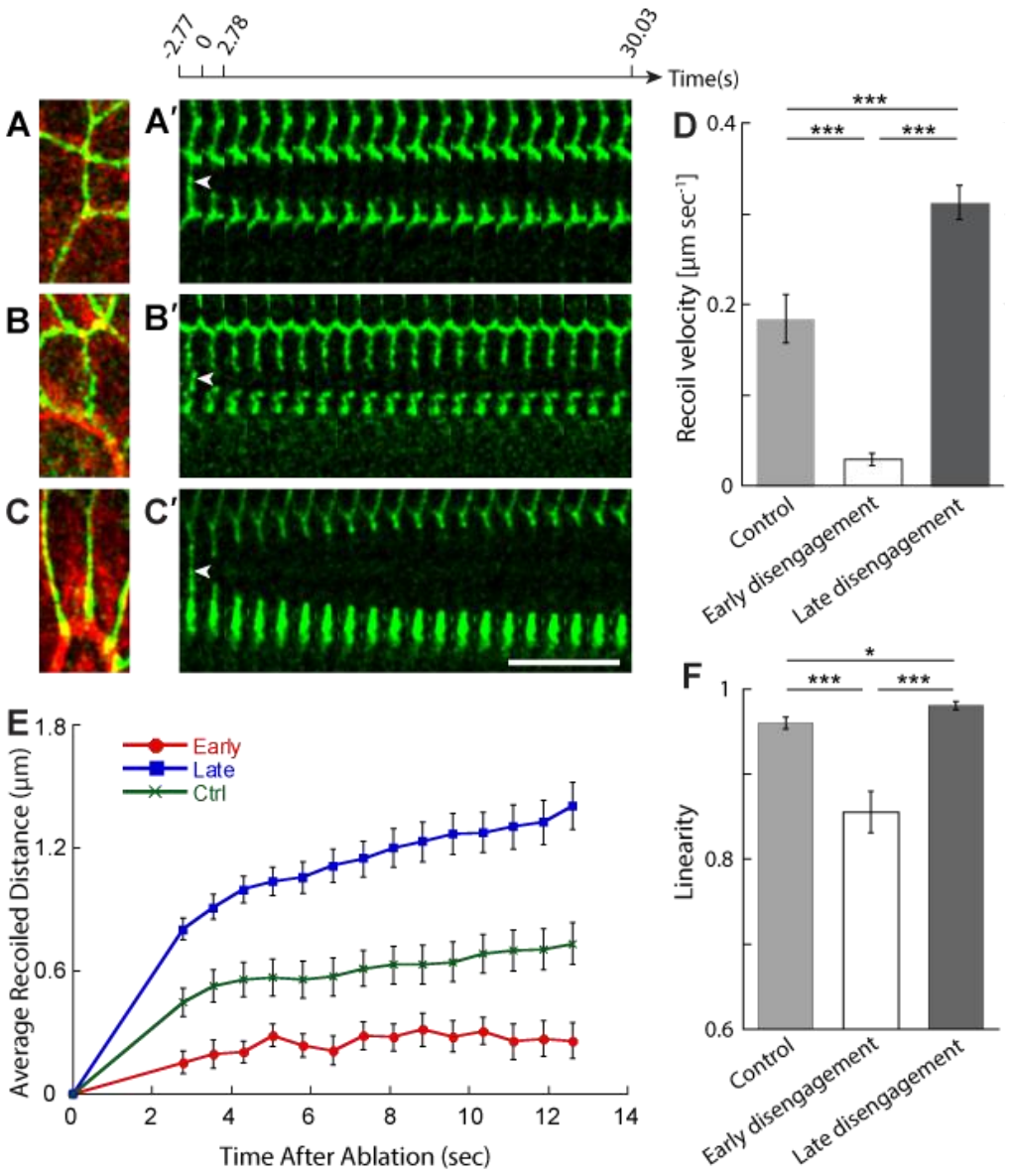

Figure 3.14 Tension is released during AJ disengagement and is rebuilt as constriction goes on

(A-C) Nano-ablation of the neighboring boundaries of histoblasts at three distinct time points: Slow Phase (A), upon AJ disengagement (B), and late disengagement (C). (A'-C') Kympgraphs of the junction recoil after nano-ablation for Slow Phase (A'), upon AJ disengagement (B'), and late disengagement (C'). Time intervals between each image are indicated by the x-axis. White arrowheads indicate the junction right before ablation (2.77 seconds before ablation). (D) Statistical analysis of the initial recoil velocities after ablation show that the initial recoil velocity upon AJ disengagement (0.0286 ± 0.007 µm/sec, n= 12, from 7 animals) significantly decreases compared with the initial recoil velocity in Slow Phase (0.184 ± 0.027 µm/sec, n= 17, from 9 animals). The difference is significant (p<0.001). Besides, the initial recoil velocity during late disengagement significantly increases (0.312 ± 0.019 µm/sec, n= 27, from 15 animals) compared with both Slow Phase control (p<0.001) and early disengagement (p<0.001). (E) Average recoiled distances after nano-ablation for all the three distinct time points: Slow Phase (green line

with crosses), early disengagement (red line with circles) and late disengagement (blue line with squares). The recoiled distances of late constriction is longer than early disengagement as well as Slow Phase control at all time points, while the distances of early disengagement are shorter than both the late constriction and the control at all time points. (F) Measurements of linearity of the neighboring boundaries connecting to the LECs showed that the neighboring boundary linearity upon AJ disengagement significantly decreased (0.856 ± 0.024, n= 12, from 7 animals) compared to the Slow Phase control (0.960 ± 0.007, n= 17, from 9 animals, $p<0.001$). Besides, the linearity significantly increased in the late disengagement (0.981 ± 0.005, n= 27, from 15 animals) compared with both the early disengagement ($p<0.001$) and the Slow Phase control ($p<0.05$). *: $p<0.05$; ***: $p<0.001$; Scale bar: 10 μm.

3.3.5 Septate junction

In epithelial tissue, the tissue integrity need to be maintained. Previous study showed that while the apoptotic events are quite frequently occurred during histoblast expansion, the tissue integrity is not compromised (Ninov et al., 2007). However, our data showed that the AJ is disengaged before the apical constriction is completed. Then I imaged the septate junction component neuroglian (Nrg) tagged with GFP. As shown in the previous results, the myosin ring at the AJ separates into two rings, so I simultaneously imaged the myosin to probe the disengagement of AJ (Movie 11). While the myosin ring separates into two rings in the late stage of apical constriction (Fig. 3.15A 5 & 10 min), septate junction maintains intact in the subapical plane (around 1.6 μm more basal than myosin rings. Myosin rings are in the same z-plane as AJ, Fig. 3.15B 5 & 10 min). The septate junction remains intact until the end of apical constriction (Fig. 3.15 A&B 20 min, Movie 11). As is shown in the previous data, new AJ between the remaining cells will form when the apical constriction finishes. Thus, septate junction maintains the tissue integrity during the late stage of apical constriction in apoptosis.

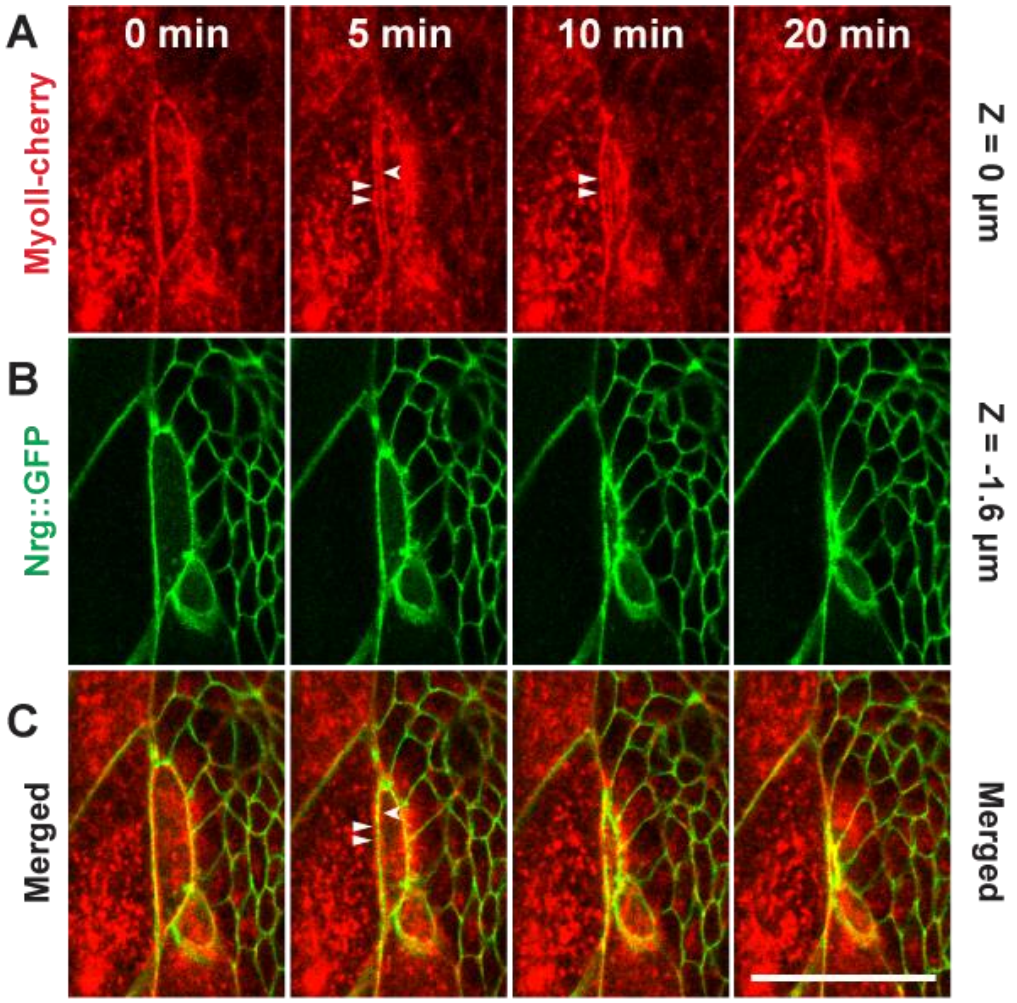

Figure 3.15 Septate Junction maintains intact during apical constriction
Septate junction is visualized by GFP tagged neuroglian (Nrg::GFP), which locates around 1.6 µm more basal than the myosin ring (AJ). Before myosin ring separation, Nrg and myosin ring roughly colocalize (A-C, 0 min). When the myosin ring separates into two, the Nrg locates between the two rings (A-C 5 & 10 min, inner ring and outer ring are indicated with single arrowhead and double arrowheads, respectively). Until the end of apical constriction, septate junction remains intact (A-C 20 min). Length of scale bar: 40 µm. See Movie 11.

3.4 Roles of two actomyosin cables formed upon apoptosis

In MDCK cells, it has been shown that there were two rings formed during the apical constriction. One actomyosin ring forms inside the apoptotic cell, and the other actomyosin ring, or the actomyosin purse string forms inside the neighboring cells (Rosenblatt et al., 2001). Previously we have shown that the actomyosin ring will separate into two rings during the late stage of apoptotic extrusion. Where are the two rings accumulated and when they start to accumulate is not clear. Besides, how the two rings play their role to cooperate and facilitate the extrusion is unknown neither.

3.4.1 Location of two actomyosin rings

To investigate where the two rings are formed, I conducted the tissue specific expression: with tissue specific Gal4 lines, I drove the expression of GFP tagged sqh (*Drosophila* non-muscle myosin II light chain) only in LECs or only in histoblasts. With the co-expression of *sqh*-sqh-cherry, I was able to examine the co-localization of the rings in two channels. As expected, in the early stage of apoptosis (before two rings separate) or after the apical constriction finishes, the rings in two channels colocalize very well (Fig. 3.16A 0-60 & 90 min, Fig. 3.17A 0, 30 & 80 min, Movie 12 & Movie 13).

However, when two rings separate from each other, while the inner ring is intact in the LEC specific expression channel, there is only partial outer ring forms in that channel (Fig. 3.16B 80 min & Movie 12). The two rings from the ubiquitously expressed sqh-cherry channel colocalize well with the inner ring and partial outer ring in the GFP channel, but not with the missing outer ring

part. This result indicates that the apoptotic LEC at least participates in forming the inner ring, but do not participate in forming the neighboring ring. In other words, the outer ring is formed by the neighbors.

But the possibility is still not ruled out that maybe both the apoptotic LEC and the neighbors participate in forming the inner ring. In the histoblast specific expression, when the two rings separate from each other in the late stage of Fast Phase, there is only partial myosin ring formed. This partial ring only colocalize with the outer myosin ring but not the inner ring from the ubiquitously expressed sqh-cherry channel (Fig. 3.17A 60&70 min, Movie 13). This result indicates that the histoblasts, or the neighbors do not participate in forming the inner ring. Taken together with the conclusion from LEC specific expression experiment that the apoptotic LEC at least participates to form the inner ring, I conclude that the inner ring is formed by the apoptotic LEC only.

Taken the results together, it is clear that the outer ring is formed inside histoblasts, or the neighbors, while the inner ring is formed inside the apoptotic LEC.

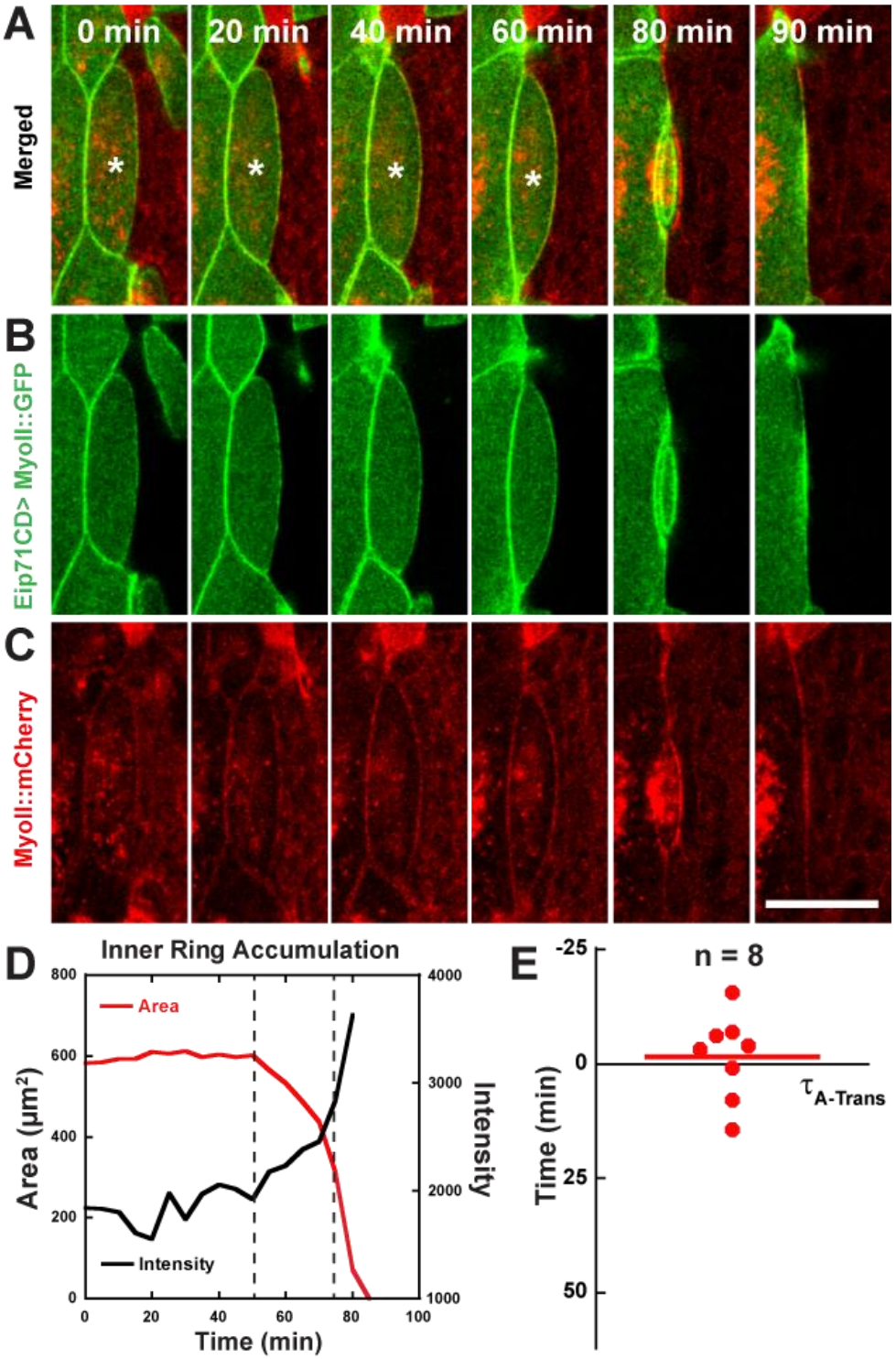

Figure 3.16 LEC specific expression of sqh-GFP

(A-C) Tissue specific expression of *UAS*-sqh-GFP inside LECs is driven by *Eip71CD*-Gal4. *Sqh*-sqh-cherry is expressed ubiquitously. The expression pattern of GFP and RFP colocalize well in LECs before the ring separation (A-C, 0-60 min, the apoptotic LEC is marked with asteroids). The myosin intensity of the boundary of apoptotic LEC connecting with histoblasts seems increasing before ring separation (B, 0-60 min). When the myosin ring separates, only partial outer ring is formed within the LECs while the other part is only visible in RFP channel (A-C, 80 min). When apical constriction completes, GFP and RFP signal colocalizes well again (A-C, 90 min). Length of scale bar: 30 μm.

See Movie 12. (D) Quantification of inner ring intensity (black line, right Y-axis) and apical surface area (red line, left Y-axis) dynamics. Left dashed line indicates the phase transition of apoptosis. Right dashed line indicates the ring separation (AJ disengagement) point. (E) Statistical analysis showing the inner ring starts to accumulate myosin at -1.5 ± 3.29 min (n = 8 cells, from 2 animals), which is around phase transition point. X-axis represents the phase transition point of apoptosis ($\tau_{A\text{-}Trans}$), and Y-axis represents the time of apoptosis. Negative value means the time in Slow Phase and positive value means the time in Fast Phase.

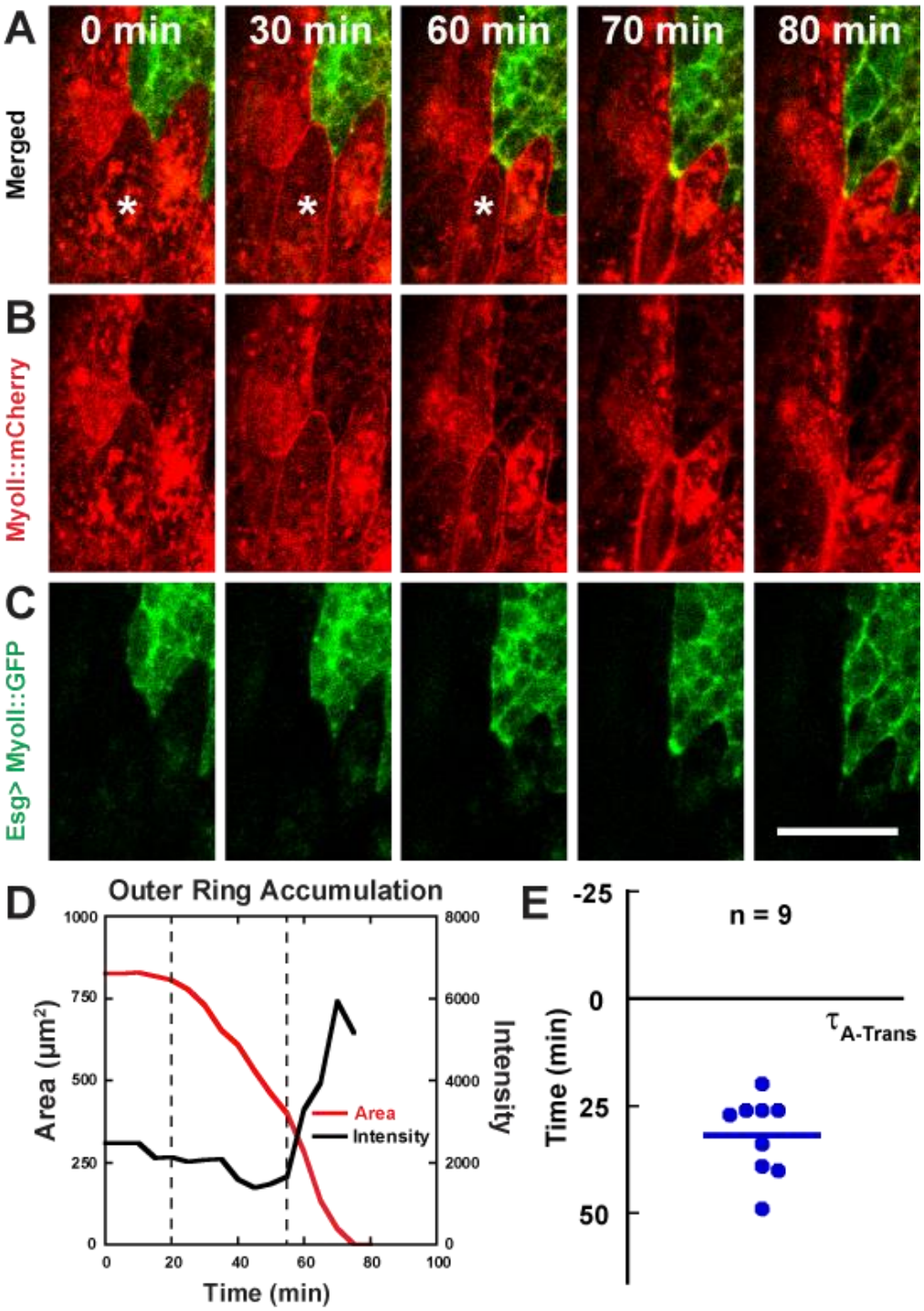

Figure 3.17 Histoblast specific expression of sqh-GFP

Tissue specific expression of *UAS*-sqh-GFP inside histoblasts is driven by *esg*-Gal4. *Sqh*-sqh-cherry is expressed ubiquitously under the endogenous promoter. The expression pattern of GFP and RFP colocalize well in LECs before the ring separation (A-C, 0&30 min, the apoptotic LEC is marked with asteroid). The myosin intensity of the boundary of neighboring histoblasts connecting with apoptotic LEC seems not increasing before ring separation (B, 0&30 min). When the myosin ring separates, partial outer ring is formed within the histoblasts while inner ring is missing from the GFP channel. Double myosin rings are visible in RFP channel (A-C, 60&70 min). Meanwhile, the myosin intensity of the partial outer ring increases a lot (C, 60&70 min). Length of scale

bar: 30 μm. See Movie 13. (D) Quantification of outer ring intensity (black line, right Y-axis) and apical surface area (red line, left Y-axis) dynamics. Left dashed line indicates the phase transition of apoptosis. Right dashed line indicates the ring separation (AJ disengagement) point. (E) Statistical analysis showing the outer ring starts to accumulate myosin at 31.89 ± 3.20 min (n = 9 cells, from 6 animals), which is around AJ disengagement point. X-axis represents the phase transition point of apoptosis ($\tau_{A\text{-}Trans}$), and Y-axis represents the time of apoptosis. Negative value means the time in Slow Phase and positive value means the time in Fast Phase.

3.4.2 Timing of actomyosin cable formation

After I answered the question of where the two myosin rings are formed, which is about spatially how the two rings are accumulated, the next question is temporally how the two rings are accumulated, that is, when the two rings accumulated. However, before the two rings separate, I was not able to separate the intensity of inner ring from the outer ring as the two rings overlap with each other. To solve the problem, I again took advantage of the tissue specific expression. For instance, in the LEC specific expression, while the inner ring overlaps with the neighboring ring before separation, I could know that signals of the partial inner ring, which is connected to the histoblast, comes from the inner ring only. By measuring the intensity of the partial inner ring, I could probe the dynamics of the inner ring accumulation. Similarly, in the histoblast specific expression setting, I could measure the intensity of the partial neighboring ring in the histoblast neighbors to probe the dynamics of the neighboring ring accumulation.

First of all, I measured the dynamics of inner ring intensity (cell is shown in Fig. 3.16 & Movie 12). The results showed that the inner ring start to accumulate around the phase transition of apical constriction (left dashed line in Fig. 3.16D), which is much earlier than the AJ disengagement hallmarked by two rings separation (right dashed line in Fig. 3.16D). Statistical results confirmed the observation that the inner ring accumulation starts at -1.5 ± 3.29 min (n= 8, from 2 animals, Fig. 3.16E), which is around the phase transition of apical constriction, and is far from the AJ disengagement ($p < 0.001$, Fig. 3.18 left part & right part).

Then I measured the dynamics of neighboring ring intensity (cell is shown in Fig. 3.17 & Movie 13). The results showed that the inner ring start to accumulate way after the phase transition of apical constriction (left dashed line in Fig. 3.17D), and is around the AJ disengagement hallmarked by two rings separation (right dashed line in Fig. 3.17D). Statistical results confirmed the observation that the inner ring accumulation starts at 31.89 ±3.20 min (n = 9, from 6 animals, Fig. 3.17E), which occurs almost at the same time as AJ disengagement (p = 0.567, Fig. 3.18 middle part & right part). Besides, the inner ring and outer ring accumulates at different time ($p < 0.001$, Fig. 3.18 left part & middle part).

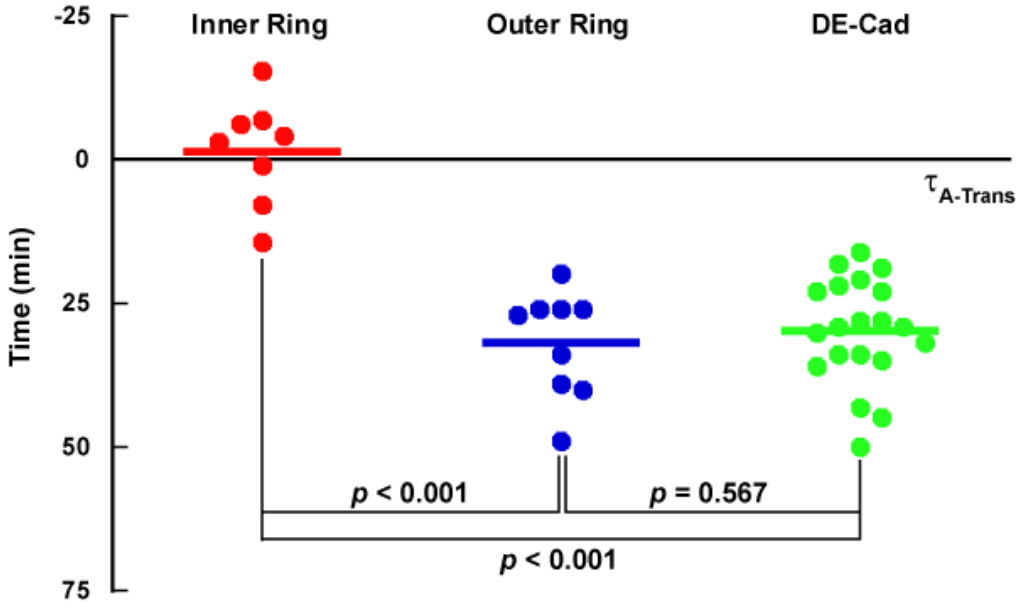

Figure 3.18 Two rings accumulate at different timing
Summary of the statistical analysis of the accumulation time of two rings and the comparison to DE-cadherin dissociation time. X-axis represents the phase transition time of apoptosis ($\tau_{A\text{-}Trans}$). Y-axis represents the time of apoptosis. Negative value indicates Slow Phase while positive value indicates Fast Phase. Bars indicate the mean values of myosin accumulation or DE-cadherin degradation time. Each dot indicates one sample cell from. Average myosin accumulation time for inner ring, outer ring are -1.5 ± 3.29 min (n = 8, from 2 animals), 31.89 ± 3.20 min (n = 9, from 6 animals), respectively. Average DE-cadherin dissociation time is 29.75 ± 2.05 min (n = 20, from 11 animals). The accumulation times of the inner ring and outer ring are significantly different ($p < 0.001$). While inner ring accumulation and DE-cadherin dissociation occur at significantly different timing ($p < 0.001$), the outer ring accumulation and DE-cadherin dissociation occur at similar timing ($p = 0.567$).

3.4.3 Disruption of outer actomyosin cable by MARCM

While the inner ring and outer ring are accumulated differently in both spatial and temporal way, the next question is what their roles are during apical extrusion.

I investigated the role of neighboring ring. I conducted the clonal expression of *sqh* RNAi in the LECs. The experimental settings are indicated in the materials & methods part (Chapter II 2.2.2). The RNAi positive cells had double copy of histone-RFP expression, which resulted in the brighter red nucleus (white cross in Fig. 3.19A). There are two categories of wild type cells: one group is generated during flippase mediated homologous recombination during mitosis. These cells had no expression of histone-RFP in the nucleus (white circle in Fig. 3.19A). On the other hand, the cells which had not conducted the flippase mediated recombination had one copy of histone-RFP expression heterozygously (white asteroid in Fig. 3.19A). From the brightness of the nucleus, one was able to distinguish the RNAi expression cells from the wild type cells.

Here, one wild type cell (white circle in Fig. 3.19A) underwent apoptosis with one of its neighbors expressing myosin RNAi (white cross in Fig. 3.19A). As the control, one wild type LEC (white asteroid in Fig. 3.19A) with all of its neighbors in wild type also underwent apoptosis at the similar timing. The results showed that compared with the control cell, the cell with *sqh* RNAi neighbour completed the apical constriction much slower (Fig. 3.19B). In addition, contour plots of the apoptotic cell in Fast Phase indicated that the cell constrict more towards the posterior side (Fig. 3.19C right part). However, the

contour plots of control cell in Fast Phase is self-similar (Fig. 3.19D right part). Considering the myosin knock-down neighbour on the posterior side of the apoptotic LEC, the results indicated that the disruption of part of the outer actomyosin ring may lead to the broken of self-similar constriction in Fast Phase.

To confirm the results, I conducted the statistical analysis to compare the behavior of apoptotic LEC with *sqh* knock-down neighbors to the wild type cells with all wild type neighbors. Results showed that while the apical area of the cells when they enter the Fast Phase are not significantly different ($p = 0.056$. 620.87 ± 49.61 μm^2, n = 20 from 11 animals, for control cell and 427.41 ± 54.29 μm^2, n = 6 from 4 animals, for apoptotic LECs with *sqh* knock-down neighbour. Shown in Fig. 3.19E right panel), the duration of Fast Phase are significantly elongated compared with the wild type cells ($p < 0.05$, 43.00 ± 2.14 min, n = 20 from 11 animals, for control cell and 55.00 ± 6.15 min, n = 6 from 4 animals, for apoptotic LECs with *sqh* knock-down neighbour. Shown in Fig. 3.19E middle panel). In addition, the maximum speed of apical constriction, which is measured by d_{Area}/ d_{Time} is also significantly decreased compared with wild type cells ($p < 0.05$, 20.95 ± 2.09 μm^2/ min, n = 20 from 11 animals, for control cell and 12.17 ± 1.44 μm^2/ min, n = 6 from 4 animals, for apoptotic LECs with *sqh* knock-down neighbour. Shown in Fig. 3.19E left panel).

These results in together indicated that knocking down of myosin in neighbors to attenuate the neighboring ring results in the deceleration of apical constriction. In other words, the neighboring ring is important to completes the apical constriction in time, and punctually extrude the apoptotic cell.

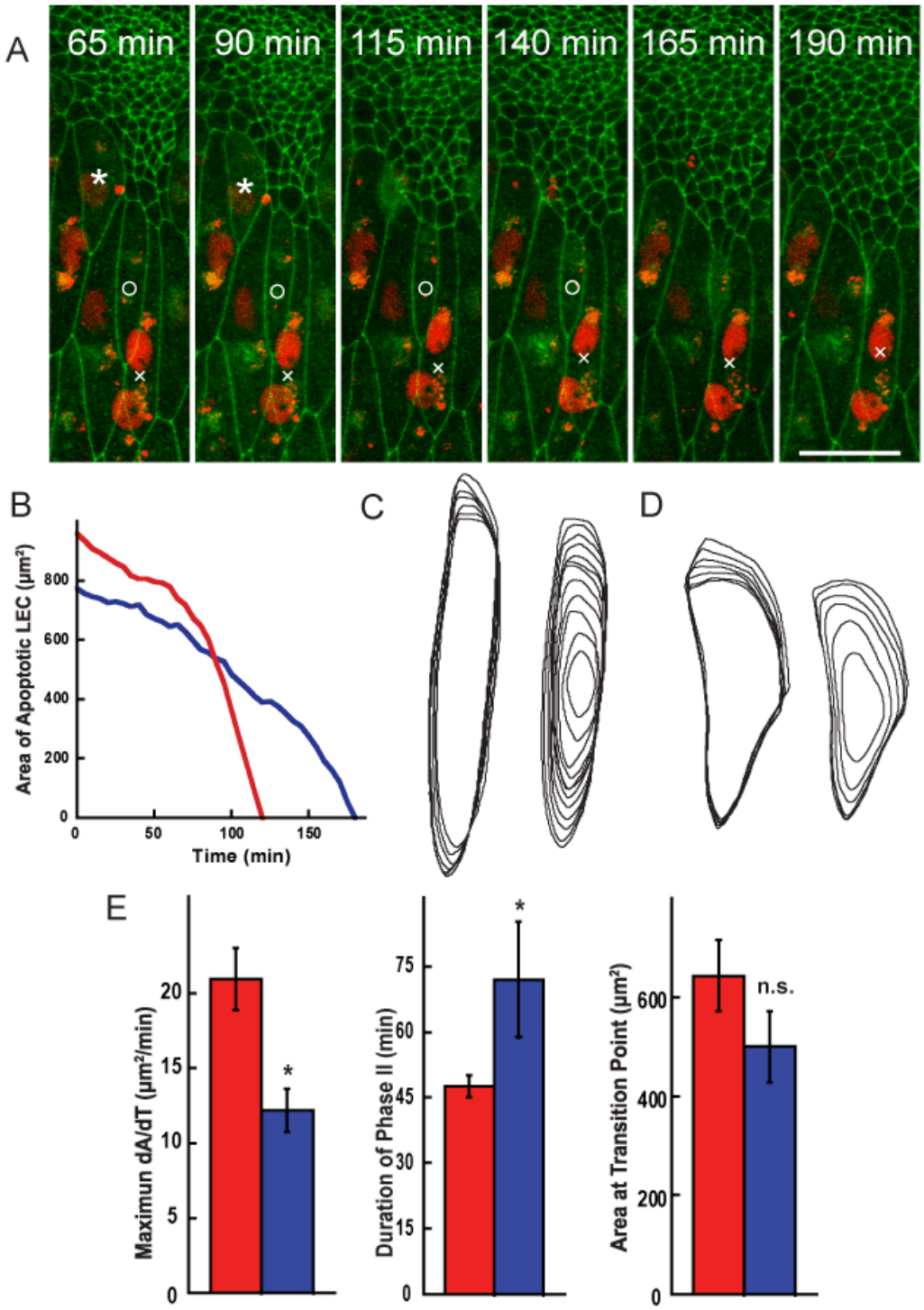

Figure 3.19 *Sqh* knock down in neighbour slows down apical constriction
(A) Time lapse images showing the apical constriction of target LEC (marked with circle) with *sqh* knock down by RNAi in one of the neighboring cells (marked with cross), and the apical constriction of control LEC (marked with asteroid). RNAi positive cells have much brighter nucleus with double copy expression of nucleus-RFP. Length of scale bar: 40 μm. See Movie 14. (B) Quantification of surface area dynamics. Control cell (red curve) finishes apical constriction much earlier than the target cell (blue curve). (C) Contour plots showing the ell shape change of the target cell in Slow Phase (left) and Fast Phase (right). The target cell deforms in the directional way in Fast Phase. (D) Contour plots showing the ell shape change of the control cell in Slow Phase

(left) and Fast Phase (right). The control cell deforms in the self-similar way in Fast Phase. (E) Statistical analyses between the control apoptotic LECs and the apoptotic LECs with *sqh* knocking down neighbour. Mean area at transition point for control cells (red column in right panel) is 620.87 ± 49.61 μm^2 (n = 20 from 11 animals). Mean area at transition point for target cells (blue column in right panel) is 427.41 ± 54.29 μm^2 (n = 6 from 4 animals). They are not significantly different (p = 0.056). Meanwhile, the target cells have longer duration of Fast Phase (55.00 ± 6.15 min, n = 6 from 4 animals, blue column in middle panel) compared with control cells (43.00 ± 2.14 min, n = 20 from 11 animals, red column in middle panel). The difference is significant ($p<0.05$). Besides, the target cells have slower maximum constriction rate (20.95 ± 2.09 μm^2/ min, n = 20 from 11 animals, blue column in left panel) compared with control cells (12.17 ± 1.44 μm^2/ min, n = 6 from 4 animals, red column in left panel). The difference is significant ($p<0.05$). *: $p<0.05$; n.s.: not significant.

3.4.4 Disruption of inner actomyosin cable

To investigate the role of inner ring, I also conducted the clonal expression to express the *sqh* RNAi only in the apoptotic cell to knock down the myosin in the apoptotic cell and attenuate the inner ring. However, there were very few examples to show the single isolated cell expressing myosin RNAi. Here was one example: the cell marked with asteroid expressed the myosin RNAi (Fig. 3.20A), which was indicated by the bright expression of histone-RFP in the nucleus (Fig. 3.20B). While the cell was fast constricting in its apical area at the beginning of the movie (Fig. 3.20A 0 & 40 min), the constriction rate slowed down (Fig. 3.20A 40-120 min). Analysis of the apical area over time indicated the decreased constricting rate, and the constriction almost ceased in the late stage (Fig. 3.20C). The contour plot of the cell confirmed the slowdown of apical constriction (Fig. 3.20D): the contours in the centre (cell shapes in the late stage of the movie) are much condensed compared with the contours in the outer region (cell shapes in the beginning of movie).

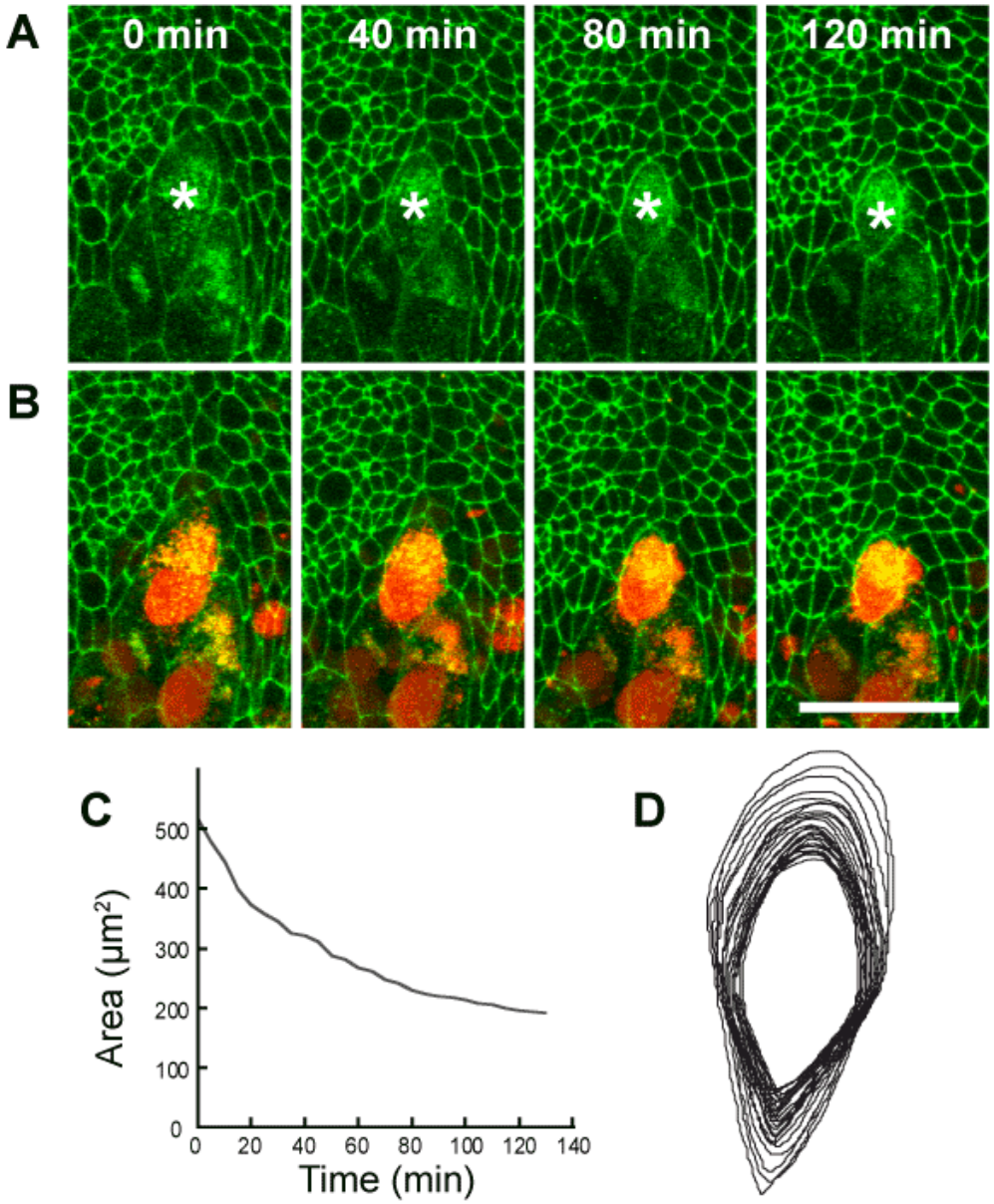

Figure 3.20 *Sqh* knock down in the LEC impedes its apical constriction
(A) Time lapse image showing the constriction of *sqh* knock down cell (marked with asteroid). Duration is 2 hours. (B) The same image overlapped with nucleus-RFP. The RNAi positive cell has much brighter expression. Length of scale bar: 40 μm. See Movie 15. (C) Apical surface area dynamics of the RNAi positive cell. (D) Contour plots showing the cell shape change of the RNAi positive cell.

3.4.5 Multiple apoptotic cell extrusion

The apoptotic events is one of the major events happened during histoblast expansion. All of the LECs will undergo apoptosis during the process and replaced by the histoblasts. Interestingly, sometimes neighboring LECs undergo apoptosis at the similar timing. To better understand the role of actomyosin purse string during apoptosis, I investigated the multi-cellular apoptosis. Two apoptotic LECs shared one boundary (Fig. 3.21 & Movie 16). Before the ring separation, the shared boundary was constricted much more than other boundaries (two opposing white arrowheads, Fig.3.21A 0&35 min). On the other hand, the histoblast neighbors generated the very sharp tip toward the boundary with very low myosin accumulation (white arrowheads in Fig. 3.21B 35 min, the cell boundary surrounding the two cells is shown by red line in Fig. 3.22A), which may indicate the contraction force before ring separation mainly comes from the boundary from the apoptotic LECs. When the two ring separated, which was the indication of AJ disengagement, the tip of the histoblast neighbors retracted back (white arrowheads in Fig.3.21A 40 min, also shown by the cell boundary surrounding the two cells in Fig. 3.22A). This retraction was the indication of junctional tension release when AJ disengages. After the ring separation, the outer ring accumulates in myosin, and simultaneously, the outer ring is smoothened (white arrowheads in Fig. 3.21A 45&50 min, illustrated in Fig. 3.22 D&E). This indicates the corporation of two parts of outer ring. In the end, the supra-cellular actomyosin purse string finished the apical constriction of the both apoptotic LECs (Fig. 3.21 65 min & Fig. 3.22F).

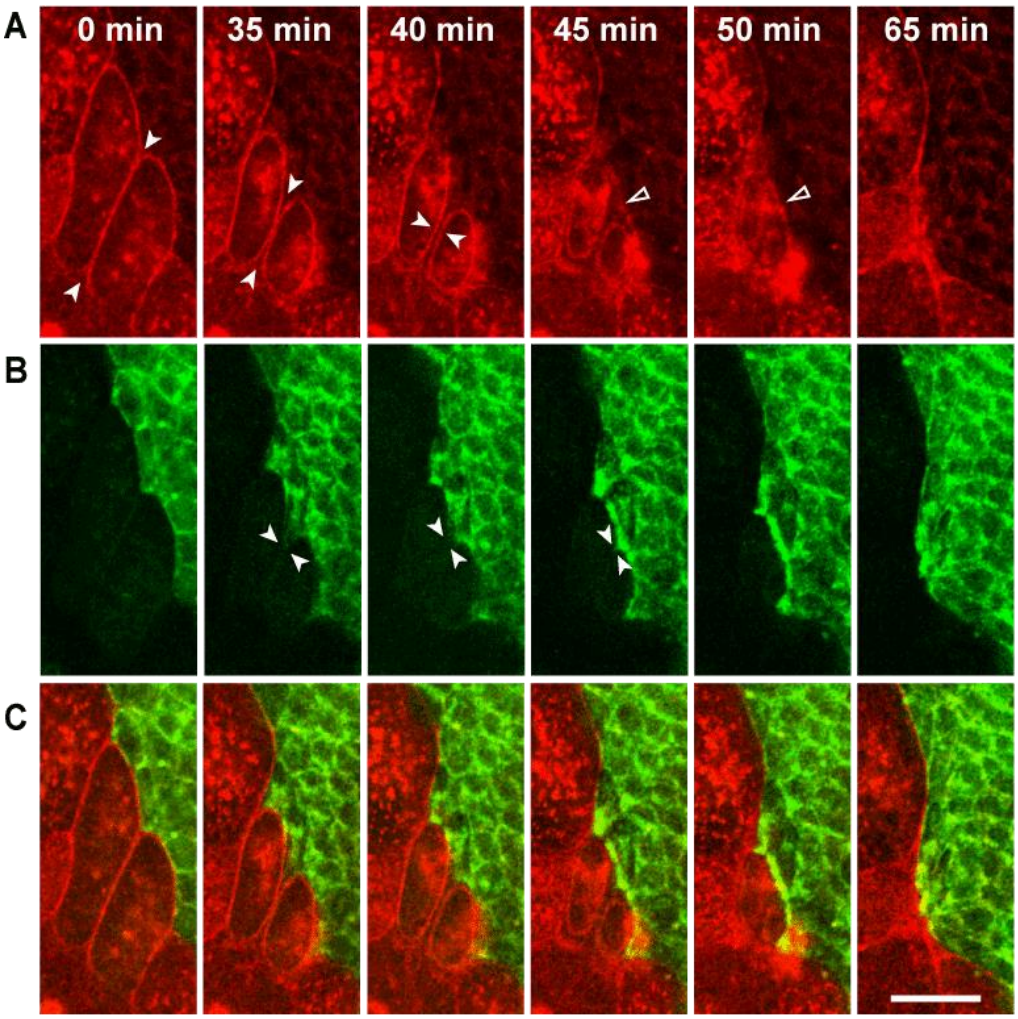

Figure 3.21 Supra-cellular actomyosin ring drives the multi-cellular apoptotic extrusion

Two LECs underwent apoptosis at the similar timing. *UAS*-sqh-GFP was specifically expressed in histoblasts under *esg*-Gal4, and sqh-cherry was ubiquitously expressed with the endogenous promoter. Before myosin ring separation, the junction shared by two apoptotic cell constricts faster than other boundaries (A, 35&40 min, indicated by two arrowheads), and the connecting boundary from histoblast neighbour was elongated with low myosin expression (B, 35 min, indicated by two opposing arrowheads). When myosin rings separated, the boundary tip from histoblasts retracted (B, 40&45 min, indicated by two arrowheads), and a supra-cellular myosin purse string was formed surrounding the two inner rings from the apoptotic LEC (A&C, 45&50 min, indicated by empty arrowheads). In the end, the supra-cellular purse string completed the apical constriction (A-C, 65 min). Length of scale bar: 20 μm. See Movie 16.

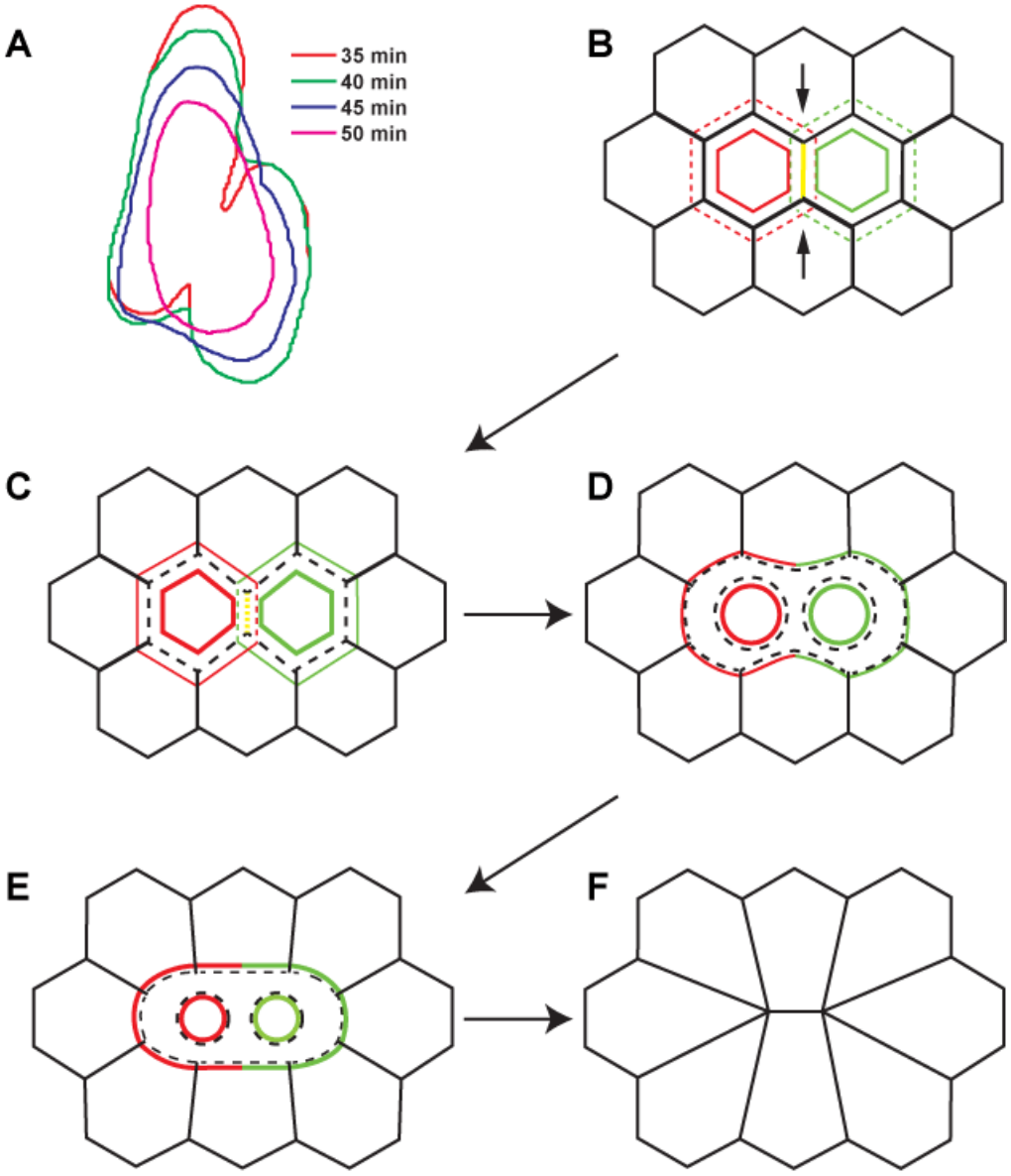

Figure 3.22 Schematic illustration of the multi-cellular apical constriction
(A) Cell shapes of the two apoptotic cell in Fig. 3.20 & Movie 16 at time point 35, 40, 45 and 50 min are shown as contour plot in red, green, blue and magenta, respectively. (B-F) Schematic illustrations of the constriction. Inner myosin rings in two cells are represented in red and green lines (B-E). Dashed red and blue lines indicate the weak outer ring before rings separation (B). Yellow line indicates the faster constricted boundary shared by both apoptotic cell (B, indicated by two opposing arrows). When rings separate, the AJ disengages (C-E, dashed black lines). The outer ring of two apoptotic cell reorganized, and fused (D-E). In the end, the two inner rings and the supra-cellular purse string together completes the constriction (F).

Chapter IV: Discussion and Conclusion

4.1 Contributions of apoptotic force in histoblast expansion

4.1.1 Mechanical contribution of apoptosis to developmental processes

It is still under debate how much apoptotic force could contribute to development during *Drosophila* dorsal closure, while it has been proved to be essential for development processes to occur in time (Gorfinkiel et al., 2009; Toyama et al., 2008). Besides, whether mechanical role of apoptosis is limited to only dorsal closure, or as predicted, the apoptotic force could help other developmental processes is not very clear (Teng and Toyama, 2011). Here, my study showed the mechanical contribution of apoptosis to histoblast expansion, which is a strong support for the global appliance of mechanical role of apoptosis to development and tissue dynamics. As pointed out in the pioneer study, apoptotic force could be an important source of mechanical forces for the organism development during evolution (Toyama et al., 2008). Taking advantage of the force generated during apoptosis could be more economic throughout evolution.

While it is demonstrated the contribution of apoptotic force to development, whether the effects of apoptotic force are local, that means supra-cellular level, or in the tissue level has not been clearly studied previously. Here, my study showed that not just the direct neighbour of the apoptotic cells could be stretched, but also the non-directly contacting cells are elongated (Fig. 3.2 & Movie 3). In addition, the tissue level quantitative analysis revealed the tissue level mechanical contribution of apoptosis. My results indicate that the apoptotic force, which is one type of mechanical force generated by the organism, could propagate through the tissue and the effects are in the tissue level. On the other hand, this tissue level effects then feedback to play a role as

the extrinsic force to influence the migration of histoblasts, and contributes to tissue dynamics.

4.1.2 Mechanical contribution of apoptosis to tissue tension homeostasis

While the force generated during apoptosis contributes to the histoblast expansion, which is one of the developmental processes, in the mechanical aspect, the force also contributes to the tissue tension homeostasis. My results showed that the tissue tension is released upon the AJ disengagement (Fig. 3.13 & Fig. 3.14). Meanwhile, the supra-cellular actomyosin purse string, or the outer ring starts to accumulate in the neighbors surrounding the apoptotic LEC (Fig. 3.17 & Fig. 3.18). The contraction of the actomyosin rings generate the mechanical force, which rebuilds the tension inside the tissue (Fig. 3.14). At the late stage of outer ring contraction, the tissue tension is recovered from AJ disengagement, and is even higher than control (Fig. 3.14). My results showed that the mechanical contribution from apoptosis well maintains the tissue tension homeostasis. Histoblast has been regarded as a type of stem cell, which could differentiate into the sensor organ cells or epithelial cells (Ninov et al., 2007), while mechanical tension has long been shown to be important in stem cell differentiation (Hinz et al., 2001). Interestingly, the tissue tension is significantly higher than the control in the late stage of actomyosin ring contraction mediated apical constriction (Fig. 3.14). From the results, it is clear that the myosin accumulated during apical constriction need to be recycled from the loci of new junction. However, how the myosin recycling occurs and how the process is mediated remains to be discovered.

In further, detailed study of the apoptotic force generation revealed that the process of LEC apoptosis itself is affected by both the intrinsic force and extrinsic force: the force generated by the inner ring, or the intrinsic force, initiates the apical constriction of apoptotic LEC, and the force generated by the neighboring rings, or the extrinsic force, brings together the neighboring cell after the AJ disengagement and maintains the vulnerable tissue integrity (Fig. 3.16- 3.20, Movie 12-15).

4.2 Anchoring of actomyosin rings after AJ disengagement

AJ is one of the key players in maintaining the epithelial tissue integrity. On the other hand, the junctions need to be loosen for the cell to facilitate extrusion. Thus, how AJ is regulated during apoptotic extrusion is one of the major focus for studying apoptosis. Previous study in *Drosophila* embryogenesis reported that in the induced global apoptosis, the Dβ-catenin will be cleaved on the N terminus. The remaining Dβ-catenin stays on the plasma membrane. Meanwhile, Dα-catenin, which is not cleaved, stay on the plasma membrane and DE-cadherin, which is also not cleaved, detach from the cell membrane with unknown mechanism (Kessler and Muller, 2009). In the later stage, the catenins will detach from the membrane. In the end, new junction forms between remaining cells (Kessler and Muller, 2009). Different from previous report, my results showed that the AJ molecules, including DE-cadherin, Dβ-catenin and Dα-catenin are all dissociated from the plasma AJ, and be internalized during the late stage of apical constriction (Fig. 3.5, Fig. 3.6 & Fig. 3.7). One possible explanation for the inconsistency with previous study in Dα-catenin during

apoptosis is that Dα-catenin indeed dissociates from the boundary upon apoptosis as I observed; however, the dissociated Dα-catenin re-distributes to the surface of the cell along with actin as a result of the cytoskeleton remodelling during apoptosis. As a consequence, the Dα-catenin seems not detached from the cell membrane.

This disengagement occurs at the junction between the apoptotic LEC and its neighbors, which means, not just the AJ molecules in the apoptotic cell are dissociated from the boundary, but also the AJ molecules from the living neighbors. Meanwhile, the outer actomyosin ring start to accumulate inside the living neighbors. The most straight-forward questions would be: Where the two actomyosin rings are anchored while the AJ disengages? Whether and how they are constricted?

4.2.1 Actomyosin purse string in neighboring cells

To start, I would like to discuss on the anchoring of outer ring. First of all, while the AJ disengages in the living neighbors, which is represented by the attenuation in the intensity of fluorescent protein tagged junctional molecule, it is not fully eliminated. On the nascent edge of the neighboring cells, which is next to the junctional gap, there is still weak AJ molecules remaining there (Fig. 3.5, Fig. 3.6 & Fig. 3.7). In fact, there is a similar process occurred during cytokinesis. During cell cytokinesis, the E-cadherin will be down regulated in the septin required manner at the furrow zone between dividing cell and its neighbors (Founounou et al., 2013; Guillot and Lecuit, 2013; Herszterg et al., 2013). In *Drosophila* embryonic ectoderm cells, this down regulation of E-

cadherin and the constriction of cytokinesis actomyosin ring together resulted in the disengagement of AJ between the dividing cell and its neighbors at the furrow zone. Yet, the remaining E-cadherin in the neighboring cells still manage to keep the cortical actomyosin along the AJ belt (Founounou et al., 2013; Guillot and Lecuit, 2013; Herszterg et al., 2013). Similarly, during late stage of apoptosis, the remaining AJ molecule, which is not functioning well to maintain the tissue integrity and a gap is formed accordingly, could still function well to anchor the actomyosin purse string. Indeed, my data showed that the actomyosin purse string colocalizes with the weak remaining AJ (Fig. 3.9, Fig. 3.10 & Fig. 3.11).

Besides, according to the way of linkage between AJ and actin filaments, the AJ could be categorized into two types: linear AJ, which is also called zonula adherens, and punctate AJ (Takeichi, 2014). In mature epithelial tissues, actin filaments are parallel to the plasma membrane, and perpendicular to the AJ. This is the linear AJ, which is linearly distributed along the plasma membrane. For the cultured cells on the colony edge, their AJs are in the punctate morphology, and the actin filaments are perpendicular to the plasma membrane and pull the AJs. This is the punctate AJ. Linear AJ and punctate AJ have been reported to be interchangeable (Taguchi et al., 2011). During the late stage of apoptosis, when the AJ disengages, punctate accumulation of DE-cadherin and Dβ-catenin is observed at the nascent edge of the neighbors (Fig. 3.9, Fig. 3.10 & Fig. 3.11). Meanwhile, the actomyosin purse string seems to be linked (colocalized) through the punctate DE-cadherin and Dβ-catenin. While the transition between linear AJ and punctate AJ still remains an open question in LEC apoptosis, the

colocalization of actomyosin ring and punctate AJs in the Late Fast Phase could answer the question of where the actomyosin ring is in fact located.

Combining the above two scenarios described, the actomyosin purse string formed inside the living neighbors could anchor on both the punctate AJ and the disengaged, yet remaining linear AJ. By pulling perpendicular against the plasma membrane through the punctate AJ, the actomyosin purse string is able to generate the mechanical force.

4.2.2 Actomyosin ring in apoptotic cell

When it comes to the inner actomyosin ring, things are more complicated. I would like to remind two facts before the discussion:

1. The tissue tension is released upon AJ disengagement.
2. The inner actomyosin ring keeps constricting after ring separation.

From Fact 1, one could infer that the tissue tension along the junction is still maintained before AJ disengagement, and this tension is released upon the disengagement. From Fact 2, one could infer that the inner actomyosin ring itself is still constricting even after AJ disengagement. But whether this constriction could have the mechanical output? In other words, is the inner ring still anchored to the plasma membrane after AJ disengagement? In vitro study of extracted cytokinetic actomyosin ring from fission yeast showed the ATP dependent ex vivo constriction without plasma membrane (Mishra et al., 2013). In fact, after the AJ disengagement, the AJ molecules are not sharp enough to tell exactly where the boundary of apoptotic cell is. In addition, the fluorescent protein tagged AJ molecules are not representative for the location of plasma

membrane anymore. To answer this question, I conducted an additional experiment using spider-GFP. Spider is one of the widely used membrane marker in *Drosophila*. By coexpressing ubiquitous spider-GFP and sqh-cherry under the endogenous promoter, I found that in the earlier phase before ring separation, the spider and sqh colocalize well (Fig. 4.1A). After ring separation, similarly as the E-cadherin results, inner ring colocalizes with the condensed inner apoptotic cell, while the outer ring colocalizes with the nascent edge of neighboring cells (Fig. 4.1B). These results indicated the inner actomyosin ring is still anchored to the membrane after AJ disengagement.

The next question is how the inner ring is anchored, which is largely unknown. One possibility is that, while AJs disengage from the plasma membrane of apoptotic cell, they are not devoid. The remaining AJs could still support the anchoring of the inner actomyosin ring. In fact, there is a highly stable pool of AJs called Spot AJs residing at the plasma membrane (Cavey et al., 2008).

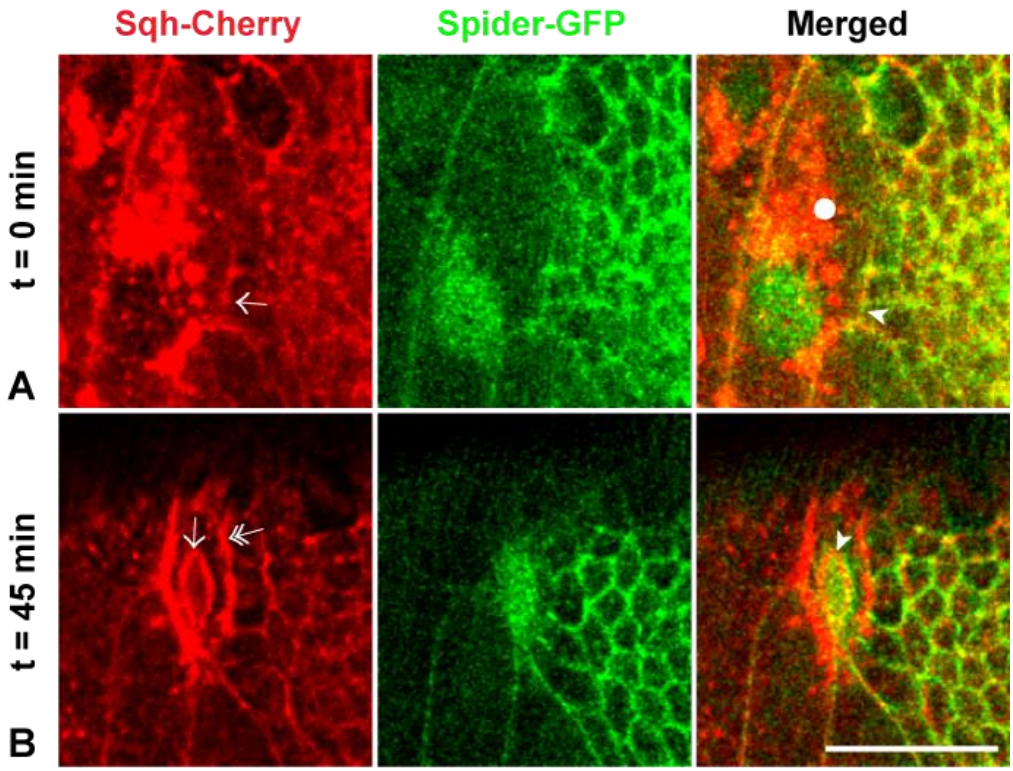

Figure 4.1 Inner actomyosin ring colocalize with membrane marker
(A) Myosin ring (indicated with arrow in RFP channel) and membrane marker (spider-GFP) colocalized well in the early stage (indicated with arrowhead in merged channel). Cell of interest is marked with circle. (B) When the myosin rings separate, the membrane marked from apoptotic LEC colocalized with the inner ring (single arrow in B, RFP channel, and arrowhead in B, merged channel), but not the outer ring. Length of scale bar: 20 μm.

4.3 Role of two actomyosin rings in apoptosis

Pioneered study on cultured cell revealed the roles of two actomyosin rings during apoptosis in MDCK cells by injecting the Rho GTPase inhibitor- C3 toxin into the living neighbors or the apoptotic cell. They concluded from the results that the inner ring formed inside the apoptotic cell is dispensable for extrusion while the supra-cellular actomyosin purse string formed in the neighbour cells is essential for the extrusion (Rosenblatt et al., 2001). Interestingly, recent study of epithelial cell extrusion in MDCK cultured cells have different opinions, although it is not apoptotic extrusion (Kuipers et al., 2014). They first of all identified two different phases during extrusion of MDCK cells: the early apical constriction phase, and the later apical extrusion phase. They inhibited the RhoA activity in the extrusion cell, with which only 50% of the cells could finish the apical constriction phase. On the other hand, while they inhibited RhoA activity in all the neighbors, apical constriction phase could finish as usual. Further numerical modelling confirmed that the inner ring itself is sufficient to facilitate the apical constriction phase (Kuipers et al., 2014).

Here, my data answered the question in the in vivo manner. I knocked down myosin regulatory light chain, *sqh* in LECs by clonal expression. Statistical analysis showed that knocking down the myosin in neighboring cells results in the longer Fast Phase, and slower constriction speed. But all the apoptotic LECs succeed in finishing the extrusion. The results indicated that the attenuation of neighboring ring will slow down the apical constriction rate, but will not totally block the extrusion. Different from previous in vitro studies, my results indicate that the neighboring ring do contribute to the apical constriction and is essential

for controlling the apoptosis timing, but is not essential for completing the extrusion.

On the other hand, the data I have showed that knocking down of myosin in the LEC only will result in the failure of extrusion. The myosin knock down cell decreased in the constricting speed and stop the constriction in the end, which further indicated that inner actomyosin ring is essential for the initiation of apical constriction. This result is consistent with the recent study which showed that the inner actomyosin ring is essential for constriction phase, which is the early phase, in MDCK cell extrusion. They also commented that the conclusion of previous study that the inner actomyosin ring is dispensable may be the result of inhibition of Rho GTPase in late phase of apoptosis, which is the apical extrusion phase. In this phase, the inner ring may be not essential (Kuipers et al., 2014).

Besides the knocking down experiments as a way to perturb, one could also investigate the role of two rings through their spatial-temporal expression pattern. My quantitative analysis results from tissue specific expression showed that the inner ring start to accumulate from Slow Phase and Fast Phase transition (Fig. 3.15 & Fig. 3.17). The myosin intensity of the inner ring continue to accumulate during Fast Phase. On the other hand, the outer ring start to accumulate in intensity only around the separation of two rings, or the disengagement of AJs. After the disengagement, which I called the Late Fast Phase, the intensity of outer ring increases in the intensity dramatically (Fig. 3.16 & Fig. 3.17). Combining these results, it seems to be more favourable for me that the inner ring activates during the Slow Phase and Fast Phase transition, and the apoptotic cell start to constrict itself and pull the neighbors. Once the

AJs disengages during Late Fast Phase, the outer actomyosin purse string start to accumulate inside the living neighbors and fill in the gap left by the apoptotic cell. At this moment, the inner ring is still constricting and contribute to apical constriction of apoptotic cell. Whether inner ring constriction contribute to large scale tissue dynamics after the AJ disengagement remains an open question.

4.4 Mechanism of actomyosin ring formation in neighboring cells

The mechanism of outer actomyosin ring accumulation is still elusive. However, some of my data indicate some possible mechanisms. My data showed the retraction of outer ring and the constriction of inner ring upon AJ disengagement (Fig. 3.13), which indicates the disengagement of AJ suddenly releases the tissue tension surrounding the apoptotic cell. Further results from nanoablation and the quantification of boundary linearity confirm that the tissue tension is released during AJ disengagement, and is rebuilt during the late constriction (Fig. 3.14). Interestingly, during the AJ disengagement, while the tissue tension is released, the outer ring also starts to accumulate at the similar time (Fig. 3.17& Fig. 3.18). It is likely that the tissue tension release upon AJ disengagement may play a role as the trigger for outer ring accumulation. During LEC apoptosis, while the tissue tension is all of a sudden released during AJ disengagement, it could be possible that the neighboring cells may sense the tension release through the mechano-sensors. The supra-cellular actomyosin purse string formation surrounding the apoptotic cell could be the response to the junctional tension release. A number of proteins located at the AJ or focal adhesion have been revealed as mechano-sensors like vinculin, talin, zyxin and

so on (le Duc et al., 2010; Lee et al., 2007; Vogel and Sheetz, 2006). Besides, the cytoskeleton itself could also sense mechanical force and responds to the force (Hayakawa et al., 2011). In fact, tissue tension homeostasis and actomyosin contraction has been reported to be coupled. Previous study working on dorsal closure showed that the subcellular cytoplasm laser perturbation, which will not damage the plasma membrane but disrupt the cellular cytoskeleton, will trigger the delamination of amnioserosa cells (Meghana et al., 2011). The cytoskeleton disturbing induced the tension release in the cell, and the cell expanded. In respond to the tension release, while there is no wound created during the process, myosin II inside the neighboring cells flowed toward the boundary of injured cell, and then facilitated the cell delamination (Meghana et al., 2011).

4.5 Similarity between apoptotic cell extrusion and embryonic wound healing

Wound healing process is a very critical process for the animal to respond to injury. Interestingly, there are many similarities between the epithelial apoptotic apical constriction and the wound healing, especially the embryonic wound healing, which is not involved in the clot formation (Sonnemann and Bement, 2011):

First of all, both of the processes are driven by actomyosin ring contraction. Both the apoptotic apical constriction and embryonic wound healing involves the actomyosin ring formation and contraction to close the gap formed in each process, and to maintain the tissue integrity. In wound healing, actomyosin purse string is formed at the leading edge surrounding the wound region, and

the contraction of actomyosin purse string could lead the migration of the surrounding cells and facilitate wound closure (Sonnemann and Bement, 2011). In apoptotic apical constriction of LEC, when the AJs disengage, there will be a gap formed on the apicolateral sides between the apoptotic cell and the living neighbors. Similar as wound healing, an actomyosin purse string will be formed in the surrounding neighbors, and will fill the gap left by the apoptotic cell.

Second, both of the processes involve the mechanical tension release. When a wound is created in epithelial tissues, previously balanced mechanical tension inside the tissue will be suddenly released. This mechanical signal could trigger the status adjustment of ion channels on the membrane, which is responsible for the calcium influx during wound initiation (Cordeiro and Jacinto, 2013). While previously not reported, my results showed that upon the AJ disengagement, similar as wound healing, the pre-balanced mechanical tension will be suddenly released. No doubt, this tension release could be the mechanical signal which has long distance effects. Whether this signal could trigger the actomyosin ring formation needs further study.

Besides, both wound healing and apical constriction could elongate the neighboring cells. In wound healing, the actomyosin purse string will contract the tissue towards the wounding site, and the cells at the wound edge are elongated, which will further reduce the area of wound. Similarly, in apoptosis, my data showed that the apoptotic cell will elongate its directly contacting neighbors, and also the non-contacting neighbors, which confirms the tissue level mechanical effects of apoptosis.

While embryonic wound healing and apoptotic apical constriction share many similar processes, one of the major difference between them is the cell

protrusion. Cell protrusion is essential for embryonic wound closure. Upon wound creation, actin rich protrusions, including lamellipodia and filopodia will form at the wounding edge together with actomyosin purse string. More generally, while there is new gap formed inside the cultured cell sheet, which is not necessarily a real "wound", cells will close the gap through both actomyosin purse string contraction and lamellipodia formation (Anon et al., 2012). In apoptosis, the formation of lamellipodia and filopodia has not been reported yet. Interestingly, here in LEC apoptosis, my data suggested the gap will be formed in the apical side between the big apoptotic cell and the living neighbors in the late stage of apical constriction. Whether the actin rich protrusions will help the gap closure is still an open question. Although there is not much data to support the hypothesis, some of my preliminary data do suggest the potential participation of lamellipodia and filopodia in apoptotic extrusion.

For example, in some of the apoptotic cells, in the late stage of apoptosis, the actomyosin ring seems to be fused in the centre, which created two connecting actomyosin rings in the "8" shape (Fig. 4.2 A&B, 10-20 min, Movie 17). These two rings then contract and completes the apical constriction (Fig. 4.2 A&B, 25 min, Movie 17). These data suggest the potential participation of filopodia at least in the late stage of apoptosis. The filopodia may be generated by the opposing neighbors. These neighbors may fuse with each other and reshape the actomyosin ring like the zippering process during dorsal closure.

On the other hand, preliminary data from tissue specific expression showed that the lamellipodia may be generated and participate in the apical constriction (Fig. 4.3, Movie 18). Before the AJ disengages, boundary of moesin from histoblast specific expression colocalize with the AJ boundary at the tissue interface (Fig.

4.3 A to D, 0 min). My previous data showed that upon AJ disengagement, the outer actomyosin ring will colocalize with the nascent edges of the neighboring cells, which are characterized by the punctate accumulation of AJ molecules (Fig. 3.9, Fig. 3.10 & Fig. 3.11). However, the results from tissue specific expression of cherry-moesin, which is the satellite protein for F-actin, showed the accumulation inside the nascent edges of the neighbors after AJ disengagement. These actin-rich protrusions co-exist with the actomyosin ring structure formed inside the neighbors (Fig. 4.3 A-D, 10 to 20 min). When the apical constriction completes and new AJ is formed between the remaining cells, the protrusions are diminished (Fig. 4.3 A-D, 35 min). However, the data is low in time resolution and cannot show the dynamics of lamellipodia, and the image quality is also not good enough to resolve the stereotypic microspikes. Still, I think it is a good starting point and worth further study.

Lamellipodia is usually generated at the front of migrating cell, and is an indication of cell migration. If the cells want to migrate, firstly they need to adhere. In fact, for histoblasts and LECs, besides the ECM at the basal, there is also a layer of cuticle sitting at the apical surface (Ninov et al., 2007). Besides, with the paracrine effects of Dpp signal from boundary LECs, the boundary histoblasts do not have β-integrin at the basal part of the cell (Ninov et al., 2010). The ECM for histoblasts will be degraded around 26h APF. It is further reported that they adhere to the cuticle apically through actin-rich villa to facilitate the migration (Ninov et al., 2010). Consistently, opposite from the normal migrating cell, which generates the lamellipodia in the basal part, here the potential lamellipodia is generated at the very apical part of the histoblasts.

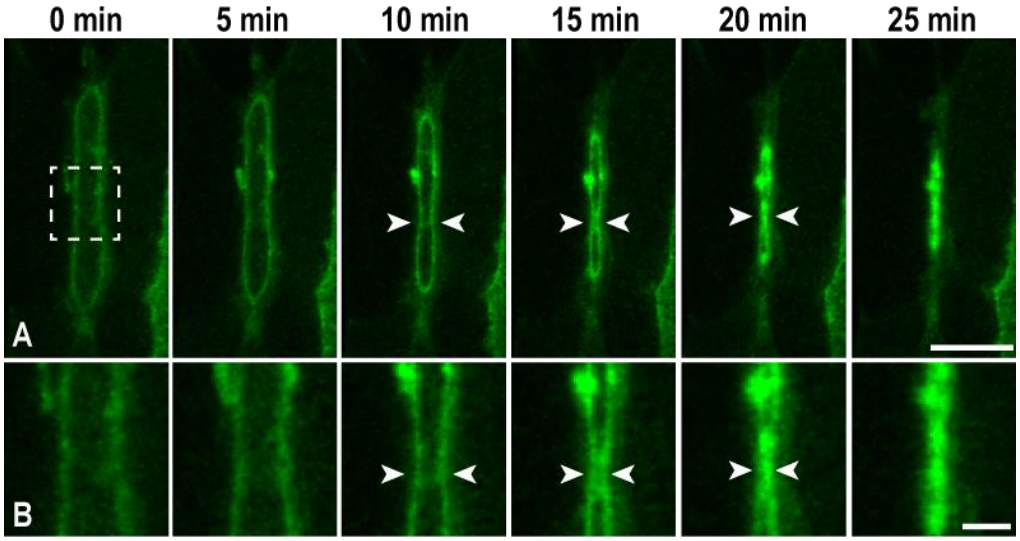

Figure 4.2 "8" shape actin ring is formed in the late stage of apoptosis
(A) Time lapse images showing the apical constriction of LEC in the late stage of apoptosis. F-actin is visualized by lifeact-GFP. The dashed square region from A is zoomed in (B). Ring started to fuse in the central part (A&B, 10-20min, indicated by opposing arrowheads). In the end, the ring completed the constriction as a line (A&B, 25 min). Lengths of scale bars: 20 μm in A, and 5 μm in B. See Movie 17.

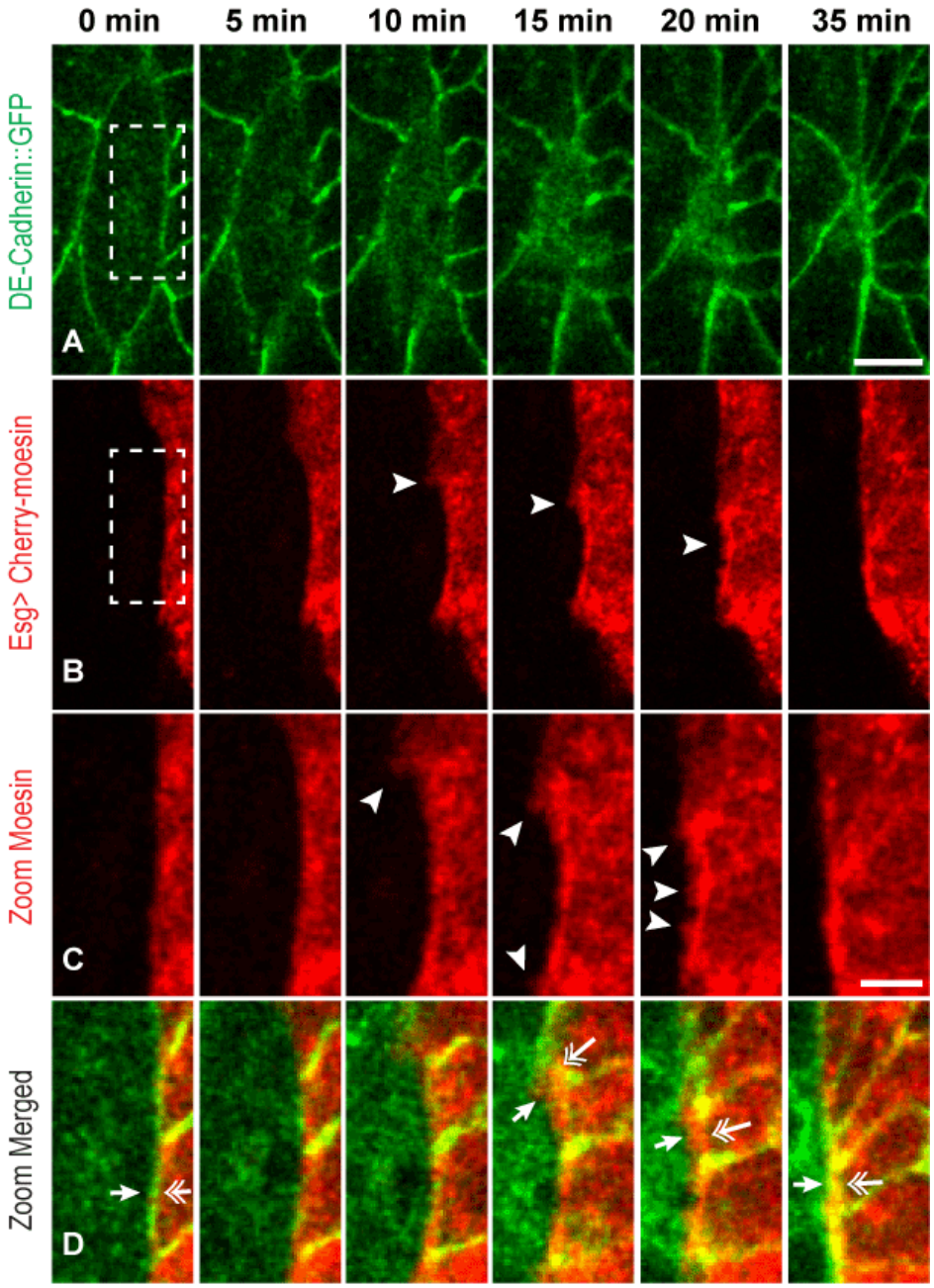

Figure 4.3 Actin-rich protrusion is formed in the leading edge of neighboring cells during late stage of apoptosis

Endo-DE-cadherin::GFP was ubiquitously expressed under the driven of endogenous promoter. Moesin-cherry was expressed specifically in histoblasts to visualize F-actin. C&D are the zooming of the dashed region. Before AJ disengagement, the moesin from histoblasts neighbour colocalized well with AJs (D 0 min, arrow indicates the boundary of moesin, double-headed arrow indicates the boundary of AJ). After the AJ disengagement, protrusions start to form at the edges of histoblasts (A-D, 10-20 min, indicated by arrowheads). The protrusions localized inside the actin ring formed by histoblast neighbors (D, 10-20 min, protrusions are indicated with arrows and actin rings are indicated with double headed arrows). Moesin and AJ colocalized again after the apical constriction finished (D, 35 min). Length of scale bar: 10 μm in A, 5 μm in C. See Movie 18.

4.6 Conclusions

In summary, the following conclusions could be drawn based on my results: (1) the apoptotic process of LEC could mechanically contribute to the histoblast expansion process. (2) The force generation is the spatial-temporal coordination of both the intrinsic ring contraction and extrinsic ring contraction, which also contributes to the maintenance of tissue integrity and tissue tension homeostasis. (3) Tissue integrity during apoptosis is maintained by septate junction while the AJ is disengaged.

Besides, the model of apoptotic events is summarized here to better describe the timing sequence of apoptosis (Fig. 4.4): while there is no clear boundary for the beginning of apoptosis, I first quantitatively separated the apoptosis into two distinct phases: Slow Phase and Fast Phase (see Chapter 2.4.1 for more details). The transition from Slow Phase to Fast Phase is not just the transition of apical constriction rate, but also the beginning of the accumulation of inner actomyosin ring. Ahead of the transition, or in Slow Phase, the caspase-3, the executive protease of apoptosis, has already been activated, and keeps increasing in the activity. Caspase-3 has powerful downstream mechanical effectors like ROCK and LIMK, which activate the myosin activity and reorganize the cytoskeleton, and later drive the apical constriction of the apoptotic cell. Upon the transit to Fast Phase, the actomyosin ring is firstly accumulated in the apoptotic cell, and constrict the apoptotic cell, while the neighbors are now pulled by the apoptotic cell. The intrinsic force plays the key role at this moment. When the activity of caspase-3 reaches the highest, the AJs between the apoptotic cell and the neighbors are disengaged and a gap is formed between the apoptotic cell and the neighbors, which is another milestone for apical constriction. Here I in

further divided the Fast Phase into Early Fast Phase, when the AJ is still intact and outer ring hasn't accumulated yet, and Late Fast Phase, when the AJ is disengaged and outer ring forms. Due to the disengagement, the tissue tension is released, and the boundaries connecting to the apoptotic LEC are wiggled. Meanwhile, the AJ molecules accumulate in the punctate manner at the sides of the nascent edges of the neighboring cells, and the actomyosin purse string starts to accumulate surrounding the apoptotic cell, which is likely to occur in response to AJ disengagement. The purse string and the inner ring together, constrict the apoptotic cell and filling the gap. As a result of the constriction, the tissue tension is rebuilt and the tension homeostasis is maintained. While there is no clear evidence to show the inner ring constriction could mechanically contribute to the neighbors without AJs, at least the supracellular purse string here plays the role as extrinsic force to facilitate the gap closure. Disruption of the outer ring will significantly slow down the apical constriction, while the inner ring could be essential for the initiation of apoptotic constriction. Potentially, the filopodia and lamellipodia may also play a role here to close the gap left by the apoptotic cell in Late Fast Phase. Last but not the least, throughout the whole process, while the AJs are disengaged at the beginning of Late Fast Phase, the septate junction remains intact and keeps the tissue integrity.

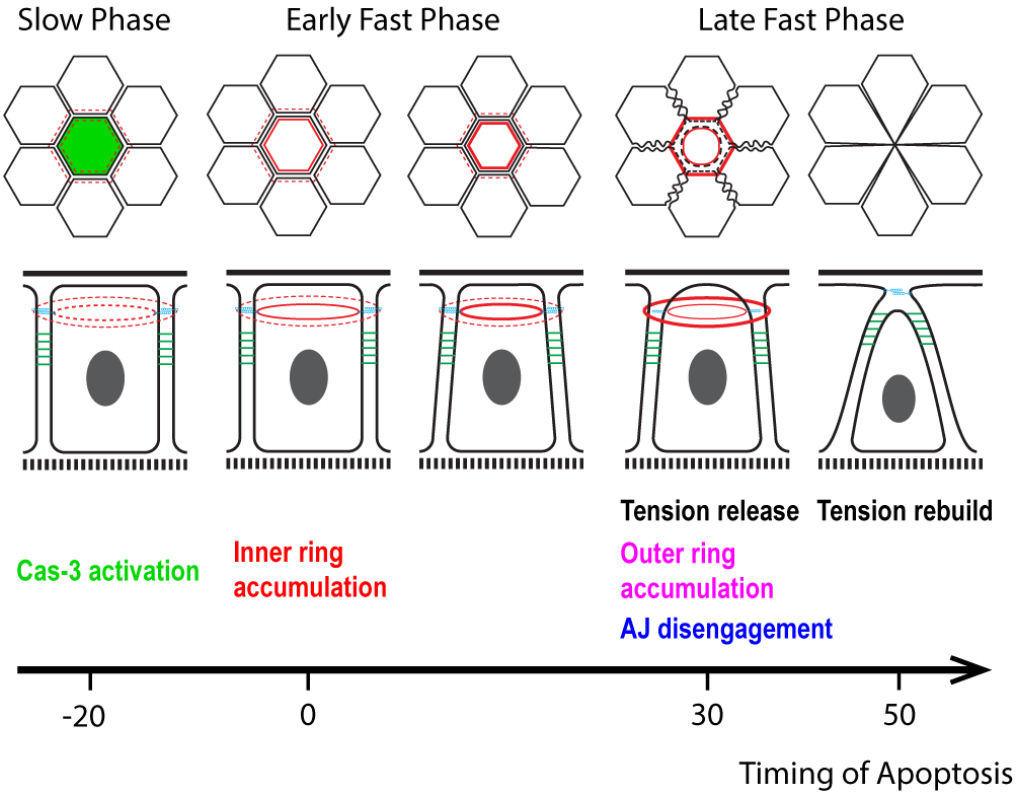

Figure 4.4 Overview of the timing of apoptotic events

Schematic illustration which mapped the events occurred in the axis of apoptosis timing. Whole apical constriction was separated with Slow Phase, Early Fast Phase and Late Fast Phase. Caspase-3 is activated inside the apoptotic LEC from proenzyme Slow Phase (green color), which occurs around 20 minutes before apoptotic LEC enters the Fast Phase. At this period, neither the inner ring nor the outer ring is accumulated (both indicated with red dashed lines). Inner ring starts to accumulate during the transition from Slow Phase to Early Fast Phase, which is marked as 0 minute in the axis of apoptosis timing. After that, the inner ring is strengthened and constricts the apoptotic cell in the Early Fast Phase (inner ring indicated with red lines, outer ring indicated with dashed red lines). AJ (blue lines in lateral view) and septate junction (green ladders in lateral view) were intact. AJ is disengaged when apoptosis transits from Early Fast Phase to Late Fast Phase (around 30 minutes in the axis), and the tissue tension is released, which is indicated with wiggled neighboring boundaries. Simultaneously, the outer ring starts to accumulate (indicated with thickened red lines). At this stage, the outer ring and inner ring together constrict the cell. In the end, new AJ forms between remaining cells and the tissue tension is rebuilt as constriction goes on, till the new junction formation. The septate junction remains intact throughout the whole process.

4.7 Future direction

The study in this thesis opens up the following intriguing questions. Here, I list them in the temporal sequence of apoptosis:

Does the lamellipodia involve in the apoptotic cell extrusion?

My preliminary data have suggested the potential involvement of lamellipodia in the late stage of apoptosis, which needs further confirmation in the future. As reported previously, both lamellipodia and actomyosin purse string are generated to close the gap in cultured cells (Anon et al., 2012). If it is further proved the involvement of lamellipodia in the apoptotic apical constriction, it may suggest the evolutionally conserved machinery for gap closure, which may close the gap in the more efficient way and shortening the window period when the tissue integrity has higher chance to be disturbed. Naturally, the subsequent study could be investigation of the function of lamellipodia during the apoptotic apical constriction. In further, LECs are really huge cells. To fill the gap left by the gigantic apoptotic cell, histoblasts might generate the lamellipodia to fill the gap. On the other hand, as neighbors, living LECs are also involved in the process. Whether they also generate the protrusive machinery is an interesting question to be investigated as well. If not, how the cells sense the size of gap and decide the way they adopt for gap closure is even more interesting. Indeed, cultured cell close the gap with different methods depending on the size of the gap (Anon et al., 2012).

How the septate junction is remodelled after the apical constriction?

To be fully extruded, the apoptotic cell has to break the adhesion to its neighbors. During the extrusion of intestinal epithelial cells, it has been reported that the TJ of the neighboring cells will redistribute basally and facilitate the apical extrusion (Marchiando et al., 2011). While my data have shown that the SJ remains intact throughout the apical constriction process of apoptosis, one of the question remains to be answered is when and how the SJ is loosened between the apoptotic cell and its neighbors. By answering this question, I could investigate the role of junctions during basal extrusion, and may shed some light on the knowledge of basal extrusion, which is the starting events of carcinogenesis (Slattum and Rosenblatt, 2014).

How the engulfment of apoptotic cell by haemocytes relates to cell delamination?

My data have shown the importance of apical actomyosin rings and the force generation that drives the apical constriction. However, when the apical constriction completes, the total extrusion process hasn't finished yet. While the circulating haemocytes will engulf the apoptotic body, the cells are still able to be extruded with the inhibition of haemocytes, although the apoptotic body remains not cleared (Ninov et al., 2007). Thus, how the apoptotic cell is fully extruded out remains to be answered. In fact, after apical constriction, the apoptotic cell blebs (Coleman et al., 2001). One possibility could be that the directional apoptotic blebbing towards the basal could drive the basal movement of apoptotic cell. Besides, the formation of new AJs may play a role to seal on

the lateral boundary, which may also contribute to the basal movement of the apoptotic cell. On the other hand, some of the apoptotic cells, like brain cells in zebrafish, show remarkable motility and may migrate from the extruding place (van Ham et al., 2012). Whether these speculations are true or not needs further investigation.

How the contractile machinery is removed?

After the actomyosin rings driven apical constriction finishes, the contractile machinery needs to be recycled to prevent the over-stretching of the tissue, which is essential to reduce the scar formation during would healing. However, how the contractile machinery is recycled is not well studied yet. On one hand, the actomyosin accumulation will disappear when the constriction finished. Thus, the recycling could be mechanical tension related. For example, cofilin, the actin depolymerisation faction, could severe the actin filaments by sensing the tension of the filaments (Hayakawa et al., 2011). On the other hand, the actomyosin removing is temporarily related to new AJs formation. During this process, the punctate AJs anchoring the actomyosin purse string will convert to the linear AJs. This process may lead to the remodelling of the actomyosin in the new boundary. In fact, in vitro studies showed that the AJ formation between cells will trigger the inhibition of RhoA, which may inhibit the actomyosin at the new junction (Maitre and Heisenberg, 2013).

Chapter V References

Aigouy, B., R. Farhadifar, D.B. Staple, A. Sagner, J.C. Roper, F. Julicher, and S. Eaton. 2010. Cell flow reorients the axis of planar polarity in the wing epithelium of Drosophila. *Cell*. 142:773-786.

Anon, E., X. Serra-Picamal, P. Hersen, N.C. Gauthier, M.P. Sheetz, X. Trepat, and B. Ladoux. 2012. Cell crawling mediates collective cell migration to close undamaged epithelial gaps. *Proceedings of the National Academy of Sciences*.

Bershadsky, A. 2004. Magic touch: how does cell-cell adhesion trigger actin assembly? *Trends in cell biology*. 14:589-593.

Bertet, C., L. Sulak, and T. Lecuit. 2004. Myosin-dependent junction remodelling controls planar cell intercalation and axis elongation. *Nature*. 429:667-671.

Bonnay, F., E. Cohen-Berros, M. Hoffmann, S.Y. Kim, G.L. Boulianne, J.A. Hoffmann, N. Matt, and J.M. Reichhart. 2013. big bang gene modulates gut immune tolerance in Drosophila. *Proceedings of the National Academy of Sciences of the United States of America*. 110:2957-2962.

Brock, J., K. Midwinter, J. Lewis, and P. Martin. 1996. Healing of incisional wounds in the embryonic chick wing bud: characterization of the actin purse-string and demonstration of a requirement for Rho activation. *The Journal of cell biology*. 135:1097-1107.

Carlson, S.D., J.L. Juang, S.L. Hilgers, and M.B. Garment. 2000. Blood barriers of the insect. *Annual review of entomology*. 45:151-174.

Cavey, M., M. Rauzi, P.F. Lenne, and T. Lecuit. 2008. A two-tiered mechanism for stabilization and immobilization of E-cadherin. *Nature*. 453:751-756.

Coleman, M.L., E.A. Sahai, M. Yeo, M. Bosch, A. Dewar, and M.F. Olson. 2001. Membrane blebbing during apoptosis results from caspase-mediated activation of ROCK I. *Nature cell biology*. 3:339-345.

Copp, A.J., and N.D. Greene. 2010. Genetics and development of neural tube defects. *The Journal of pathology*. 220:217-230.

Cordeiro, J.V., and A. Jacinto. 2013. The role of transcription-independent damage signals in the initiation of epithelial wound healing. *Nature reviews. Molecular cell biology*. 14:249-262.

Ebrahim, S., T. Fujita, B.A. Millis, E. Kozin, X. Ma, S. Kawamoto, M.A. Baird, M. Davidson, S. Yonemura, Y. Hisa, M.A. Conti, R.S. Adelstein, H. Sakaguchi, and B. Kachar. 2013. NMII forms a contractile transcellular sarcomeric network to regulate apical cell junctions and tissue geometry. *Current biology : CB*. 23:731-736.

Edwards, K.A., M. Demsky, R.A. Montague, N. Weymouth, and D.P. Kiehart. 1997. GFP-moesin illuminates actin cytoskeleton dynamics in living tissue and demonstrates cell shape changes during morphogenesis in Drosophila. *Developmental biology*. 191:103-117.

Eisenhoffer, G.T., P.D. Loftus, M. Yoshigi, H. Otsuna, C.B. Chien, P.A. Morcos, and J. Rosenblatt. 2012. Crowding induces live cell extrusion to maintain homeostatic cell numbers in epithelia. *Nature*. 484:546-549.

Eisenhoffer, G.T., and J. Rosenblatt. 2013. Bringing balance by force: live cell extrusion controls epithelial cell numbers. *Trends in cell biology*. 23:185-192.

Fan, Y., and A. Bergmann. 2008. Apoptosis-induced compensatory proliferation. The Cell is dead. Long live the Cell! *Trends in cell biology*. 18:467-473.

Fernandez-Gonzalez, R., and J.A. Zallen. 2011. Oscillatory behaviors and hierarchical assembly of contractile structures in intercalating cells. *Physical biology*. 8:045005.

Founounou, N., N. Loyer, and R. Le Borgne. 2013. Septins Regulate the Contractility of the Actomyosin Ring to Enable Adherens Junction Remodeling during Cytokinesis of Epithelial Cells. *Developmental Cell*. 24:242-255.

Gates, J., and M. Peifer. 2005. Can 1000 reviews be wrong? Actin, alpha-Catenin, and adherens junctions. *Cell*. 123:769-772.

Gorfinkiel, N., G.B. Blanchard, R.J. Adams, and A. Martinez Arias. 2009. Mechanical control of global cell behaviour during dorsal closure in Drosophila. *Development*. 136:1889-1898.

Greenspan, R.J. 2004. Fly Pushing: The Theory and Practice of Drosophila Genetics. Cold Spring Harbor Laboratory Press.

Guillot, C., and T. Lecuit. 2013. Adhesion Disengagement Uncouples Intrinsic and Extrinsic Forces to Drive Cytokinesis in Epithelial Tissues. *Developmental Cell*. 24:227-241.

Hayakawa, K., H. Tatsumi, and M. Sokabe. 2011. Actin filaments function as a tension sensor by tension-dependent binding of cofilin to the filament. *The Journal of cell biology*. 195:721-727.

Held, L.I., L.I. Held, and J.B.L. Bard. 2005. Imaginal Discs: The Genetic and Cellular Logic of Pattern Formation. Cambridge University Press.

Hengartner, M.O. 2000. The biochemistry of apoptosis. *Nature*. 407:770-776.

Herren, B., B. Levkau, E.W. Raines, and R. Ross. 1998. Cleavage of beta-catenin and plakoglobin and shedding of VE-cadherin during endothelial apoptosis: evidence for a role for caspases and metalloproteinases. *Molecular biology of the cell*. 9:1589-1601.

Herszterg, S., A. Leibfried, F. Bosveld, C. Martin, and Y. Bellaiche. 2013. Interplay between the dividing cell and its neighbors regulates adherens junction formation during cytokinesis in epithelial tissue. *Dev Cell*. 24:256-270.

Hinz, B., D. Mastrangelo, C.E. Iselin, C. Chaponnier, and G. Gabbiani. 2001. Mechanical Tension Controls Granulation Tissue Contractile Activity and Myofibroblast Differentiation. *The American Journal of Pathology*. 159:1009-1020.

Hirano, S., N. Kimoto, Y. Shimoyama, S. Hirohashi, and M. Takeichi. 1992. Identification of a neural alpha-catenin as a key regulator of cadherin function and multicellular organization. *Cell*. 70:293-301.

Ivanova, S., U. Gregorc, N. Vidergar, R. Javier, D.S. Bredt, P. Vandenabeele, J. Pardo, M.M. Simon, V. Turk, L. Banks, and B. Turk. 2011. MAGUKs, scaffolding proteins at cell junctions, are substrates of different proteases during apoptosis. *Cell death & disease*. 2:e116.

Jacinto, A., S. Woolner, and P. Martin. 2002. Dynamic Analysis of Dorsal Closure in Drosophila: From Genetics to Cell Biology. *Developmental Cell*. 3:9-19.

Jacobson, M.D., M. Weil, and M.C. Raff. 1997. Programmed cell death in animal development. *Cell*. 88:347-354.

Kerr, J.F., A.H. Wyllie, and A.R. Currie. 1972. Apoptosis: a basic biological phenomenon with wide-ranging implications in tissue kinetics. *British journal of cancer*. 26:239-257.

Kessler, T., and H.A. Muller. 2009. Cleavage of Armadillo/beta-catenin by the caspase DrICE in Drosophila apoptotic epithelial cells. *BMC developmental biology*. 9:15.

Kiehart, D.P., C.G. Galbraith, K.A. Edwards, W.L. Rickoll, and R.A. Montague. 2000. Multiple forces contribute to cell sheet morphogenesis for dorsal closure in Drosophila. *Journal of Cell Biology*. 149:471-490.

Kim, H.Y., V.D. Varner, and C.M. Nelson. 2013. Apical constriction initiates new bud formation during monopodial branching of the embryonic chicken lung. *Development*. 140:3146-3155.

Kroemer, G., L. Galluzzi, P. Vandenabeele, J. Abrams, E.S. Alnemri, E.H. Baehrecke, M.V. Blagosklonny, W.S. El-Deiry, P. Golstein, D.R. Green, M. Hengartner, R.A. Knight, S. Kumar, S.A. Lipton, W. Malorni, G. Nunez, M.E. Peter, J. Tschopp, J. Yuan, M. Piacentini, B. Zhivotovsky, and G. Melino. 2009. Classification of cell death: recommendations of the Nomenclature Committee on Cell Death 2009. *Cell death and differentiation*. 16:3-11.

Kuipers, D., A. Mehonic, M. Kajita, L. Peter, Y. Fujita, T. Duke, G. Charras, and J.E. Gale. 2014. Epithelial repair is a two-stage process driven first by dying cells and then by their neighbours. *Journal of cell science*. 127:1229-1241.

Kuranaga, E. 2012. Beyond apoptosis: caspase regulatory mechanisms and functions in vivo. *Genes to cells : devoted to molecular & cellular mechanisms*. 17:83-97.

Kurokawa, M., and S. Kornbluth. 2009. Caspases and kinases in a death grip. *Cell*. 138:838-854.

le Duc, Q., Q. Shi, I. Blonk, A. Sonnenberg, N. Wang, D. Leckband, and J. de Rooij. 2010. Vinculin potentiates E-cadherin mechanosensing and is recruited to actin-anchored sites within adherens junctions in a myosin II-dependent manner. *The Journal of cell biology*. 189:1107-1115.

Lee, S.E., R.D. Kamm, and M.R. Mofrad. 2007. Force-induced activation of talin and its possible role in focal adhesion mechanotransduction. *Journal of biomechanics*. 40:2096-2106.

Lee, T., and L. Luo. 1999. Mosaic analysis with a repressible cell marker for studies of gene function in neuronal morphogenesis. *Neuron*. 22:451-461.

Lindsten, T., A.J. Ross, A. King, W.X. Zong, J.C. Rathmell, H.A. Shiels, E. Ulrich, K.G. Waymire, P. Mahar, K. Frauwirth, Y. Chen, M. Wei, V.M. Eng, D.M. Adelman, M.C. Simon, A. Ma, J.A. Golden, G. Evan, S.J. Korsmeyer, G.R. MacGregor, and C.B. Thompson. 2000. The combined functions of proapoptotic Bcl-2 family members bak and bax are essential for normal development of multiple tissues. *Molecular cell*. 6:1389-1399.

Lubkov, V., and D. Bar-Sagi. 2014. E-cadherin-mediated cell coupling is required for apoptotic cell extrusion. *Current biology : CB*. 24:868-874.

Madara, J.L. 1990. Maintenance of the macromolecular barrier at cell extrusion sites in intestinal epithelium: physiological rearrangement of tight junctions. *The Journal of membrane biology*. 116:177-184.

Madhavan, M.M., and K. Madhavan. 1980. MORPHOGENESIS OF THE EPIDERMIS OF ADULT ABDOMEN OF DROSOPHILA. *Journal of Embryology and Experimental Morphology*. 60:1-31.

Mahajan, R.K., and J.D. Pardee. 1996. Assembly mechanism of Dictyostelium myosin II: regulation by K+, Mg2+, and actin filaments. *Biochemistry*. 35:15504-15514.

Maitre, J.L., and C.P. Heisenberg. 2013. Three functions of cadherins in cell adhesion. *Current biology : CB*. 23:R626-633.

Marchiando, A.M., L. Shen, W.V. Graham, K.L. Edelblum, C.A. Duckworth, Y. Guan, M.H. Montrose, J.R. Turner, and A.J. Watson. 2011. The epithelial barrier is maintained by in vivo tight junction expansion during pathologic intestinal epithelial shedding. *Gastroenterology*. 140:1208-1218 e1201-1202.

Marinari, E., A. Mehonic, S. Curran, J. Gale, T. Duke, and B. Baum. 2012. Live-cell delamination counterbalances epithelial growth to limit tissue overcrowding. *Nature*. 484:542-545.

Martin, A.C., M. Kaschube, and E.F. Wieschaus. 2009. Pulsed contractions of an actin-myosin network drive apical constriction. *Nature*. 457:495-499.

Mazumdar, A., and M. Mazumdar. 2002. How one becomes many: blastoderm cellularization in Drosophila melanogaster. *BioEssays : news and reviews in molecular, cellular and developmental biology*. 24:1012-1022.

Meghana, C., N. Ramdas, F.M. Hameed, M. Rao, G.V. Shivashankar, and M. Narasimha. 2011. Integrin adhesion drives the emergent polarization of active cytoskeletal stresses to pattern cell delamination. *Proceedings of the National Academy of Sciences of the United States of America*. 108:9107-9112.

Mishra, M., J. Kashiwazaki, T. Takagi, R. Srinivasan, Y. Huang, M.K. Balasubramanian, and I. Mabuchi. 2013. In vitro contraction of cytokinetic ring depends on myosin II but not on actin dynamics. *Nature cell biology*. 15:853-859.

Mogilner, A., and G. Oster. 2003. Force generation by actin polymerization II: the elastic ratchet and tethered filaments. *Biophysical journal*. 84:1591-1605.

Monier, B., A. Pelissier-Monier, A.H. Brand, and B. Sanson. 2010. An actomyosin-based barrier inhibits cell mixing at compartmental boundaries in Drosophila embryos. *Nature cell biology*. 12:60-65; sup pp 61-69.

Nakajima, Y.-i., E. Kuranaga, K. Sugimura, A. Miyawaki, and M. Miura. 2011. Nonautonomous Apoptosis Is Triggered by Local Cell Cycle Progression during Epithelial Replacement in Drosophila. *Molecular and Cellular Biology*. 31:2499-2512.

Nava, P., R. Kamekura, and A. Nusrat. 2013. Cleavage of transmembrane junction proteins and their role in regulating epithelial homeostasis. *Tissue barriers*. 1:e24783.

Niederman, R., and T.D. Pollard. 1975. Human platelet myosin. II. In vitro assembly and structure of myosin filaments. *The Journal of cell biology*. 67:72-92.

Ninov, N., D.A. Chiarelli, and E. Martin-Blanco. 2007. Extrinsic and intrinsic mechanisms directing epithelial cell sheet replacement during Drosophila metamorphosis. *Development*. 134:367-379.

Ninov, N., C. Manjón, and E. Martín-Blanco. 2009. Dynamic Control of Cell Cycle and Growth Coupling by Ecdysone, EGFR, and PI3K Signaling in <italic>Drosophila</italic> Histoblasts. *PLoS Biol*. 7:e1000079.

Ninov, N., and E. Martin-Blanco. 2007. Live imaging of epidermal morphogenesis during the development of the adult abdominal epidermis of Drosophila. *Nat. Protocols*. 2:3074-3080.

Ninov, N., S. Menezes-Cabral, C. Prat-Rojo, C. Manjón, A. Weiss, G. Pyrowolakis, M. Affolter, and E. Martín-Blanco. 2010. Dpp Signaling Directs Cell Motility and Invasiveness during Epithelial Morphogenesis. *Current Biology*. 20:513-520.

Oda, H., and S. Tsukita. 2001. Real-time imaging of cell-cell adherens junctions reveals that Drosophila mesoderm invagination begins with two phases of apical constriction of cells. *Journal of cell science*. 114:493-501.

Oshima, K., and R.G. Fehon. 2011. Analysis of protein dynamics within the septate junction reveals a highly stable core protein complex that does not include the basolateral polarity protein Discs large. *Journal of cell science*. 124:2861-2871.

Roh-Johnson, M., G. Shemer, C.D. Higgins, J.H. McClellan, A.D. Werts, U.S. Tulu, L. Gao, E. Betzig, D.P. Kiehart, and B. Goldstein. 2012.

Triggering a cell shape change by exploiting preexisting actomyosin contractions. *Science*. 335:1232-1235.

Rosenblatt, J., M.C. Raff, and L.P. Cramer. 2001. An epithelial cell destined for apoptosis signals its neighbors to extrude it by an actin- and myosin-dependent mechanism. *Current Biology*. 11:1847-1857.

Rubin, G.M., and E.B. Lewis. 2000. A brief history of Drosophila's contributions to genome research. *Science*. 287:2216-2218.

Sellers, J.R. 2000. Myosins: a diverse superfamily. *Biochimica et biophysica acta*. 1496:3-22.

Shaevitz, J.W., and D.A. Fletcher. 2007. Load fluctuations drive actin network growth. *Proceedings of the National Academy of Sciences of the United States of America*. 104:15688-15692.

Slattum, G.M., and J. Rosenblatt. 2014. Tumour cell invasion: an emerging role for basal epithelial cell extrusion. *Nat Rev Cancer*. 14:495-501.

Solon, J., A. Kaya-Çopur, J. Colombelli, and D. Brunner. 2009. Pulsed Forces Timed by a Ratchet-like Mechanism Drive Directed Tissue Movement during Dorsal Closure. *Cell*. 137:1331-1342.

Sonnemann, K.J., and W.M. Bement. 2011. Wound repair: toward understanding and integration of single-cell and multicellular wound responses. *Annual review of cell and developmental biology*. 27:237-263.

Steinhusen, U., J. Weiske, V. Badock, R. Tauber, K. Bommert, and O. Huber. 2001. Cleavage and shedding of E-cadherin after induction of apoptosis. *The Journal of biological chemistry*. 276:4972-4980.

Taguchi, K., T. Ishiuchi, and M. Takeichi. 2011. Mechanosensitive EPLIN-dependent remodeling of adherens junctions regulates epithelial reshaping. *The Journal of cell biology*. 194:643-656.

Takeichi, M. 2014. Dynamic contacts: rearranging adherens junctions to drive epithelial remodelling. *Nature reviews. Molecular cell biology*. 15:397-410.

Takemoto, K., T. Nagai, A. Miyawaki, and M. Miura. 2003. Spatio-temporal activation of caspase revealed by indicator that is insensitive to environmental effects. *The Journal of cell biology*. 160:235-243.

Teng, X., and Y. Toyama. 2011. Apoptotic force: active mechanical function of cell death during morphogenesis. *Development, growth & differentiation*. 53:269-276.

Thornberry, N.A., H.G. Bull, J.R. Calaycay, K.T. Chapman, A.D. Howard, M.J. Kostura, D.K. Miller, S.M. Molineaux, J.R. Weidner, J. Aunins, and et al. 1992. A novel heterodimeric cysteine protease is required for interleukin-1 beta processing in monocytes. *Nature*. 356:768-774.

Toyama, Y., X.G. Peralta, A.R. Wells, D.P. Kiehart, and G.S. Edwards. 2008. Apoptotic force and tissue dynamics during Drosophila embryogenesis. *Science*. 321:1683-1686.

van Ham, T.J., D. Kokel, and R.T. Peterson. 2012. Apoptotic cells are cleared by directional migration and elmo1- dependent macrophage engulfment. *Current biology : CB*. 22:830-836.

Vogel, V., and M. Sheetz. 2006. Local force and geometry sensing regulate cell functions. *Nature reviews. Molecular cell biology*. 7:265-275.

Yamada, S., S. Pokutta, F. Drees, W.I. Weis, and W.J. Nelson. 2005. Deconstructing the cadherin-catenin-actin complex. *Cell*. 123:889-901.

Yamaguchi, Y., N. Shinotsuka, K. Nonomura, K. Takemoto, K. Kuida, H. Yosida, and M. Miura. 2011. Live imaging of apoptosis in a novel transgenic mouse highlights its role in neural tube closure. *The Journal of cell biology*. 195:1047-1060.

Yonemura, S., Y. Wada, T. Watanabe, A. Nagafuchi, and M. Shibata. 2010. alpha-Catenin as a tension transducer that induces adherens junction development. *Nature cell biology*. 12:533-542.

Yu, F., and O. Schuldiner. 2014. Axon and dendrite pruning in Drosophila. *Current opinion in neurobiology*. 27C:192-198.